

**ANALYSIS OF FLUORESCENCE CORRELATION SPECTROSCOPY
& FLUORESCENCE ANISOTROPY MEASUREMENTS OF
FLUORESCENT NANOPROBES IN LINEAR
POLYMER SOLUTIONS**

BY

ZAKARIA M'RAH

A DISSERTATION

**SUBMITTED IN PARTIAL FULFILLMENT OF THE REQUIREMENTS
FOR THE DEGREE OF DOCTOR OF PHILOSOPHY
IN THE OPTICS GRADUATE PROGRAM OF
DELAWARE STATE UNIVERSITY
DOVER, DELAWARE**

May 2017

This thesis is approved by the following members of the Committee:

Dr. Hacene Boukari, Committee Chairperson, Department of Physics & Engineering, Delaware State University

Dr. Yuri Markushin, Committee Member, Department of Physics & Engineering, Delaware State University

Dr. Amir Khan, Committee Member, Department of Physics & Engineering, Delaware State University

Dr. Qi Lu, Committee Member, Department of Physics & Engineering, Delaware State University

Dr. Jennie Leach, External Committee Member, Department of Chemical, Biochemical & Environmental Engineering, University of Maryland Baltimore County

DEDICATION

I dedicate this dissertation to the late *ALI M'RAH ben OMAR*, my beloved grandparent.

ACKNOWLEDGMENTS

I would like to say thank you to Dr Hacene Boukari, my PhD advisor and mentor, who, without his guidance and support this would not have been possible. His patience and never ending encouragement as well as his belief in my potential has allowed me to grow into the scientist I am today.

I would like to thank my committee members, Dr Jennie Leach, Dr Amir Khan, Dr Qi Lu and Dr Yuri Markushin. Thank you all for your willingness to be part of my committee. I also appreciated the input you gave me on my dissertation.

I would like to express my gratitude to Dr Qi Lu for her guidance in lab meetings and always having an open door. I would like to thank my professors in the department of physics and engineering as well as Dr Nouredine Melikechi for being supportive over the years.

I am indebted to INBRE and OSCAR for providing me the financial support throughout my doctoral studies at DSU. I would like to thank the staff, Ms Jackie Jones, Vanessa Nesbit and Amal Juracka for their support as well.

I would like to thank my brothers, and my sister. Thank you for redirecting me whenever I lost the enthusiasm to keep pushing.

I am grateful to my fellow graduate students, Elton Jhamba, Isaac Basaldua and Angela Landberg Their encouragement made graduate school more bearable.

ABSTRACT

We combine fluorescence correlation spectroscopy (FCS), fluorescence anisotropy (FA) and fluorescence imaging microscopy methods to measure the rotational diffusion and the translational diffusion of fluorophores mixed in non-fluorescent –hence “invisible”- aqueous Linear polymers solutions under thermal fluctuations.

We measured changes of the emission spectrum, the lifetime, and the apparent rotational and translational diffusion coefficients of the fluorophores with systematic increase of the polymer concentration up to 1200 mg/ml for PEG and up to 120 mg/ml for PVA, at room temperature. The spectrum and the lifetime appear to be insignificantly altered by the polymer solutions. The fluorescence correlation functions can be readily fit with the expression describing normal particle diffusion. We then determine changes of the apparent rotational and translational diffusion coefficients with systematic increase of polymer concentration. Notably, the changes cannot be accounted for by the corresponding changes of the bulk viscosity of the linear polymer solutions as would be suggested by the Stokes-Einstein relations for both diffusion coefficients. Instead, we analyze the data with the entropic model proposed by de-Gennes and fit each set of data with a stretched exponential $[\exp(-\alpha c^n)]$ with n being related to the quality of the solvent. The fits yield n -value close to $3/4$, suggesting a good behavior of the host polymer-water system. Moreover, the α -value for translation is similar to that of rotation, indicating similar local entropic effects on the rotation and translation, which is predicted by the model.

TABLE OF CONTENTS

CHAPTER I: INTRODUCTION & FUNDAMENTALS

1.1 Overview.....	01
1.2 Basic Concepts in Polymers.....	04
1.2 Poly (ethylene glycol):	07
1.3 Poly (vinyl alcohol) PVA.....	08
1.4 Nanoprobe Diffusion in Polymer Solutions	09
1.5 Fluorescence correlation spectroscopy (FCS):	10
1.6 Fluorescence anisotropy (FA):	13
1.6 Selection of a Fluorescent Label:	15
1.7 Structure of the dissertation.....	16

CHAPTER II: Translational Diffusion & Fluorescence Correlation Spectroscopy Measurements

2.1. Introduction.....	18
2.2 Mathematical background.....	20
2.3. Materials and Sample Preparations	25
2.3.1. PEG, PVA and Fluorescent Nanoprobes.....	25
2.3.2 Lab work and preparation.....	26
2.3.3 Hybridization chamber.....	30

2.3.4. Schematic of an FCS setup.....	32
2.3.5. FCS Instrument and Components:	36
2.3.6. Q2 system Components.....	38
2.4.1. FCS Calibration:.....	39
2.4.2. Laser Power Calibration:.....	40
2.4.3. Absence of fluorophore (background) Vs presence of fluorophore (Fluorescence Signal).....	42
2.4.4. Effect of PEG solutions on the fluorescence of Alexa488 and Fluorescein.....	44
2.5. Results and Discussion	50
2.5.1. Analysis of Correlation functions:.....	50
2.5.2 Probe Diffusion in Polymeric Solutions.....	58
2.5.3. Volume Fraction Vs. Concentration.....	63
2.6. Conclusions:.....	68
 CHAPTER III : ROTATIONAL DIFFUSION of Alexa488 in PEG and PVA Solutions	
3.1 Introduction.....	70
3.2 Fluorescence Anisotropy Method.....	70
3.3 Theoretical Background and Frequency Domain Measurements.....	72
3.4 ISS K2 Spectrofluorimeter INSTRUMENT.....	76

3.4.1 Photomultiplier tube (PMT) configuration and Light source.....	76
3.4.2 Excitation/Emission Monochromators and Polarizers.....	78
3.4.3 Software.....	81
3.5 Experimental Results:.....	82
3.5.1 Polymers and Nanoprobes:.....	82
3.5.2 Calibration Test with Raman Spectrum.....	83
3.5.3 Background Suppression, Sample, and Reference Preparation:.....	84
3.5.4 Lifetime Measurements:.....	87
3.5.5 Alexa488 in PEG and PVA Solutions:.....	88
3.5.6 Rotational Correlation Times of Alexa488 Vs. Polymer Concentration:.....	92
3.6 Summary and Conclusions of Chapter 3:	100
 CHAPTER IV: DISCUSSION & CONCLUSIONS	
4.1 Results from Fluorescence Spectroscopy:.....	103
4.2 Results from FCS Measurements:.....	103
4.3 Results from FA Measurements:.....	104
4.4 Analysis of FCS Data with Viscosity Data.....	106
4.5 Linear PEG or PVA vs Branched Ficoll Solutions:.....	108
REFERENCES:.....	114

LIST OF FIGURES AND ILLUSTRATIONS

Figure 1.1: Overlap concentration of polymer solutions.....	06
Figure 1.2: cross-linked polymer Vs. Linear polymer	07
Figure 1.3: PEG polymer molecular structure.....	08
Figure 1.4: PEG polymer molecular structure.....	09
Figure 1.5: Schematic diagram of FCS.....	11
Figure 1.6. Geometry of fluorescence anisotropy experiment.....	12
Figure 2.1: Contour plot for square detection profile of Gaussian beam where the first circle at which along the (x,y) plane intensity decreases to e^{-2}	22
Figure 2.2: A; Fluka Analytical ref: 81280-1KG Poly (ethylene glycol) bottle B:PEG solid and pure powder, C:PEG+H ₂ O vortexed for 01 hrs, D: at t=6hrs, E: at t=24hrs.....	26
Figure 2.3: A: Sigma Aldrich ref: 363146-1KG Poly(Vinyl alcohol) bottle B: PVA in beaker on hot/stir plate (around 100°C & 1150 rpm).....	29
Figure 2.4: A: dilute cross-linked and highly viscous PVA gel (5-7 days of heating and stirring). B: is a zoomed capture of A.....	29
Figure 2.5: PVA gel in Solid form (30 days of heating and stirring) A: Solid PVA in Beaker B: PVA portion was cut to show the hard & holding form.....	30
Figure 2.6: Four wells set of PEG samples in hybridization chamber, samples are air bubble-free and carefully sealed.FCS Instrument: Q2-FFS ALBA.....	31
Figure 2.10: FCS setup and schematic calibration.....	32
Figure 2.7: FCS Layout A: general overview of FCS units B: Olympus microscope C: 64-bit workstation with ISS VistaVision software.....	34

Figure 2.8: FCS units; A: FastFLIM data acquisition unit B:3-axis controller unit C:Piezo Z controller unit D:Scanning mirrors driver unit E:Q2 system unit F:Laser launcher unit.....	35
Figure 2.9: Q2 system overview.....	37
Figure 2.11: Normalized $G(\tau)$ Vs. time delay (τ) result in FCS calibration test. Cross-correlation fitting of 5 iterations using a 3-D Gaussian to recover the beam waist parameters.....	39
Figure 2.12: Correlation Plots at Background (laser power at 0%).....	40
Figure 2.13: Correlation Plots at 0.3mW laser power (25%).....	41
Figure 2.14: Correlation Plots at 0.6mW laser power (50%).....	41
Figure 2.15: Correlation function of Fluorescein fluorophore in PVA (20mg/ml concentration) and its respective photon counts Vs time duration of the experiment.....	42
Figure 2.16: Correlation function of PVA (20mg/ml concentration) without Fluorescein fluorophore and its respective photon counts Vs time duration of the experiment.....	43
Figure 2.17: Fluorescence spectra of Alexa 488 in different PVA concentrations.....	45
Figure 2.18: Fluorescence spectra of Fluorescein in different PVA concentrations	46
Figure 2.19: Fluorescence spectra of Alexa 488 in different PEG concentrations	47
Figure 2.20: Fluorescence spectra of Fluorescein in different PEG concentrations.....	48
Figure 2.21: Fluorescence lifetime of Alexa488 in different PVA concentrations	49
Figure 2.22: Fluorescence lifetime of Alexa488 in different PEG concentrations.....	49
Figure 2.23: Correlation functions of fluorescein in different PVA solutions. Fits of the equation 2.9 of Data are represented as solid lines.....	51

Fig 2.24: Normalized correlation functions of fluorescein in different PVA solutions. Fits of the equation 2.9 of data are represented as solid lines.....52

Figure 2.25: Correlation functions of Alexa 488 in different PEG solutions (from 01 to 400 mg/ml). Fits of the equation 2.9 of Data are represented as solid lines.54

Figure 2.27: Normalized correlation functions of Alexa in different PEG solutions (from 100 to 400 mg/ml). Fits of the equation 2.9 of Data are represented as solid lines.55

Figure 2.26: Correlation functions of Alexa 488 in different PEG solutions(from 500 to 1200 mg/ml). Fits of the equation 2.9 of Data are represented as solid lines.56

Figure 2.28: Correlation functions of fluorescein in different PEG solutions(from 500 to 1200 mg/ml) . Fits of the equation 2.9 of Data are represented as solid lines.....57

Figure 2.29: translational diffusion coefficient of Fluorescein fluorophores as function of PVA concentration.....61

Figure 2.30: translational diffusion coefficient of Alexa488 fluorophores as function of PEG concentration.....62

Figure 2.32: Calculated Volume fraction of PVA and PEG as a function of their respective concentrations.....64

Figure 2.31: comparable Volume fraction at~ 0.74, to the respective is about 04 folds (~150 mg/ml for Fluorescein in PVA and ~38 mg/ml forAlexa488 in PEG).....65

Figure 2.33: Translational diffusion time Vs. the polymer volume occupancy fraction in the solution of both PEG and PVA, The two fittng plots are in almost superposition.....67

Figure 3.1: Schematic drawing for the measurement of fluorescence Anisotropy.....71

Figure 3.2: ISS K2 (Champaign , IL) Spectrofluorometer.....77

Figure 3.3:MFCC Block Diagram (Multi-Frequency Cross-Correlation) setup.....80

Figure 3.4: ISS K2 spectrofluorometer components with full command displayed in Vinci Software window.....	81
Figure 3.5 : Frequency domain intensity decays of Fluorescein in H ₂ O (green and black) and Alexa in H ₂ O (blue and red)	82
Figure 3.6: Raman spectrum of H ₂ O.....	83
Figure 3.7: Fluorescence Emission Spectra of PEG 500 mg/ml (Red) and Alexa 488 in water (blue) without filter in the optical path.....	85
Figure 3.8: Figure: Fluorescence Emission Spectra of PEG 500 mg/ml (Red) and Alexa 488 in water (blue) with filter present in the optical path.....	85
Figure 3.9: Frequency domain intensity decays of Alexa in PEG 100 mg/ml (green and light blue) and Alexa 488 in 900mg/ml PEG (dark blue and red).....	86
Figure 3.10: Frequency domain intensity decays of Alexa in PVA 10 mg/ml (green and light blue) and Alexa 488 in 100mg/ml PEG (dark blue and red)	87
Figure 3.11: Frequency response of Alexa488 in PEG 500mg/ml. Data are the solid dots, Solid line represents the best single exponential fit.....	89
Figure 3.12: Differential Polarized Phase Angle and Amplitude Ratio (Frequency domain anisotropy decays) of Alexa 488 in PEG 500mg/ml.....	90
Figure 3.13: Frequency response of Alexa488 in PEG 100mg/ml. Data are the solid dots, Solid line represents the best single exponential fit.....	91
Figure 3.14: Differential Polarized Phase Angle and Amplitude Ratio (Frequency domain anisotropy decays) of Alexa 488 in PEG 100mg/ml	92
Figure 3.15: Anisotropy of Alexa488 fluorophore as function of PEG concentration.....	94

Figure 3.16: Anisotropy of Alexa488 fluorophore as function of PVA concentration.....	95
Figure 3.17: Rotational Correlation time of Alexa488 fluorophores as function of PEG concentration.....	96
Figure 3.18: Rotational Correlation time of Alexa488 fluorophores as function of PVA concentration.....	97
Figure 3.19: Rotational diffusion coefficient of Alexa488 fluorophore as function of PEG concentration.....	98
Figure 3.20: Rotational diffusion coefficient of Alexa488 fluorophore as function of PVA concentration.....	99
Figure 4.1: Changes of the translational diffusion coefficient of Alexa488 in Ficoll solutions.....	108
Figure 4.2: Changes of the translational diffusion coefficient of Alexa488 in PEG solutions...	109
Figure 4.3: Changes of the inverse of the rotational correlation time (proportional to rotational diffusion coefficient, D_R) of Alexa488 in Ficoll solutions.....	111
Figure 4.4: Changes of the inverse of the rotational correlation time (proportional to rotational diffusion coefficient, D_R) of Alexa488 in PEG solutions.....	112

CHAPTER I: INTRODUCTION & FUNDAMENTALS

1.1 Overview

We usually think of crowding as a cause of obstruction and frustration, yet all living systems appear to be highly crowded. It is an essential characteristic of all living organisms. The cell, in particular, is a heterogeneous and crowded entity, and somehow this “crowdedness” plays a vital role for many of its biological functions. Most studies show that the concentration of biological macromolecules (proteins, ribonucleoproteins, nucleic acids polysaccharides, ...) inside cells can be as high as 400 mg/mL, corresponding to 40% volume occupancy restricting considerably the amounts of free water [1]. Since no individual macromolecular species is necessarily present at high concentration [2,3], the cellular macromolecules can be considered as “crowders” or “volume-occupiers”. These macromolecules themselves have specific primary functions within the cell, but their very presence in the cellular environment has a major secondary effect, namely crowding. In addition to these macromolecules, supramolecular assemblies in the form of cellular subunits within a cell (e.g. nucleus, mitochondria) that also contribute to the heterogeneity of the crowdedness of the cell interior.

It is now recognized that macromolecular crowding plays significant roles in diverse biochemical and biophysical processes, including protein folding, enhancement of enzymatic properties, polymerization/depolymerization of macromolecules, and slowing down of diffusion [39]. Here, fundamental studies on crowding have been conducted in test-tube assays with the use of molecular crowding agents such as proteins and polymers. With recent advances in spectroscopic and imaging technologies and in designing novel molecular probes the interest has shifted to in-situ studies of live-cells, burgeoning into a growing and active interdisciplinary field

by itself. It is now possible to investigate macromolecular interactions and dynamics in the cells, and extract relevant physical and chemical parameters such polymerization rate and chemical constants. How to translate the measured complex interactions into models of biological systems remain quite challenging [40].

Before immersing into the complexity of biological systems, however, one needs to step back and look into developing and studying simple molecular models of crowded environments. One should note that interest in understanding the behavior of crowded environments and their roles in chemical and physical processes is not unique to biological systems. Rather, this understanding has been sought in other fields such as tissue engineering, drug delivery, oil recovery, colloidal science, and chemical therapeutics. For our applications, we seek models that are aqueous in nature, and we should be able to vary and control their structural characteristics such as porosity or mesh size, their viscoelastic properties, their solvent affinity, and their ionic strengths. Here, it has been suggested that biopolymeric solutions and hydrogels may be considered crowded environments [38]. This suggestion is the basic hypothesis for my work since I joined Dr. Boukari's laboratory. It follows a line of successful work and collaborative projects conducted on several aqueous polymers.

While at NIH, Dr. Boukari and his student, Dr. Ariel Michelman-Ribeiro, used Poly(Vinyl) Alcohol (PVA), *a linear polymer*. They investigated the translational diffusion of various nanoprobe dispersed in PVA solutions that were prepared at different PVA concentrations. Further, they investigated the effect of cross-linking of the PVA solutions on the diffusion of the nanoprobe. A major finding of this work is the unexpected additional slowing down of the nanoprobe due to chemical crosslinking of the PVA solutions and the apparent correlation of the slowing down with the stiffness of the formed PVA hydrogels.

Dr. Silviya Zustiak from Dr. Leach's Laboratory at University of Maryland Baltimore County used Polyethylene glycol (PEG), a linear polymer, and investigated the diffusion and interactions of various solutes (e.g. lysozyme, γ globulin) in the crosslinked PEG hydrogels [36]. Their work led to questioning the assumption that PEG hydrogels are completely inert to protein interactions. Recently, Jhamba et al. used Ficoll, a branched polysaccharide, and measured changes of both the translational and rotational diffusion of various nanoprobe (e.g. Alexa488, rhodamine 6G, FITC-Ficoll, BSA) as a function of Ficoll concentration [37]. Their findings indicate that the nanoprobe "see" a theta-behavior for the Ficoll environment in contrast to the good-solvent behavior "seen" by similar nanoprobe in PVA solutions.

Besides the studied polymeric systems, the above mentioned reports demonstrated the attributes of fluorescence correlation spectroscopy (FCS) for measuring nanoprobe diffusion and interactions at nanoscopic scale. Here fluorescence has been exploited to identify, monitor, and characterize the structural and dynamical behaviors of the fluorescent nanoprobe which is in principle dispersed in a non-fluorescent –hence "invisible"- crowded polymeric environment. FCS provides several advantages, including the use of nanomolar concentration of the fluorescent nanoprobe, the use of small volume of the samples (as little as 10 μ l), and the use of low power laser ($\sim\mu$ Watts). As such FCS has been extended by many authors to studies of dilute and concentrated solutions, gels, as well as live-cells [35], and it has been reviewed frequently [38].

My dissertation aims at extending previous work on PVA and PEG solutions to investigate systematically both the translational and rotational diffusion of nanoprobe in these systems. Two questions underlie the work: 1) how polymeric solutions affect the rotational diffusion of nanoprobe. While extensive work was done to elucidate the effect of polymeric

solutions on the translational diffusion, limited data and little is known about its effect on the rotation. More interestingly, is the concentration dependence of the translational diffusion similar to that of the rotation? 2) How, if any, does the chain structure of the host polymers affect the overall diffusion –translation and rotation- of the nanoprobe? We will contrast the results derived from linear PVA and PEG polymer solutions with those from branched Ficoll polymer solutions. Experimentally, we applied FCS to measure the translation diffusion of various fluorescent nanoprobe in the polymer solution, and we applied the fluorescence anisotropy (FA) method to determine changes of the rotational diffusion of the nanoprobe in the polymer solutions. Theoretically, we used an entropic-based model suggested by de Gennes and his collaborators to analyze and fit the data. Here, this model was applied to analyze the translational diffusion data, and it was unclear whether it would be applied to the rotational data. We have extended this model for the rotation and report our results.

1.2 Basic Concepts in Polymers

A polymer is a large molecule made up of chemical units joined together by chemical reaction. Polyethylene ($\text{CH}_3-(\text{CH}_2)_N-\text{CH}_3$) for example is a long chain-like molecule composed of ethylene molecules ($\text{CH}_2=\text{CH}_2$) [20]. Knowledge about the polymer's properties both in solutions and networks is required for analyzing this polymer.

The solution behavior changes from diluted to semi diluted to concentrated regimes [21]. Therefore, three concentration domains have been presented for polymer random coils in solution, corresponding respectively to separated chains, overlapping chains, and a concentrated solution regime (Figure 1.2).

The overlap concentration C^* is defined as follows:

$$C^* = \frac{M_W}{\frac{4}{3} R_g^3 N_A} \quad (1.1)$$

where M_W is the molecular weight of the polymer, R_g is the radius of gyration of the polymer and N_A is Avogadro's number. Also we define a geometric overlap concentration, C^θ , as:

$$C^\theta = \frac{M_W}{8 R_h^3 N_A} \quad (1.2)$$

where R_h is the hydrodynamic radius of the polymer. Hence, by definition, at the geometric overlap concentration, the polymer particles would be closely packed and touching each other. As polymer concentration increases, the space between chains decreases, below the overlap concentration, the polymer chains are freely floating in the solution, however, when polymer concentration approaches the overlap concentration, the polymer chains are tightly packed and finally at concentrations above the overlap concentration, polymer chains overlap and are physically entangled (see figure 1.2).

It is important to note that the C^* of the polymer is different for each solvent and can be easily adjusted by changing the solvent or its amount in a formulation.

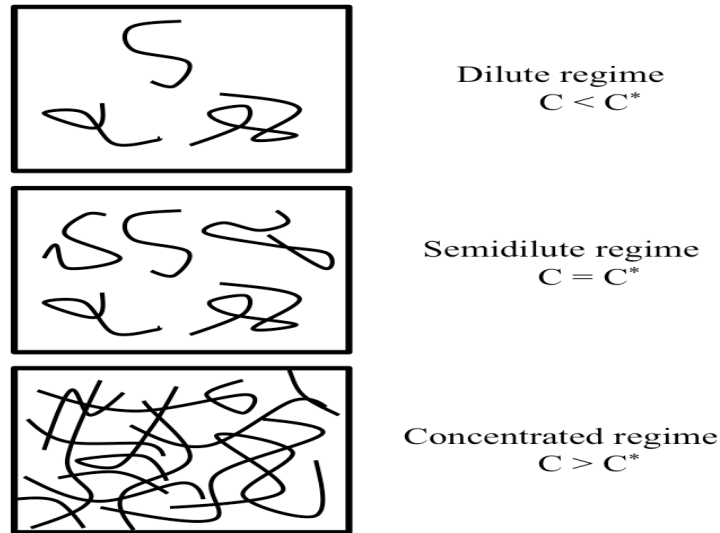


Figure 1.1: Overlap concentration of polymer solutions.

Hydrogels have been utilized due to their tunable properties in order to mimic properties of *in vivo* tissue [22, 23]. Hydrogels are ideal mimics of most soft tissue in the body, due to their overall low elastic modulus and their viscoelasticity [24]. Polymer networks, such as hydrogels, form porous structures upon crosslinking and are able to absorb and maintain a considerable amount of water [12]. Moreover, the intrinsic physical property of hydrogels is an important quality that dictates the influx of fluid for swelling and mechanical support [22, 25].

Mesh network is formed that provides a similar environment as the extracellular matrix around cells due to the three-dimensional crosslinking of the polymer networks (Figure 1-3) [26]. The extracellular matrix provides a fibrous environment for cells to grow and proliferate [27]; therefore, studying diffusion in polymers as a function of their porous structure is a crucial step for understanding transport phenomena in PEG and PVA linear polymers.

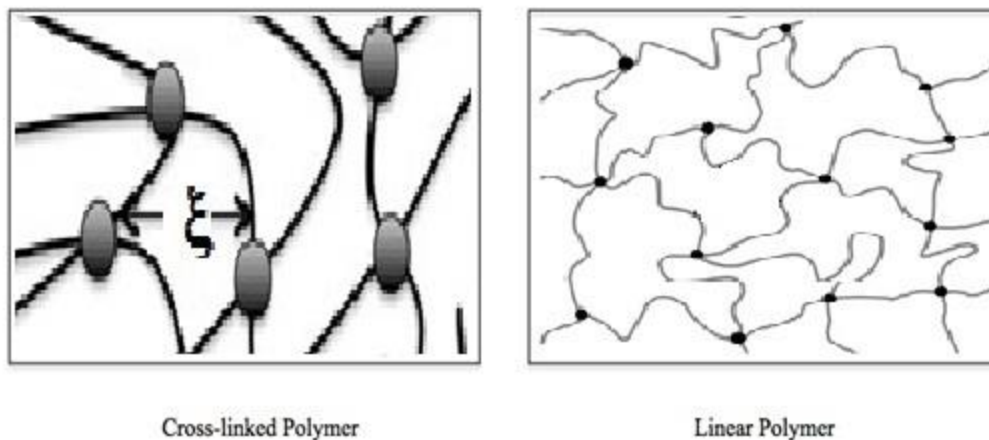


Figure 1.2: cross-linked polymer Vs. Linear polymer

ξ is the mesh size, where the polymer chains are attached to each other by cross-linkers; which is defined as the average distance between crosslinks, and it is representative of the pore space available within polymer networks.

1.2 Poly (ethylene glycol):

Poly (ethylene glycol) (PEG) is a non-toxic, water-soluble polymer, which resists recognition by the immune system. The term PEG is often used to refer to polymer chains with molecular weights below 20 kDa, while poly (ethylene oxide) (PEO) refers to higher molecular weight polymers [28]. Due to mild chemistry of PEG (Figure 1.4), it exhibits rapid clearance from the body, and has been approved for a wide range of biomedical applications. Because of these properties, hydrogels prepared from PEG are excellent candidates as biomaterials. PEG may transfer its properties to another molecule when it is covalently bound to that molecule. This could result in toxic molecules becoming non-toxic or hydrophobic molecules becoming soluble when coupled to PEG [28].

Coupling of a biological molecule to PEG usually contributes to its biological activity. This renders PEG surfaces resistant to cell and protein adsorption [29]. Proteins that are tethered to PEG are not denatured, and their rate of clearance through the body is often increased because their size is increased. Such properties make PEG-containing hydrogels excellent candidates as drug delivery systems, specifically as controlled release devices [30, 31]. Rate of drug release is typically depends on the method of hydrogel preparation, crosslinking density, molecular weight of the PEG chains, and the drug solubility in water.

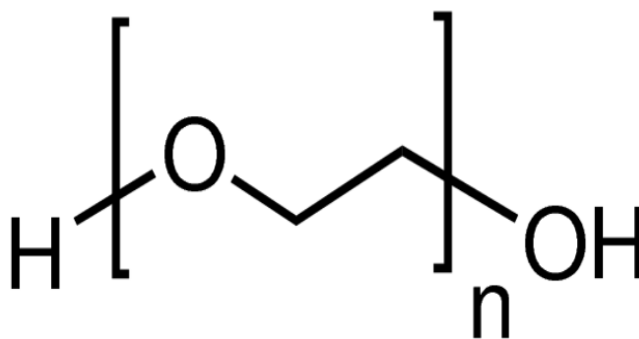


Figure 1.3: PEG polymer molecular structure.

1.3 Poly (vinyl alcohol) PVA

Poly (vinyl alcohol) PVA is a hydrophilic water-soluble environmentally friendly linear polymer produced by the polymerization of vinyl acetate to polyvinyl acetate followed by hydrolysis-that does not reach completion-of the PVAc to PVA. It is a semi-crystalline, hydrophilic polymer with good chemical and thermal stability [32]. PVA is highly biocompatible and nontoxic. It can be processed easily and has high water permeability [33] . PVA solutions can form physical gels from various types of solvent. These properties made PVA very useful in many applications in the medical, pharmaceutical, cosmetic, food fields. In order to have PVA dissolution, the

temperature must be well above 70°C because of the weak intermolecular hydrogen bonding in its structure. Furthermore, crystallization is more difficult due to the high presence of hydrolysis.

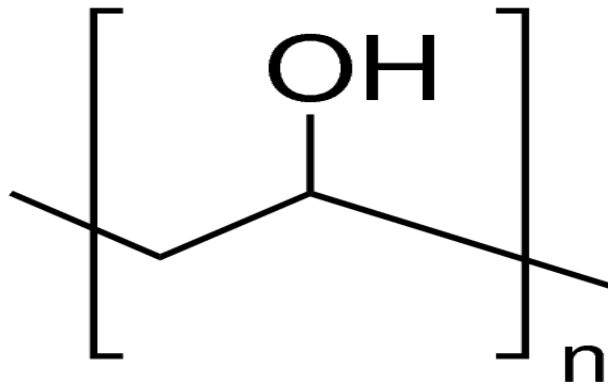


Figure 1.4: PEG polymer molecular structure

1.4 Nanoprobe Diffusion in Polymer Solutions

As defined by Cussler, diffusion is the process responsible for the movement of matter from one part of a system to another [11] and it is mainly due to random molecular motions, gases have more space between molecules, diffusion processes are fast (10 cm/min), whereas they are much slower in liquids (0.05 cm/min) and solids (0.00001 cm/min) [12]. According to Hu et al. [13], diffusion in both gases and liquids can be successfully predicted theoretically. Diffusion is known to depend on temperature, pressure, solute size and viscosity.

Diffusion in polymeric solutions and gels has been studied for decades with the use of various techniques such as gravimetry, membrane permeation, fluorescence and two dynamic light scattering [14]. Also, many new techniques have been developed for the measurement of diffusivities including pulse-field gradient nuclear magnetic resonance (NMR), forced Rayleigh scattering, and fluorescence recovery after photo bleaching (FRAP) [15].

Recently, fluorescence correlation spectroscopy (FCS), the technique used in this dissertation, has emerged as a powerful tool for the investigation of translational diffusion of solutes in various environments [41]. The diffusion studies have resulted in an enhanced knowledge of polymer morphology and structure, transport phenomena, and more recently, the controlled release of drugs from polymer carriers[16]. In addition, these studies have led to theoretical descriptions of the diffusion of solvents and/or solutes in polymer solutions, gels and even solids [17, 18]. These physical models are based on different physical concepts (the obstruction effects, the hydrodynamic interactions and the free volume theory) and their applicability varies [19].

1.5 Fluorescence correlation spectroscopy (FCS):

FCS was developed about forty two years ago by Madge et al [4]. The authors introduced the instrument's capabilities by reporting results on DNA-drug complex formation where the diffusion of the drug in DNA solutions was measured by FCS [4]. The kinetically recorded data from fluorescence molecules in the solution revealed detailed information about the sample of interest [5]. Since FCS is a single molecule technique, only very low concentration of solute must be present in the sample.

This dissertation will summarize FCS studies on polymer systems and, in particular, focus on the diffusion of differently sized molecular and macromolecular probes in polymer solutions, classical and responsive polymer gels. FCS is able to measure behavior of multiple fluorescent molecules without mixing the fluctuations of individual particles based on wavelength separation. The unique ability of FCS, which makes it stand out from other classical techniques, is to take advantage of the fluctuations of physical parameters that are reflected by the fluorescence emission of the molecules [6]. Then, the fluctuations will be recognized by FCS

based on strength and duration. FCS is a method based on observation of fluorescence intensity fluctuations that is the result of single fluorescent molecules diffusing in and out of a small detection area ($\sim 1.5\mu\text{m} \times \sim 0.3\mu\text{m}$).

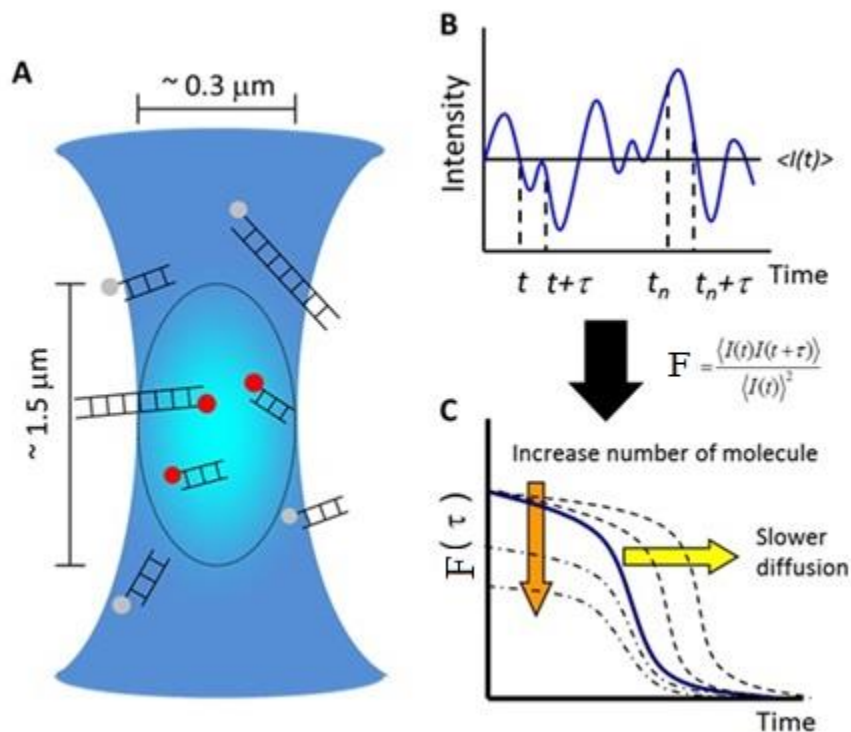


Figure 1.5: Schematic diagram of FCS[6]. Schematic of the observation area of FCS (confocal volume) (A); fluctuations in fluorescence intensity (B); autocorrelation functions ($F(\tau)$) (C).

The FCS data are interpreted in terms of autocorrelation functions ($F(\tau)$) that gives information on the diffusion time (τ_D) and the number of molecules (N) in the observation area. Diffusion constant can be estimated from τ_D and the size of the observation area [7].

FCS has a confocal set-up where excitation radiation is provided by a laser beam (dependent on the fluorescent dye) and directed into a microscope objective with a dichroic mirror and focused on the sample. The fluorescence light from the sample is collected by a water

or oil immersion objective and passed through the dichroic mirror and the emission filter. Afterwards, the light is focused onto the detector. Recorded intensity of fluctuations from fluorescent molecules is correlated in time and gives the solute translational diffusivity. Analysis of the autocorrelation function $F(\tau)$, provides information about the mechanisms underlying the intensity fluctuations [4]:

$$F(\tau) = \frac{1}{N} \left(1 + \frac{\tau}{\tau_D}\right)^{-1} \left(1 + \beta^2 \frac{\tau}{\tau_D}\right)^{-1/2} \quad (1.3)$$

where N is the average particle number in the detection volume, τ is the delay time, τ_D is the characteristic diffusion time, and $\beta = (r_0/z_0)^2$ is an ISS instrumental constant where r_0 and z_0 are the radius and axial length of the focused laser beam spot, respectively. Assuming a 3D Gaussian profile of the excitation beam, τ_D can be related to diffusivity by the following equation:

$$\tau_D = \frac{r_0^2}{4D} \quad (1.4)$$

For two independent species, the autocorrelation function becomes [4]:

$$F(\tau) = m_1 \left(1 + \frac{\tau}{\tau_1}\right)^{-1} \left(1 + \beta^2 \frac{\tau}{\tau_1}\right)^{-1/2} + m_2 \left(1 + \frac{\tau}{\tau_2}\right)^{-1} \left(1 + \beta^2 \frac{\tau}{\tau_2}\right)^{-1/2} \quad (1.5)$$

where τ_1 and τ_2 are the respective characteristic diffusion times, m_1 and m_2 are the respective fractional contributions of each components to the correlation function.

The counts per molecule are from the signal intensity of the molecules summation present, for each molecule detected during the measurement these counts are compared to a later time and correlated.

Plotting the data and extrapolating the autocorrelation curve, it intersects with the y-axis when τ is equal to 0, which equals to $F(0)$. At this point the equation changes to: $F(0) = \frac{1}{N}$ which means $F(0)$ equals the inverse of the particle number in the measurement system at $t = 0$. The fitting of the autocorrelation data is done in chapter 02 with mathematical functions which include the shape and size of the excitation volume as well as the specifics of the diffusion. In this dissertation the decay of the autocorrelation is shifted along the time axis depending on the molecules' diffusion constant while the autocorrelation function is shifted along the $F(\tau)$ axis at time zero depending on the number of molecules N present.

Knowing these characteristics, it is easier to see when a change such as the binding of two molecules occurs. With FCS, it is possible to measure the binding of fluorescent molecules quantitatively and qualitatively [8-10]. The binding and the resulting diffusion constants between a small fluorescently labeled molecule and a larger molecule in solution can be detected in a time dependent manner which conclude to the assumption that aggregation is present or not. The diffusion time through the excitation volume is characteristic for the molecule and is determined by calculating the autocorrelation and the number of particles. Based on the detected fluorescence and the measurement volume the concentration of the solution can be calculated.

1.6 Fluorescence anisotropy (FA):

Fluorescence anisotropy, also known as fluorescence polarization, is a tool for studying molecular interactions and investigating physical and chemical molecular properties by monitoring an apparent size change in fluorescent or fluorescently-labeled molecules. The basic premise of FA is that when a small fluorescent molecule is excited with plane-polarized light, the

emitted light is depolarized due to rapid tumbling in solution during its fluorescence lifetime. However if a large molecule binds the small molecule, the rotation of the small molecule is slowed and the emitted light remains polarized (Perrin, 1926). FA measurements provide useful information about flexibility of molecules. High anisotropy value means that the probe or the fluorophore does not change its molecular configuration and orientation while at the excited state.

The polarization of the small molecule (or ligand) can be obtained by titrating in the large receptive molecule. The measured anisotropy value is a weighted average of the bound and free states thereby providing a direct measurement of the fraction of bound ligand. FA is a technique that has been used for a variety of receptor ligand binding studies, including DNA-protein interactions (Kleigman et al., 2006) and RNA-RNA interactions (Schlax et al., 2001). Here , in this dissertation I describe the FA binding observations , PEG- fluorescene, PVA-fluorescene, PEG-R6G and PVA-R6G to get a further insight into the thermodynamics that lie at the foundation of the buildup of molecular networks and produce evolutionary outcomes.

There are two methods of measuring the lifetime, so measuring the rotational correlation time has two ways as well: frequency domain and time domain. In this dissertation, I have used an ISS K2 spectrometer, which is built on frequency domain method.

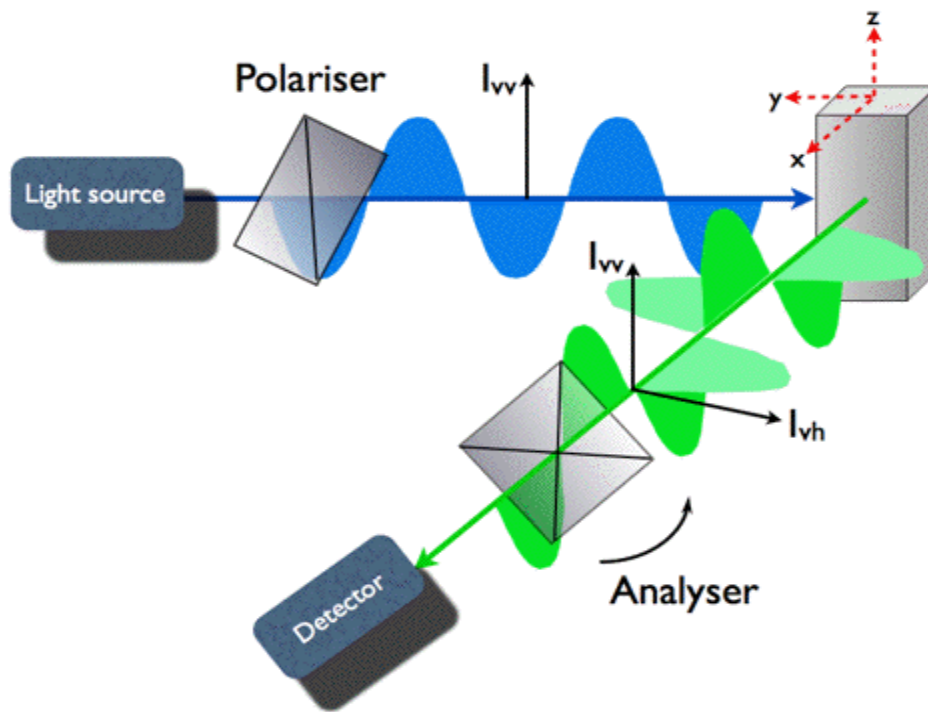


Figure 1.6. Geometry of fluorescence anisotropy experiment[34].

1.6 Selection of a Fluorescent Label:

Many conditions that must be satisfied and answered when choosing the fluorophore as a fluorescent label. The fluorophore probe must possess high molar extinction coefficient and a good fluorescence quantum yield, so that high levels of emission can be achieved at low concentrations. The emission should be well shifted so that Raman peaks from the medium and Rayleigh scattering intensity-which can be severe for polymeric systems-will not interfere with the fluorescence signal of interest. This dissertation has been conducted using Rhodamine 6G (R6g), Fluorescein and Alexa 488. Alexa 488 (average molwt 643.4) with ex/em is 494/517 nm. While fluorescein (average molwt 332.31) and R6g (average molwt 479.01) are comparable in

molecular weight however their respective excitation and emission wavelengths are different(ex/em 490/514 nm and ex/em 528/551nm) . Alexa 488 is ThermoFisher scientific made while Rhodamine 6G (R6g) and Fluorescein are acquired from Sigma-Aldrich.

For all experiments, it is essential that the presence of the probe does not cause disruption of the system and create local perturbations of the structure, so that conclusions and results obtained by the chromophore would not correctly reflect the properties of the polymer structures themselves.

1.7 Structure of the dissertation

The dissertation is structured as follows:

- **Chapter 1:** provides an overview on the main theme of my studies and the main techniques that I have used.
- **Chapter 2:** describes fluorescence correlation spectroscopy (FCS) method, the underlying theoretical principles of the technique, the data collected on Alexa488 and fluorescein fluorophores mixed in PVA and PEG solutions, the data analysis based on de Gennes model, and a brief summary of the conclusions.
- **Chapter 3:** describes fluorescence anisotropy (FA) method, the underlying theoretical principles of the technique, the data collected on Alexa488 and fluorescein fluorophores mixed in PVA and PEG solutions, the data analysis based on de Gennes model, and a brief summary of the conclusions.
- **Chapter 4:** discusses the results from Chapter 2 and Chapter 3 in a consistent way and in an attempt to extract possible similarities between the rotation and the translation of the nanoprobe, with an attempt to understand the local polymeric environment. Further, we

contrast the results obtained from the linear polymers (PVA and PEG) with those derived from the branched polymer, Ficoll.

CHAPTER II: TRANSLATIONAL DIFFUSION & FLUORESCENCE CORRELATION SPECTROSCOPY MEASUREMENTS

2.1. Introduction

Fluorescence Correlation Spectroscopy (FCS) uses temporal fluctuations of fluorescence emanating from a small illuminated volume ($\sim 10^{-15}$ liter) [42]. Typically, the temporal fluctuations are associated with either intramolecular dynamics of fluorescent probes or motion of fluorescent probes moving in and out the illuminated volume. Analysis of the temporal fluctuations is performed by generating first either the temporal intensity-intensity correlation or the photocount histogram of the measured intensities. Then, the arduous task is commonly the interpretation of the correlation function or the photocount histogram through the development of a consistent physics model (e.g. translation diffusion, chemical reaction, intermolecular transition, aggregation) and the derived expressions for fitting the data (correlation or photocount histogram).

In practice FCS is mostly used to measure the translational diffusion coefficients of fluorescent particles (e.g. proteins, polymers, DNA), and study interactions and rates of chemical reactions in biological systems, including cells [43-45]. Recent and ongoing development of fluorescent probes and fluorescent proteins enabled FCS measurements on live-cells where it is now possible to measure cellular concentration of proteins, to assess aggregation or polymerization of proteins, and to determine diffusion and mobility of proteins in the crowded cellular environment. Here, FCS depends on spontaneous fluorescence intensity fluctuations of self-fluorescent or fluorescence labeled molecules in solution and at thermodynamic equilibrium to obtain information about the concentration, reaction and translational diffusion properties of molecules in the system [46-49]. Also, the vast majority of the substances in nature do not

fluoresce meaning low background relative to the signal from the fluorescent dye in FCS experiments, while maintaining the advantages of noninvasiveness and kinetic measurements at equilibrium.

Other applications include the study of systems outside of chemical equilibrium [50] and the conformational dynamics of bio-molecules which may consist of changes in the structural properties of the molecule but not in its chemical identity [80], the rotational behavior of molecules [81], and the changes of mechanical properties of gels [67].

Key to FCS measurements is the fluorescence emission of the target molecules, which results from illuminated and focused laser of the medium sample at wavelengths sufficient enough to excite the molecules within the system to their first excited state. The excited molecules undergo various competing processes of de-excitation such as non-radiative internal conversion, non-radiative inter-system crossing, and fluorescence [51]. Internal conversion is the process where energy at excited state is converted to vibrational energy and subsequently dissipated during collisions with the solvent. Inter-system crossing, however, is a spin forbidden transition between electronic states [52,53]. Both process are non-radiative and therefore should be minimized enough in an FCS experiment to ensure that the target molecules are as fluorescently bright as possible. This point is important since the signal to noise ratio in an FCS experiment was shown by Koppel to strongly depend on the rate of photon emission per molecule per dwell time [54]. Subsequent to Koppel's work it has been proven by Qian and Kask that the signal to noise ratio further depends on concentration, the details of the observation volume, and the shot-noise in the system [55,56].

Overall, FCS is not a single-molecule method. Rather, it is a statistical method since it depends on the intensity fluctuations from fluorescent molecules, and thus requires appropriate

statistical analysis methods. The shape of the generated auto- or cross-correlation functions of the system contains information and details relating to the characteristic time scales of the processes contributing to fluorescence fluctuations. The functions also show clues about the size of the contributions of those processes to the correlation function.

In my work and this chapter of my dissertation, I have focused on collecting and analyzing temporal fluorescence fluctuations of small nanoprobe, Alexa488 and fluorescein, dispersed in polyethylene glycol (PEG) solutions prepared at different concentrations. My main objective has been to determine changes of the apparent diffusion coefficients of the nanoprobe as a function of the PEG concentration. Along the way I have had to address several questions related to the effects of PEG on the fluorescence properties of the nanoprobe, the interpretation and modeling of the underlying mechanisms of the fluctuations, and the modeling of the effects of polymeric structures on the diffusion of the nanoprobe. The fluorescence spectra and lifetimes were collected with a K2 spectrometer manufactured by ISS company, which will be briefly described in this chapter. The FCS data were collected with an ALBA/FLIM instrument by ISS, which will also be described in this chapter.

2.2 Mathematical background

Consider a model solution of fluorescent nanoparticles with concentration C of n nanoparticles in a volume V . Due to thermal fluctuations, n can be expressed at any given time in terms of concentration $C(\mathbf{r}, t)$ in 3-D space variable, \mathbf{r} , and time, t . The number of fluorescent molecules is then given by:

$$n(t) = \int_V C(\mathbf{r}, t) d\mathbf{r}^3, \quad (2.1)$$

where the integral is extended over V . Thermal fluctuations drive and induce the translational diffusion, moving the molecules in and out of the volume V while the system is in thermal equilibrium. We consider also random translational diffusion as the main mechanism that causes changes in both space and time of the concentration of the molecules within the solution.

The spatio-temporal distribution of the concentration is governed by the diffusion equation. The equation can be expressed as:

$$\frac{\partial \delta c(r,t)}{\partial t} = D \nabla^2 \delta c(r,t), \quad (2.2)$$

where D is the translational diffusion coefficient of the particles and; $\delta c(r,t) = C(r,t) - \langle C(r,t) \rangle$ denotes the local concentration fluctuations around the average concentration $\langle C(r,t) \rangle$, where the $\langle \dots \rangle$ indicates the space and time average of the concentration in the solution.

If a laser beam is directed and focused onto a sample of the solution, it will excite the fluorescent particles that are exposed in the path of the beam. Using a detector and associated electronics to turn the detector signal into photocount pulses, we measure the emitted fluorescence intensity, $I(t)$, emerging from an excitation volume, V , over the experimental time (Δt). $I(t)$ is related to concentration $c(r,t)$ of molecules in V as

$$I(t) = g \varepsilon Q \int c(\vec{r}, t) W(\vec{r}) d \vec{r}, \quad (2.3)$$

where g is an empirical factor that accounts for quantum efficiency and gain of the electronics (e.g. detection efficiency, current amplifier); ε is the optical extinction coefficient of the sample; Q is the fluorescent quantum yield of the fluorescent particles; $W(\vec{r})$ describes the 3-dimensional intensity profile of the incident beam. In practice, we focus on the intensity fluctuation, δI , over time, which is given by

$$\delta I(t) = I - \langle I \rangle = g\varepsilon Q \int d^3\vec{r} W(\vec{r}) \delta c(\vec{r}, t) \quad (2.4)$$

where $\langle \dots \rangle$ is the average intensity measured over the time period, Δt .

In FCS, the incident/detection function (MDF) is often considered to be a three-dimensional Gaussian as:

$$W(\vec{r}) = W(x, y, z) = A e^{(-2(x^2+y^2)/\omega^2)} e^{-2(z^2/\sigma^2)}, \quad (2.5)$$

where (x, y, z) are Cartesian coordinates centered at the intersection of focal plane (x, y) and the optical axis along the z direction.. ω is related to the beam waist, a characteristic width of the beam at which the intensity decreases to e^{-2} of its maximum intensity along the (x, y) plane at the center of the beam and σ is the beam elongation and width of the intensity along the z -direction (see Figure 2.1).

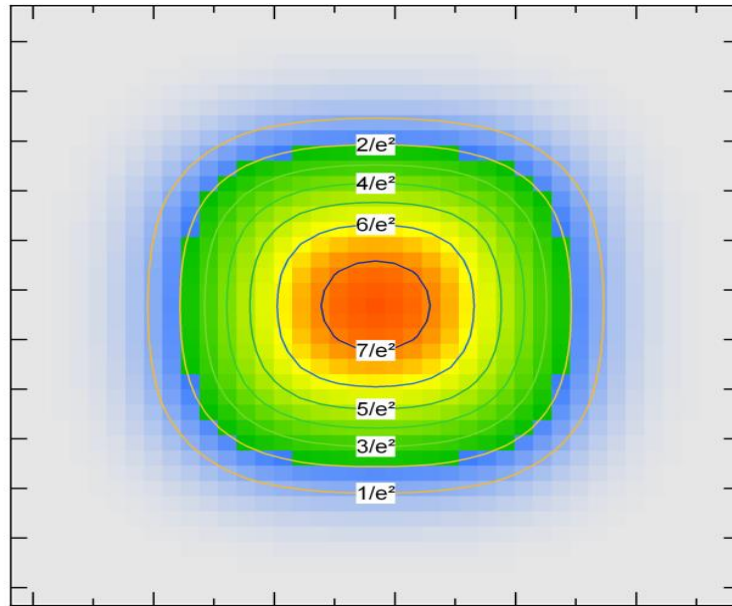


Figure 2.1: Contour plot for square detection profile of Gaussian beam where the first circle at which along the (x, y) plane intensity decreases to e^{-2}

Note that the z-direction is aligned along the optical axis of the incident beam (usually $\sigma > \omega$).

The detected volume, V , can be then defined as $V \sim \omega^2 \sigma$.

The time-correlation function, $F(\tau)$, has been introduced for signal processing which is the time average of the product of intensity fluctuations and normalized by the square of the average intensity:

$$F(\tau) = \frac{\langle \delta I(0) \delta I(\tau) \rangle}{\langle I \rangle^2} \quad (2.7)$$

where $\langle \dots \rangle$ denotes the time average correlation over the measured time, Δt . The delay time, τ , refers to delayed time from a given time measurement t to $t + \tau$. Since t is taken arbitrary, we set $t=0$. The time scale of the delay time, τ , should capture the main physical phenomenon of the fluctuations. Substituting Eq.2.4 into Eq.2.7 we get:

$$F(\tau) = \frac{(Q)^2 (\Delta t)^2}{\langle I \rangle^2} \int \int d^3 r d^3 r' W(\vec{r}) W(\vec{r}') \langle \delta c(\vec{r}, 0) \delta c(\vec{r}', \tau) \rangle, \quad (2.8)$$

Equation 2.8 indicates that the main unknown is the concentration fluctuations, which is, in principle, derived from the solution of the differential equation, Eq.2.2, under the appropriate boundary conditions. Aragon et al. [57] provided the first rigorous derivation of the integral of Eq.2.8 which they expressed as:

$$F(\tau) = \frac{1}{N} \left(1 + \frac{4D\tau}{\omega^2} \right)^{-1} \left(1 + \frac{4D\tau}{\sigma^2} \right)^{-1/2}, \quad (2.9)$$

or;

$$F(\tau) = \frac{1}{N} \left(1 + \frac{\tau}{\tau_D} \right)^{-1} \left(1 + \left(\frac{\omega}{\sigma} \right)^2 \frac{\tau}{\tau_D} \right)^{-1/2}, \quad (2.10)$$

for 3-dimensional diffusion. In contrast, for 2-dimensional diffusion we have:

$$F(\tau) = \frac{1}{\bar{N}} \left(1 + \frac{\tau}{\tau_D} \right)^{-1}. \quad (2.11)$$

in both Eqs. 2.10 and 2.11 D denotes the diffusion coefficient of the nanoparticle in the solution, $\bar{N} = \bar{C}V$ the average number of nanoparticles in the solution, $V = \pi^{3/2}\omega^2\sigma$ the effective sampling volume (~ femtoliters), and the apparent diffusion time along the x - y plane

$$\tau_D = \frac{\omega^2}{4D}. \quad (2.12)$$

At short time delays $\tau \rightarrow 0$ the amplitude of the correlation function is determined by the average number of fluorescent nanoparticles \bar{N} in the sampling volume, hence: $F(\tau \rightarrow 0) = \frac{1}{\bar{N}}$. The lower the number, the higher the amplitude of the correlation function. Equation 2.9 shows that the correlation function depends basically on three parameters: \bar{N} attributed to the sample of interest, $\left(\frac{\omega}{\sigma}\right)^2$ associated with the experimental detection setup (not the sample), and τ_D the diffusion time of the fluorescent nanoparticle along x - y plane (sample and setup). The 3-D geometry for the observed volume implies that the highest probability for detecting fluorescence is at the origin, and $\omega < \sigma$ and thus the probability of detection decays with the same distance from the origin faster in the radial direction than the axial direction.

2.3. Materials and Sample Preparations

2.3.1. PEG, PVA and Fluorescent Nanoprobes

Poly (ethylene glycol) (PEG) is water-soluble, linear polymer commercialized by Fluka Analytical, a registered trademark owned by Sigma-Aldrich Company. Although we have acquired PEG powders in different molecular weights, we present in this dissertation the results from samples prepared with PEG of MW=10000 g/mol. We prepared solutions concentrations from 100 mg/ml to 1200 mg/ml, limited only by the dissolution of the powder in Millipore-purified water.

Poly (vinyl alcohol) (PVA) is a hydrophilic linear polymer with high molecular weight of average 85 000 g/mol. It was acquired from Sigma-Aldrich. The choice of this high molecular weight is useful in preparing gel.

Concentrations of 10, 20, 50, 100, 120 mg/ml were prepared (50 mg/ml to 120 mg/ml in the case of substantially dilute cross-linked or hard gel depending on length of times the experiments were performed)

Fluorescein average MW=332.31g/mole. The excitation maximum is 490 nm and the emission maximum is 514 nm. It was acquired from Sigma-Aldrich.

Alexa 488, average MW= 643.4 g/mole. The excitation maximum of Alexa is 494nm. and the emission maximum is 517nm. It was acquired from ThermoFisher scientific.



**Figure 2.2: A; Fluka Analytical ref: 81280-1KG Poly(ethylene glycol) bottle
B: PEG solid and pure powder, C: PEG+H₂O vortexed for 01 hrs, D: at t=6hrs, E:
at t=24hrs**

2.3.2 Lab work and preparation

Sample preparation and handling were very important factors in determining the reproducibility of FCS data obtained from experiments conducted at different times. In this work I have analyzed not only my data but also those generated by other students (Ms. Ines Lattiri and Mr. Shawn Clark) who redid the experiments by preparing different PEG solutions. As shown below

in Figure 2.2, PEG powder was mixed with Millipore purified water to prepare PEG solutions at different concentrations. The powder and water mixture was vortexed and shaken for an hour, and left overnight for full dissolution of the powder in water at room temperature. All along we monitored the transparency of the mixture as a measure of dissolution.

Similar steps were also taken to prepare poly (vinyl) alcohol solutions for concentrations starting from 10 mg/ml to 120 mg/ml. However, one should point out that PVA solutions are known to crosslink through hydrogen bonds overtime to form a gel. This needs to be contrasted to PVA gels prepared with poly-functional crosslinking agents that form linkages between portions of adjacent polymer chains. Example is glutaraldehyde, a bifunctional aldehyde that reacts with hydroxyl groups on PVA [58], N-hydroxysuccinimide (NHS) esters form ester linkages through reaction with hydroxyls, though the ester bonds formed can be subject to hydrolysis in aqueous solution [59]. Boric acid and Congo red have also been used as chemical crosslinkers [79]. Radiation is another method, where electron beam, ultra-violet light or gamma irradiation are used to create chemical linkages [60]

Physical crosslinking network have been similarly developed. Particular benefits to the formation of a network via physical crosslinks, as opposed to chemical, is the absence of toxic materials that could potentially leach from the gel [61]. As a result of this technique, the formation of crystallites provides crosslinks for the formation of a three dimensional network. One common example of physical crosslinking subjects a PVA solution to successive freeze-thaw cycles. Relatively dilute solutions of PVA can form into elastic constructs, using this technique. Crystallization in PVA hydrogels plays a large role in network formation for physical crosslinking [62].

In my work, PVA was dissolved in deionized water until it was completely solubilized by employing a combination of heat and magnetic stirring to achieve uniform distribution (See figure 2.3). An example of processing steps in PVA gel preparation includes weighing 4 g of PVA which was mixed in 40mL of deionized H₂O in a beaker then adding 30mL of ethanol to make the basic PVA solution. The mixture was placed on the hot/stir plate (around 100 C). After stirring and heating for 6 hours, PVA powder weight measurements were taken and recorded according to the desired final concentrations (50 mg/ml, 100 mg/ml and 120 mg/ml) then slowly poured to the mixture.

Fluophore probes were embedded and well mixed at the very beginning of the experiment, different stages of gelation processes from highly viscous gel state (after heating and stirring for 5-7 days) to completely solid gel state (after heating and stirring for 25 and longer) were noticed and FCS as shown in figure 2.5.



**Figure 2.3: A: Sigma Aldrich ref: 363146-1KG Poly(Vinyl alcohol) bottle
 B: PVA in beaker on hot/stir plate (around 100 °C & 1150 rpm)**

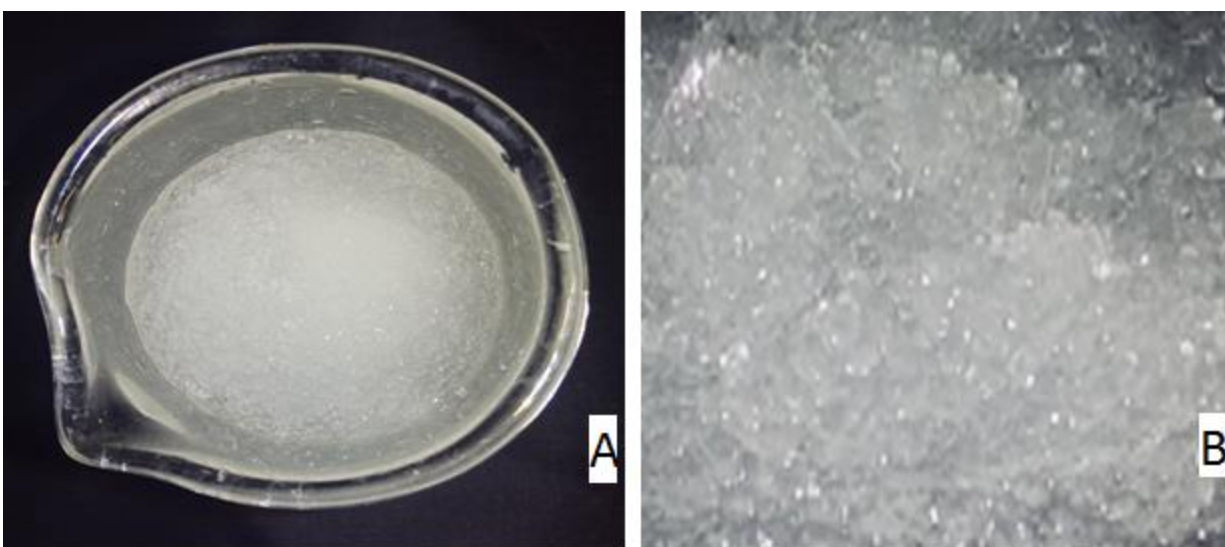


**Figure 2.4: A: dilute cross-linked and highly viscous PVA gel (5-7 days of heating and stirring).
 B: is a zoomed capture of A**

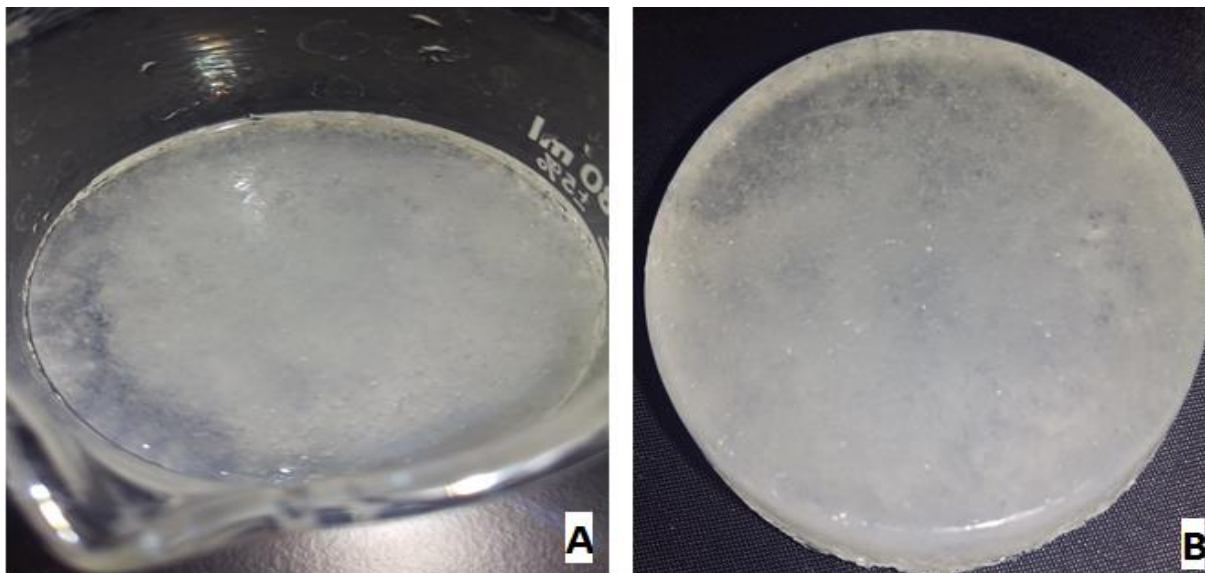


Figure 2.5: PVA gel in Solid form (30 days of heating and stirring) A: Solid PVA in Beaker B: PVA portion was cut to show the hard & holding form

2.3.3 Hybridization chamber

Secure Seal hybridization gasket chambers made by GRACE BIO-LAB have been used to load samples of the fluorophore-polymer solutions (See Figure 2.6). The fluorophore-polymer solutions were thoroughly mixed and then pipetted into each 50- μ l well. One side of the 4-well set (see Figure 2.6) was “glued” with a Corning coverslip (\sim 170 μ m thick) and this side was set on the microscope objective (NA=1.3 oil, 60X) for FCS measurements as shown in Figure 2.6.

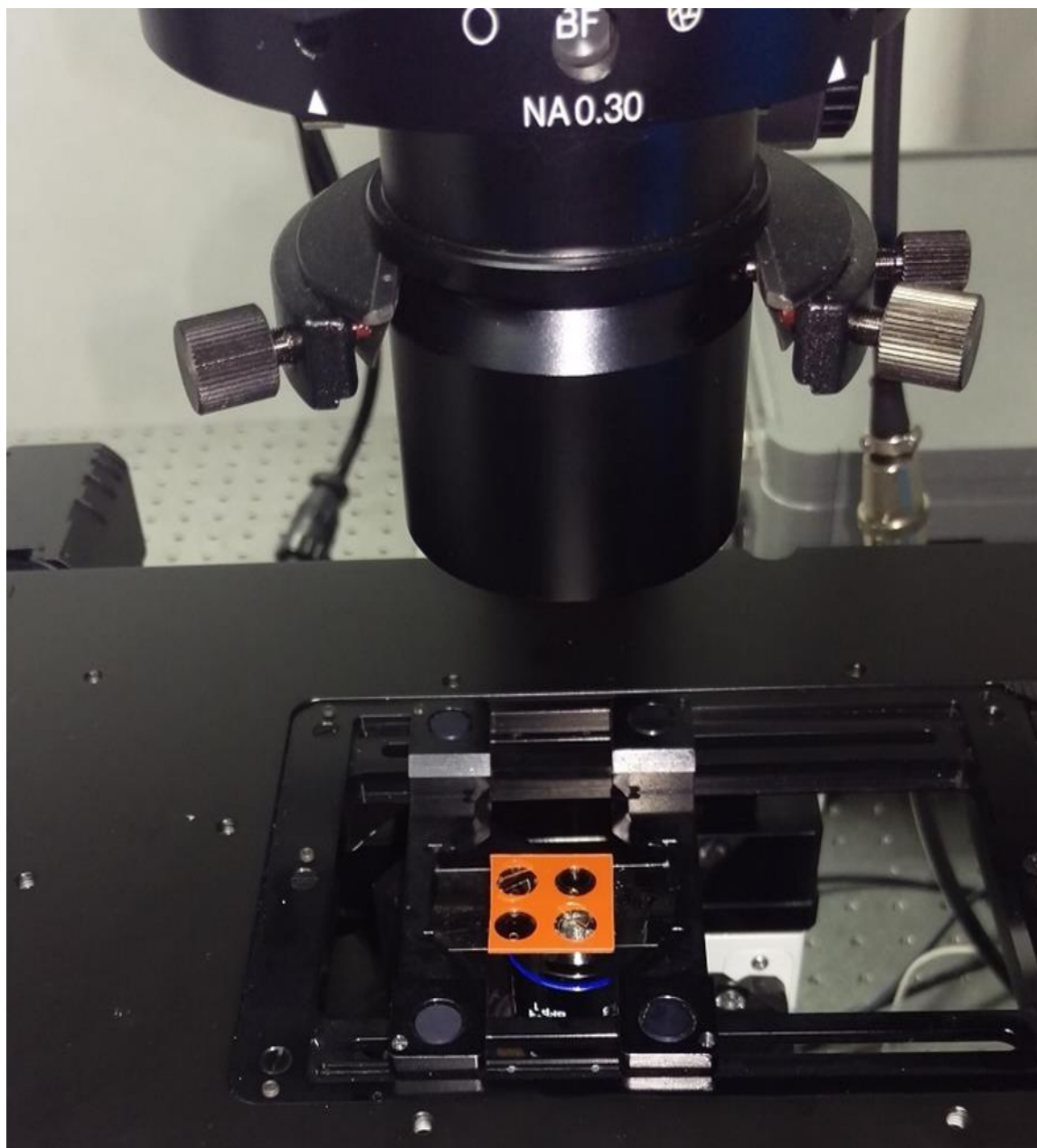


Figure 2.6: Four wells set of PEG samples in hybridization chamber, samples are air bubble-free and carefully sealed.FCS Instrument: Q2-FFS ALBA

2.3.4. Schematic of an FCS setup

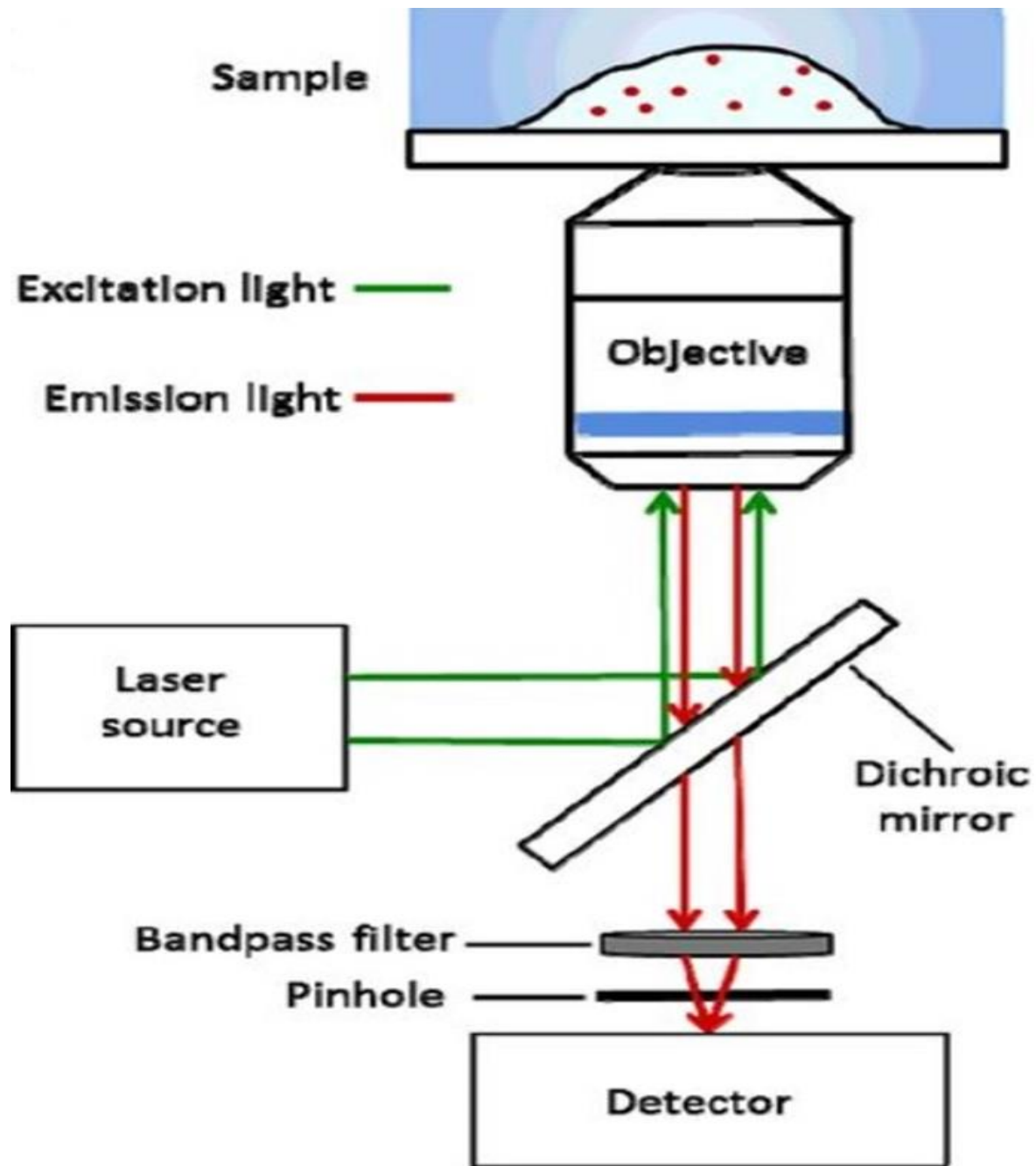


Figure 2.10[66]: FCS setup and schematic calibration

As shown in Figure 2.10, microwatts-order power laser beam is directed to the sample via a dichroic then focused onto the sample with a high numerical aperture objective. The beam excites the fluorescent probes and the emitted fluorescence is collected with the same objective, which is directed through the dichroic mirror and an optical filter to merely select the fluorescence then a micrometer pinhole ($\sim 50 \mu\text{m}$) is placed in confocal mode in front of the detector in order to restrict the collection of fluorescence to the confocal plane of the objective.

FCS measurements were performed using Q2-FFS system from ISS Inc., Champagne, Illinois

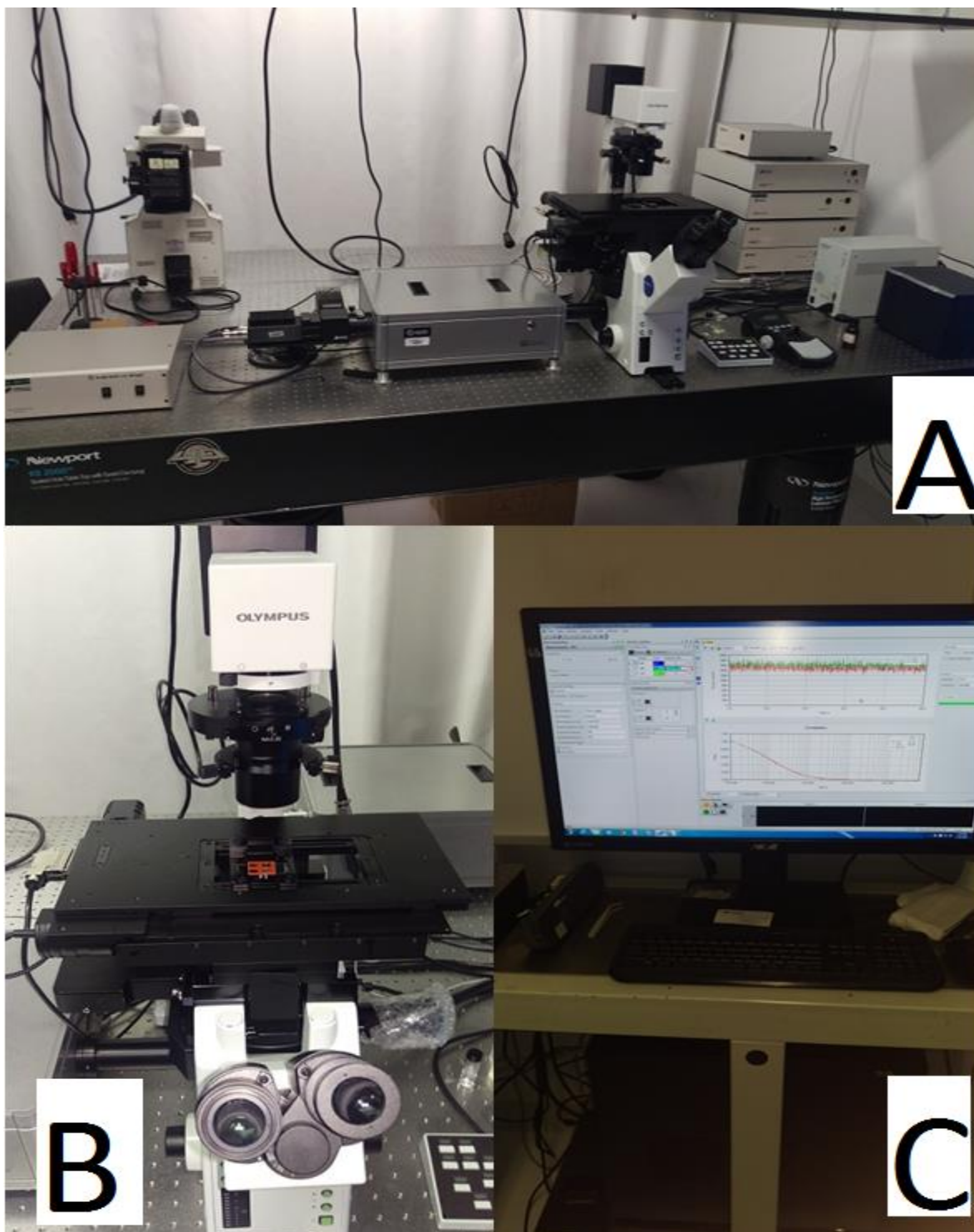
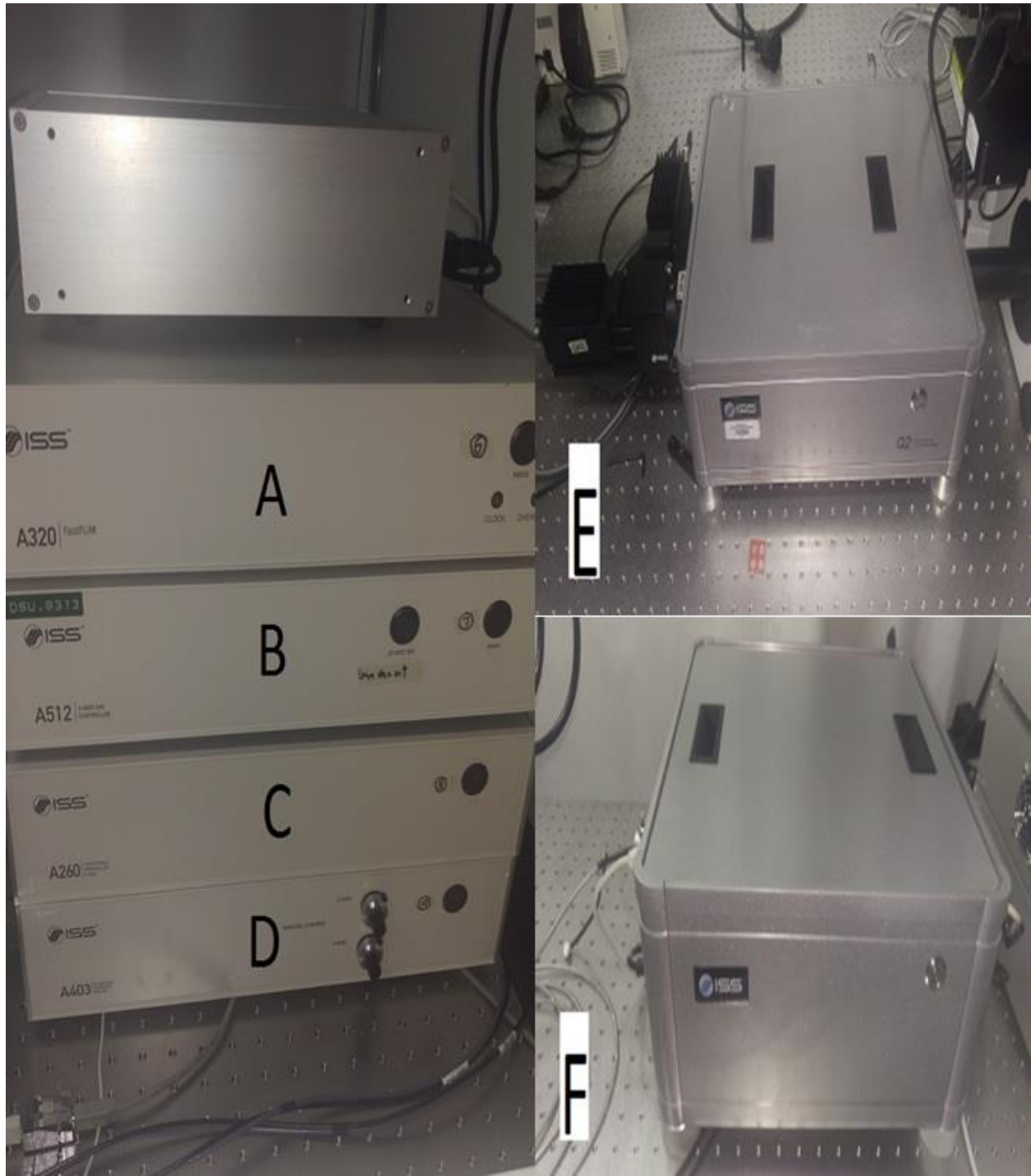


Figure 2.7: FCS Layout **A:** general overview of FCS units **B:** Olympus microscope **C:** 64-bit workstation with ISS VistaVision software



**Figure 2.8: FCS units; A: FastFLIM data acquisition unit B:3-axis controller unit
 C:Piezo Z controller unit D:Scanning mirrors driver unit E:Q2 system unit
 F:Laser launcher unit.**

2.3.5. FCS Instrument and Components:

For our FCS measurements we used ISS Alba/FLIM instrument that was acquired recently through a grant from DoD. The instrument is built around an IX81 inverted Olympus microscope which was equipped with a Prior stage (Figure 2.7) and diverse high NA microscope objectives (60X, NA:1.35 Oil; 40X, NA:0.95 Air) . The Alba/FLIM system is composed of:

1. Computer, 64-bit workstation operated by Windows 7 64-bit professional 27-in high-resolution (2560x1440) flat panel monitor
2. Software, ISS VistaVision software (Version 4.1.047, 64-bit)
3. Q2 system The Q2 scanning head equipped with the polarization module MiniTDU equipped with two H7421-40 detectors MiniTDU optical compartment accessories.
4. Laser module ISS 3-diode laser launcher ISS 445-nm and 488-nm laser diodes (CW or pulsed) Coherent Sapphire 50-mW 532-nm laser diode (CW) Single-mode polarization maintained fiber optics
5. Data acquisition unit ISS FastFLIM data acquisition unit (A320)
6. XYZ positioning control, Prior XY automated stage XY Galvo scanning mirrors (installed in Q2) and driver module (A403) Piezo Z device (installed on the microscope nosepiece) and controller module (A260) 3-axis DAC controller module (A512)

For our measurements we used the 485-nm, 1.2 mW power laser diode whose intensity was filtered to desired intensities using neutral density filters. The emitted fluorescence was collected back through the same objective and sent through to a dichroic mirror (525/50nm), that optically filtered more the emission signal and sends it to a 50/50 beam splitter for detection by the PMTs (Figure 2.9), which are typically activated in cross-correlation mode for either

correlating two different emissions or reducing the after pulsing effect at short delay times ($< 10 \mu\text{s}$).

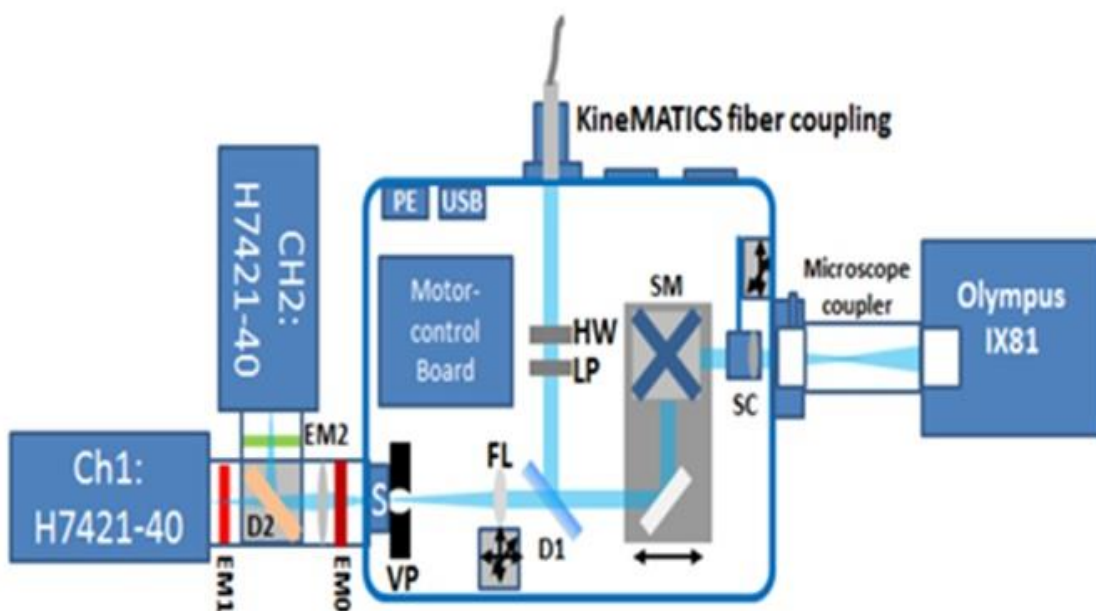


Figure 2.9: Q2 system overview

2.3.6. Q2 system Components

1. S - Motorized Shutter,
2. HW; LP - Polarization module – half wave plate (HW); linear polarizer (LP)
3. SM; SC - XY Galvo scanning mirrors (SM); scan lens
4. FL - Focusing lens, motorized in XYZ at the resolution of 1.6 μm per step
5. VP - Variable pinhole, motorized, tunable from $< 20 \mu\text{m}$ to 1 mm.
6. D1 - Main dichroic mirror to separate (reflect) excitation and (pass) emission light - Chroma ZT488/532rpc.
7. D2 - Second dichroic beam splitter mirror to separate emission light between Ch1 and Ch2 Polarization beam splitter dichroic; 50/50 beam splitter dichroic;
8. EM0 - Emission filter for both Ch1 and Ch2
9. EM1 - Emission filter for Ch1 only; EM2 – Emission filter for Ch2 only. Each filter (25 mm diameter) is mounted in a ring insert, which is then dropped into the slot.

In the detection 50 percent of the fluorescent intensity is sent to each PMT, however the photons detected by the PMT during the same acquisition time are not equal, and the detectors have different levels of accuracy. This makes it hard to calculate the uncertainty as noted in [63-65]. The error in τ_D measurement is best estimated by repeating the experiments and in our case calculated τ_D varied by less than 5%.

2.4.1. FCS Calibration:

Alexa 488 in water was used and excited by 488nm laser. At 500 kHz frequency, 10 million data points were collected for five iteration then Vista software is used to fit and calculate the cross correlation function. Figure 2.11 shows normalized correlation functions of Alexa488 mixed in water. The solid lines are fits of the data with the expression in Eq.(2.10). For a fixed $430 \mu\text{m}^2/\text{s}$ diffusion rate and 1 AU pinhole, the volume parameters are determined to be $\omega = 0.2 \mu\text{m}$ (lateral beam waist) and $\sigma = 1.67 \mu\text{m}$ (axial beam waist).

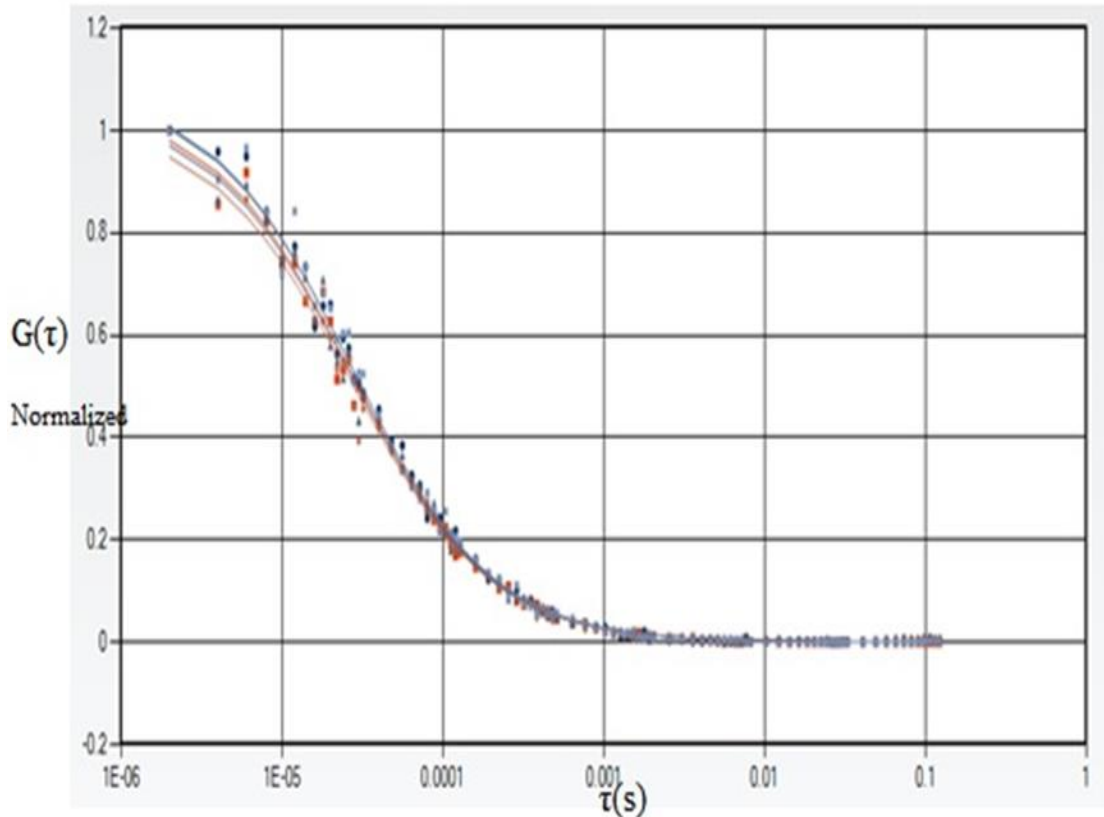


Figure 2.11: Normalized $G(\tau)$ Vs. time delay (τ) result in FCS calibration test. Cross-correlation fitting of 5 iterations using a 3-D Gaussian to recover the beam waist parameters.

The ratio $\omega/\sigma = 0.2/1.67 \approx 0.12$ was subsequently used to fit the correlation functions measured in PEG solutions and others. It is also important to adjust the vertical position (z-position) when moving the objective beneath the wells, most effective way to adjust this is by lowering the objective down from the sample bottom fused cover glass(at this point few counts (CPS) will be observed) then to sample focus which yields to very good counts and stable intensity value .

2.4.2. Laser Power Calibration:

FCS correlation functions are collected on a sample of Alexa488 dispersed in water excited with a 485 nm-laser with varying intensity. Each correlation was run over 30 second period.

Figures 2.12 to 2.14 show counts per second from channel 1 and channel 2. Signal detected by PMT detector 1 is displayed in channel 1 and signal from detector 2 is displayed in channel 2.

Cross correlation of both channel 1 and channel 2 produces is shown by channel 3(Ch1x2).

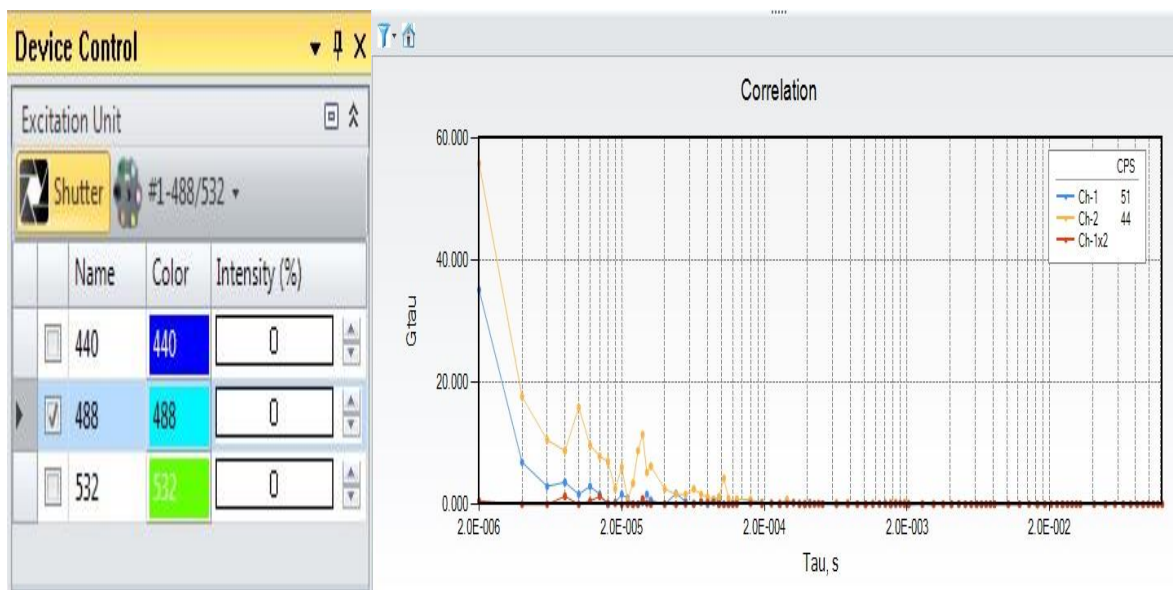


Figure 2.12: Correlation Plots at Background (laser power at 0%)

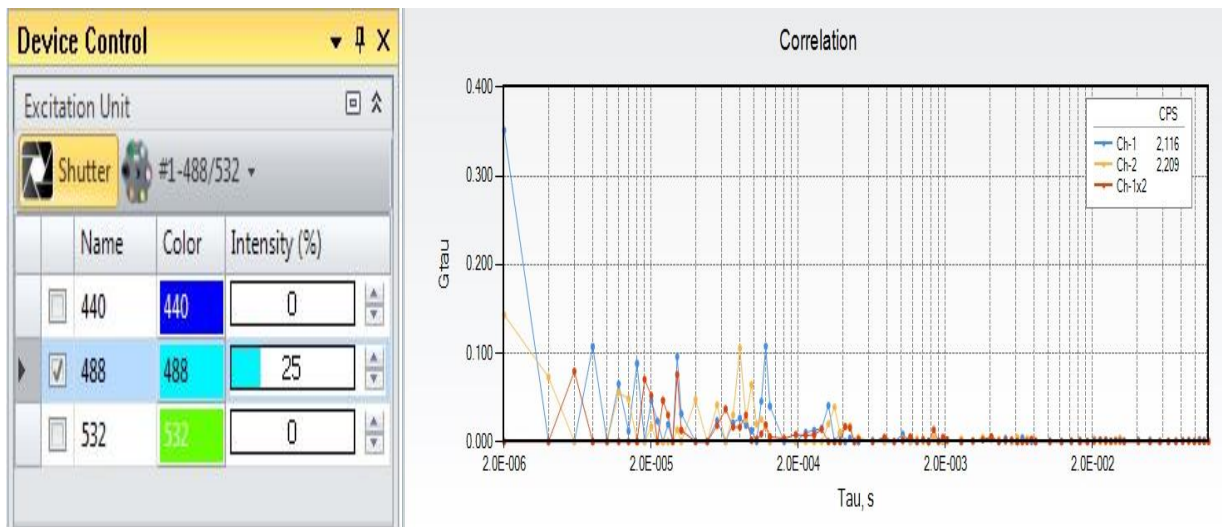


Figure 2.13: Correlation Plots at 0.3mW laser power (25%)

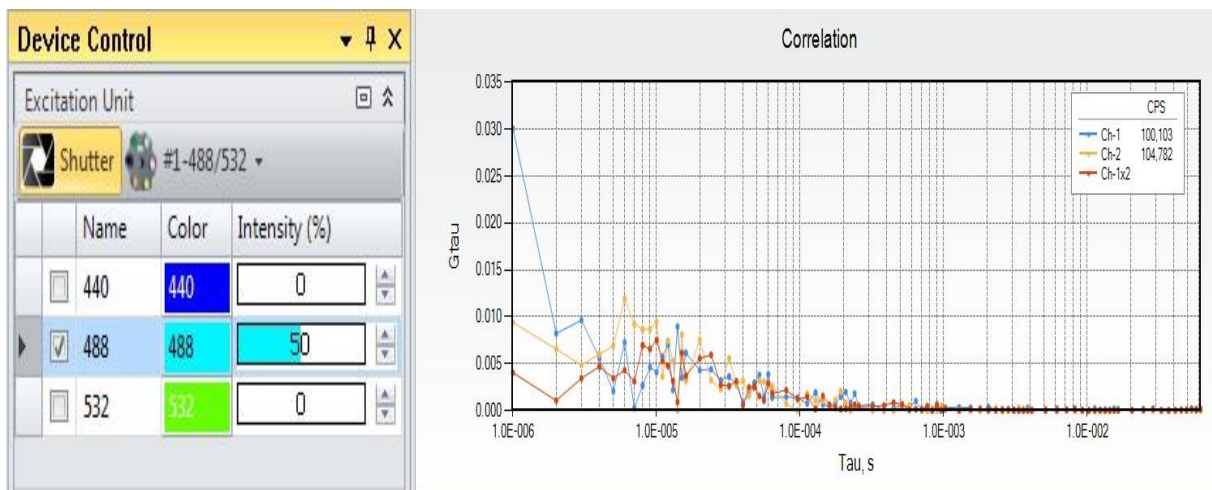


Figure 2.14: Correlation Plots at 0.6mW laser power (50%)

As the intensity was increased, the signal to noise of the correlation function improved (see Fig.2.14). The best results were obtained when the laser was between 50% and 60%; here we collected a well-defined correlation function of which we were able to extrapolate the data for delay times approaching zero. The amplitude was approaching the 0.01 value, independent of either 50% or 60% laser power, consistent with the theoretical expression in Equation 2.9.

However, we noticed that high laser powers would eventually induce photo-bleaching, meaning the destruction of the fluorophore.

2.4.3. Absence of fluorophore (background) Vs presence of fluorophore (Fluorescence Signal):

The contribution of the background to the overall fluorescence signal from the fluorophores was measured and assessed. We loaded samples of PVA (or PEG) solutions with or without fluorophores and loaded in the chambers. We collected correlation functions and photon counts for both samples. Then, the laser was turned on for both samples containing the same PVA solutions of the same concentration with (Figure 2.15) and without (2.16) fluorescein, which represents a 0.3 % of drop in intensity.

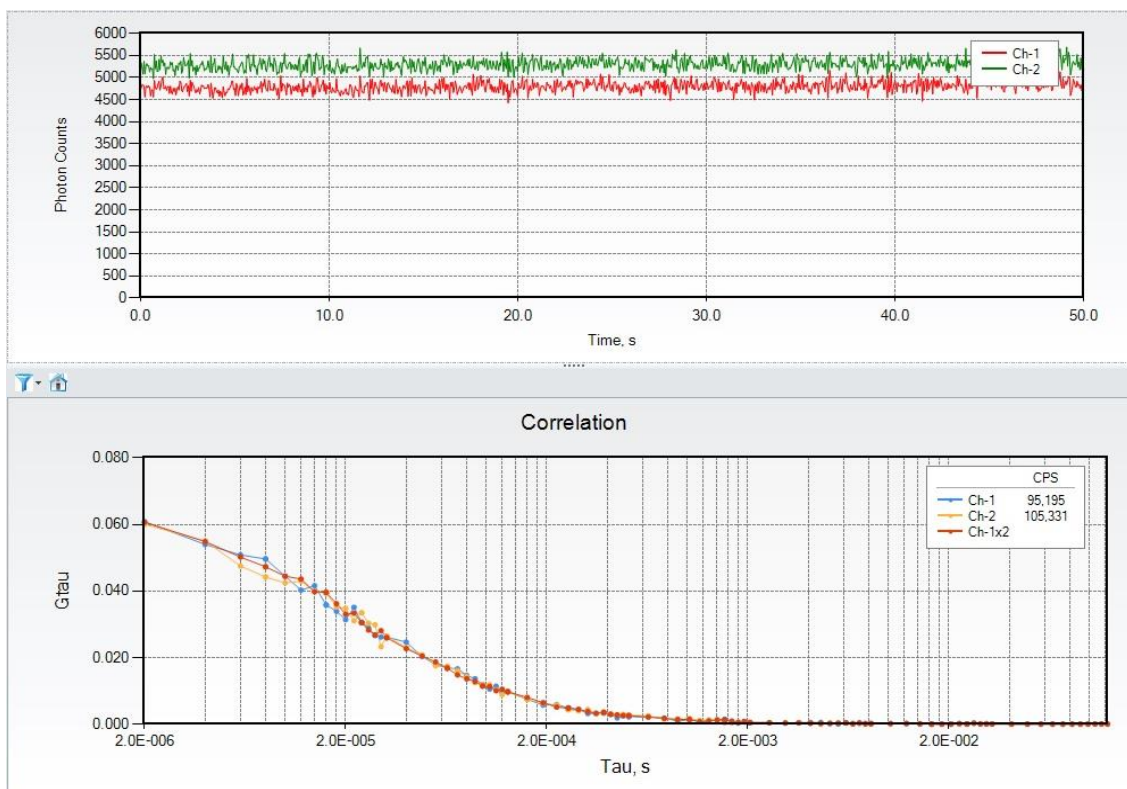


Figure 2.15: Correlation function of Fluorescein fluorophore in PVA (20mg/ml concentration) and its respective photon counts Vs time duration of the experiment

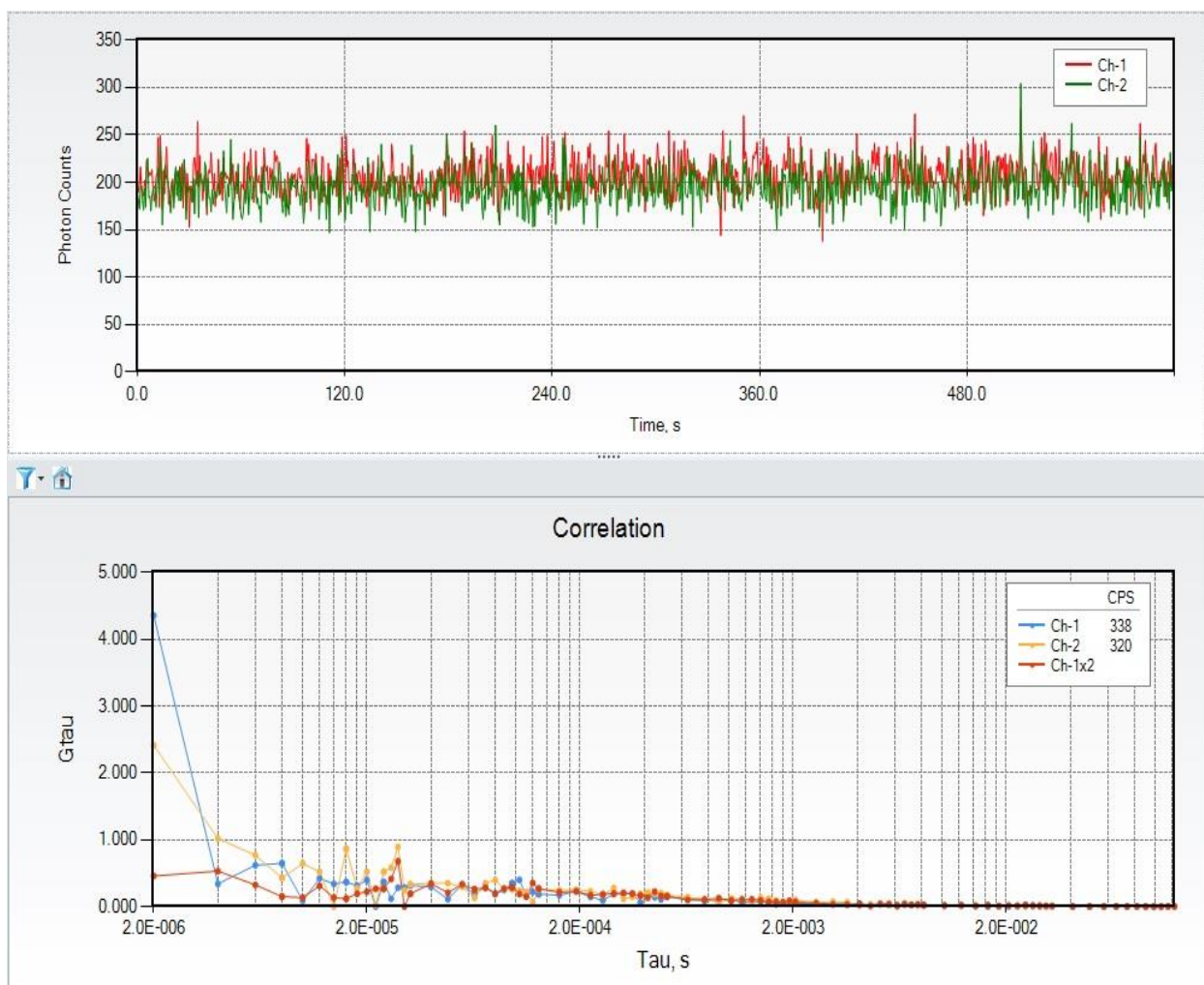


Figure 2.16: Correlation function of PVA (20mg/ml concentration) without Fluorescein fluorophore and its respective photon counts Vs time duration of the experiment

The presence of photon counts emanating from the polymers (no fluorescein) was mainly due to autofluorescence (endogenous sample constituents) or reagent background (unbound or nonspecifically bound probes) which justify low counts being (Ch-1=338 and Ch-320) in Figure 2.16 and therefore no correlation was present even at longer times. On the other side, a clear correlation function was displayed when fluorescein was present in the polymer solution -the

count rates were much higher on the channels (Ch-1=95195 and Ch2= 105331) in Figure 2.15, and a clear correlation function emerged, which could be now readily associated with the presence of fluorescein, not any possible auto-fluorescence for the polymeric solutions.

2.4.4. Effect of PEG solutions on the fluorescence of Alexa488 and Fluorescein

Before investigating the molecular mobility and dynamics of fluorescent nanoprobe dispersed in the PVA or PEG polymeric solutions we first measured the effect of the polymers on the fluorescence properties of the nanoprobe.

In Figures 2.17-2.20 show changes of the fluorescence spectra of Alexa488 and Fluorescein as a function of the concentration of PVA or PEG. Despite small shifts of the peak to longer wavelengths we see no significant changes in the overall profiles of the emitted fluorescence spectra. Similarly, Figure 2.21 and Figure 2.22 indicate little effect of the polymers on the fluorescence lifetime of the fluorophores. Both these results set the stage then for the interpretation of measured FCS correlation functions and the fluorescence anisotropy data. That is, the molecular structure of each fluorescent nanoprobe was not affected by the polymers, and as such the fluorescence fluctuations in FCS and changes of the fluorescence anisotropy could be associated with translational motion of the nanoprobe and slowing down of the rotation, respectively.

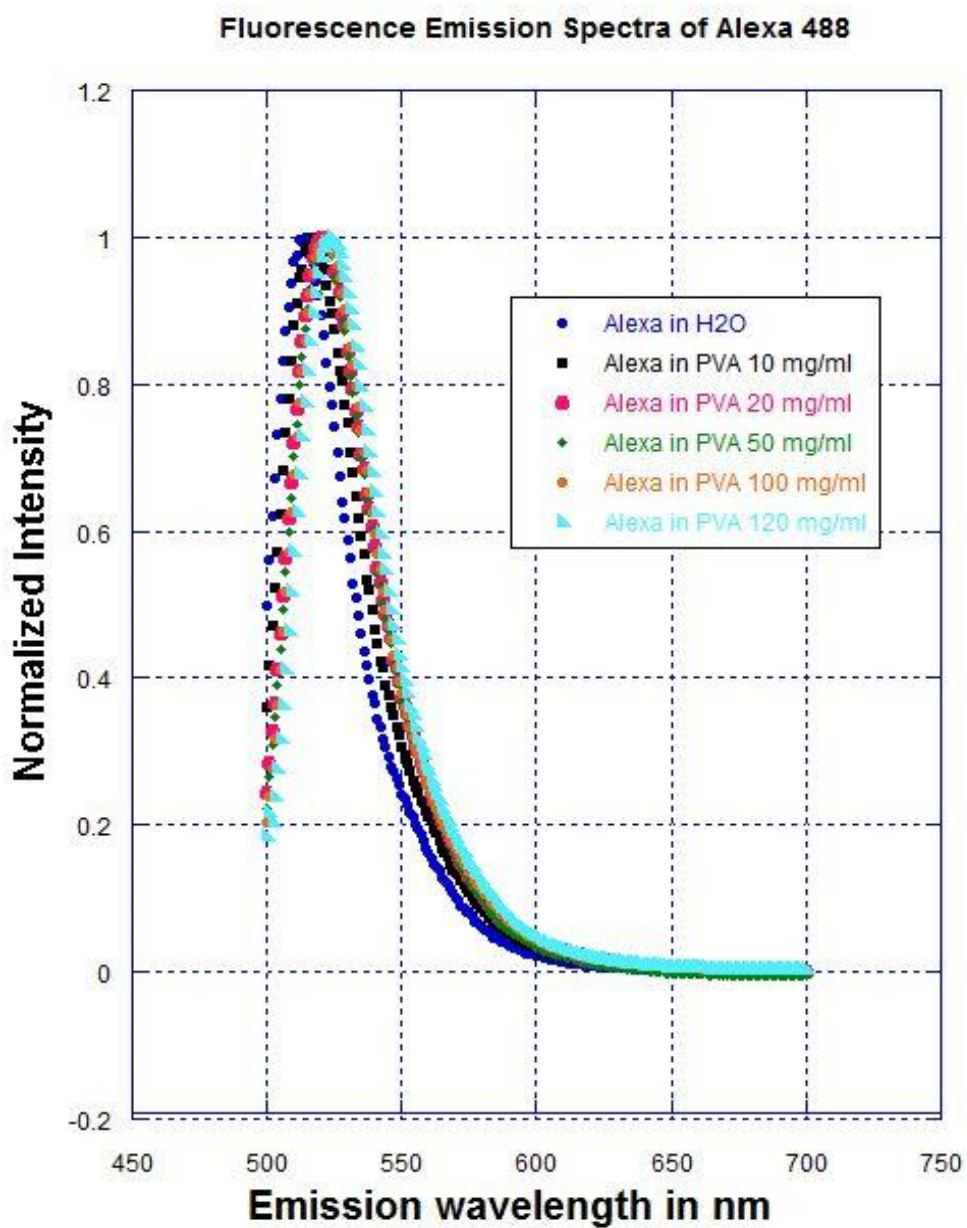


Figure 2.17: Fluorescence spectra of Alexa 488 in different PVA concentrations

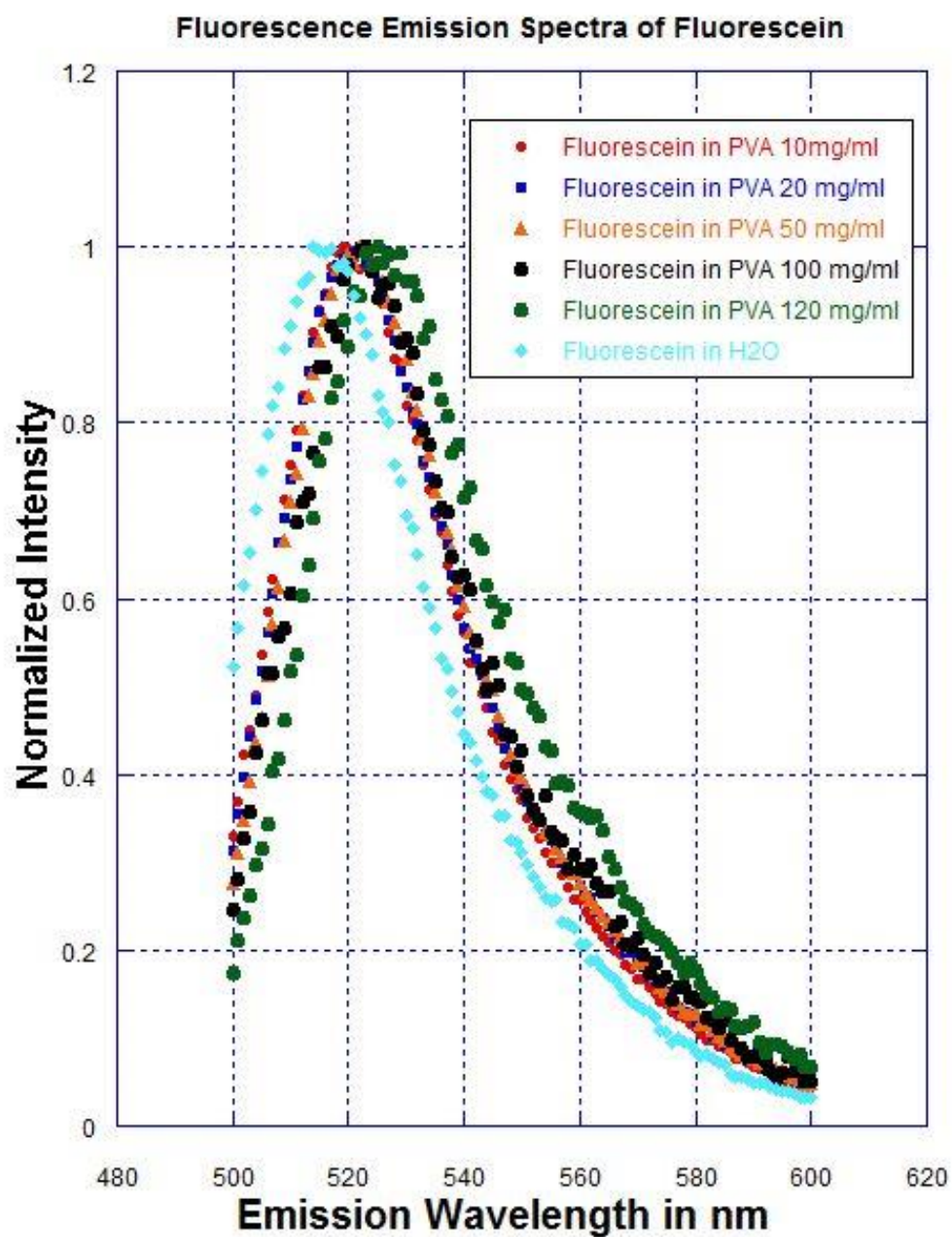


Figure 2.18: Fluorescence spectra of Fluorescein in different PVA concentrations

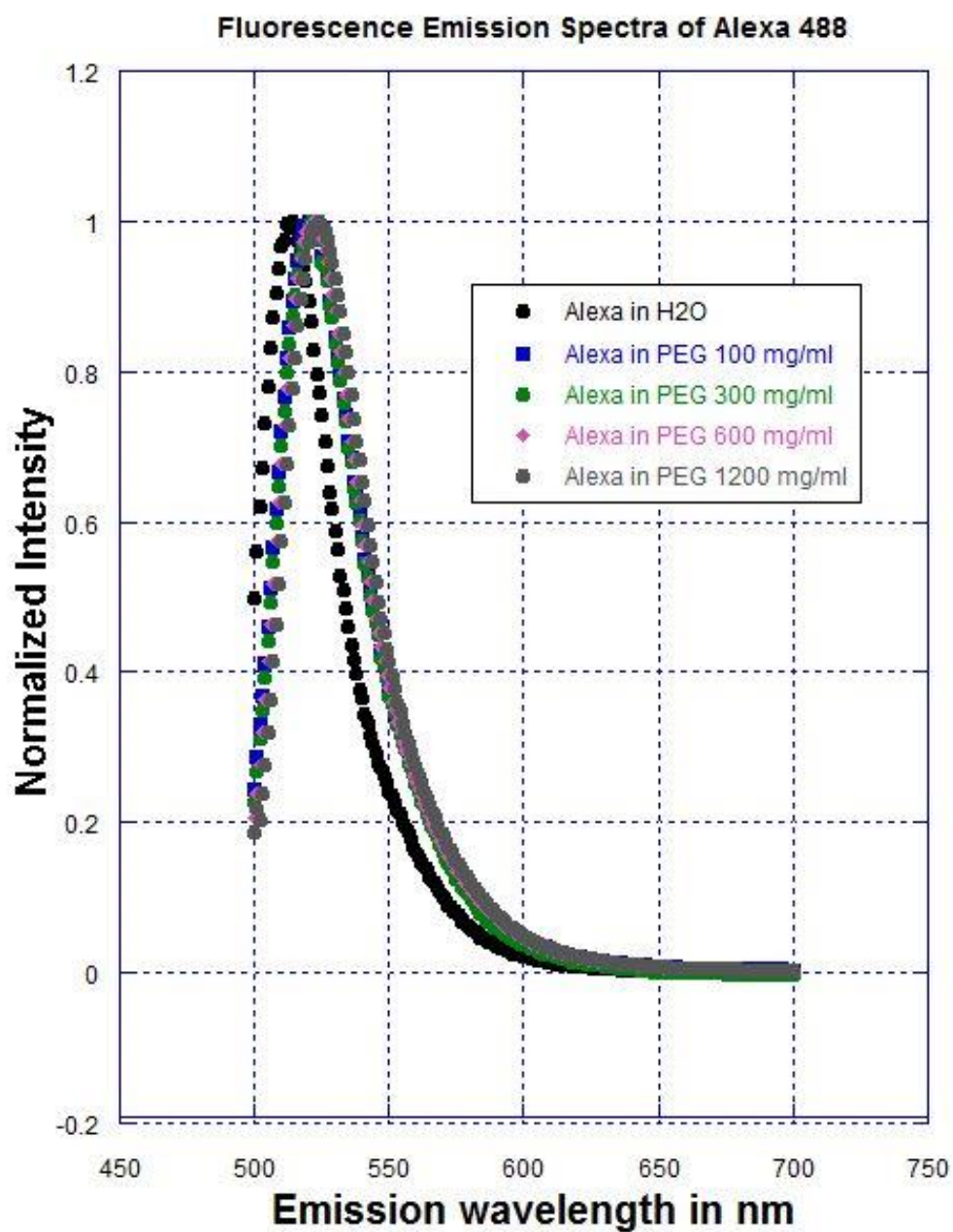


Figure 2.19: Fluorescence spectra of Alexa 488 in different PEG concentrations

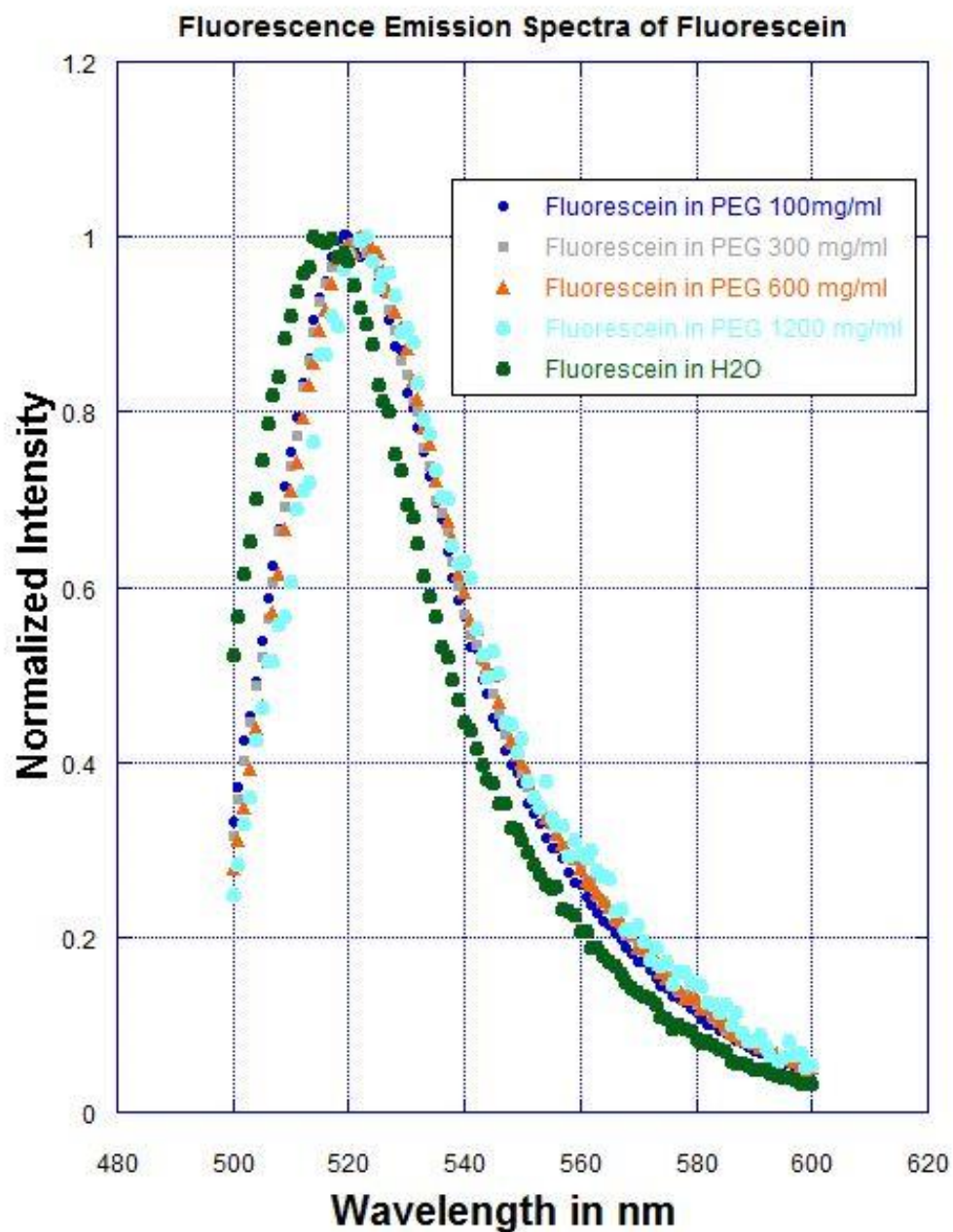


Figure 2.20: Fluorescence spectra of Fluorescein in different PEG concentrations

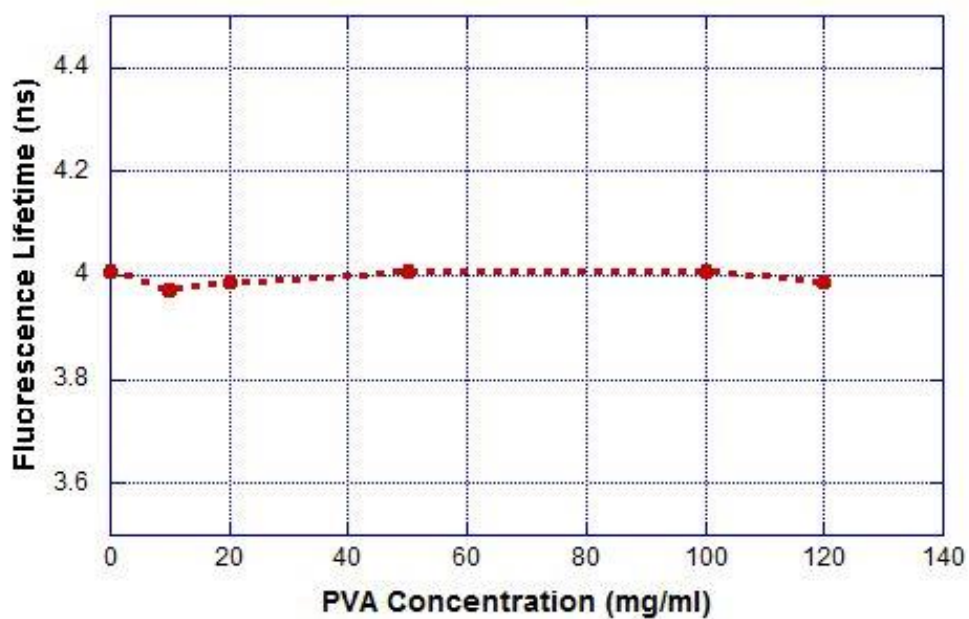


Figure 2.21: Fluorescence lifetime of Alexa488 in different PVA concentrations

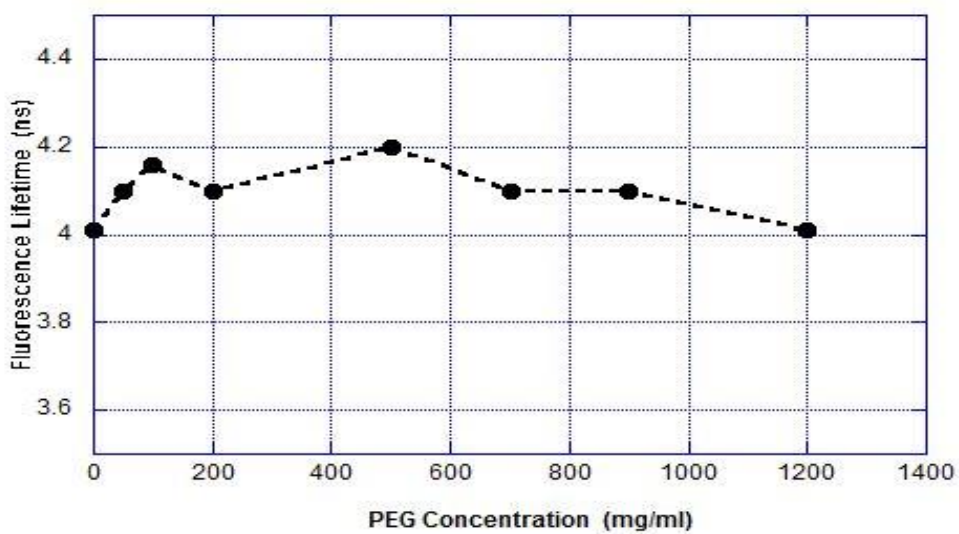


Figure 2.22: Fluorescence lifetime of Alexa488 in different PEG concentrations

2.5. Results and Discussion

2.5.1. Analysis of Correlation functions:

Assuming the confocal volume, which is defined by our optical setup of FCS remains the same then, $\left(\frac{\omega}{\sigma}\right)^2$ is kept constant at the same value obtained from Alexa488 diffusing in water. Below (Figures 2.23 to Figures 2.28) show plots of measured FCS functions of Alexa488 in PEG and Fluorescein in PVA as a function of delay time τ . Then, with respect to their respective amplitudes at $\tau \rightarrow 0$, the functions were normalized and studied. These collected normalized correlations at different PEG and PVA concentrations show a systematic shift to longer times with increase of both polymers concentration, a 17 fold shift in PEG from 100mg/ml to 1200 mg/ml and 40 fold shift in PVA from 10mg/ml to 120 mg/ml. We fit the measured correlations with the expression in Equation 2.10 where N and τ_d are the two fitting parameters.

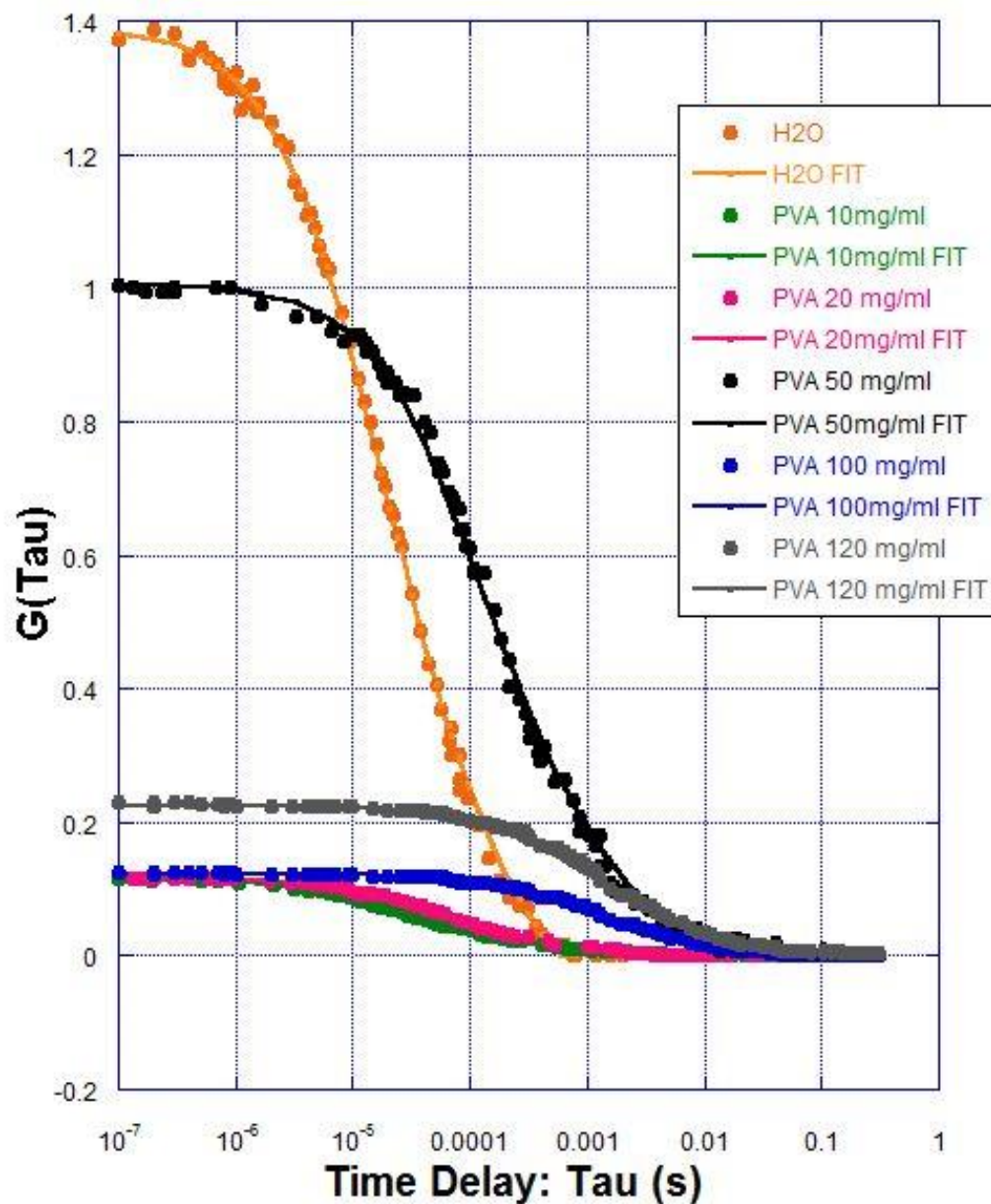


Figure 2.23: Correlation functions of fluorescein in different PVA solutions. Fits of the equation 2.9 of Data are represented as solid lines.

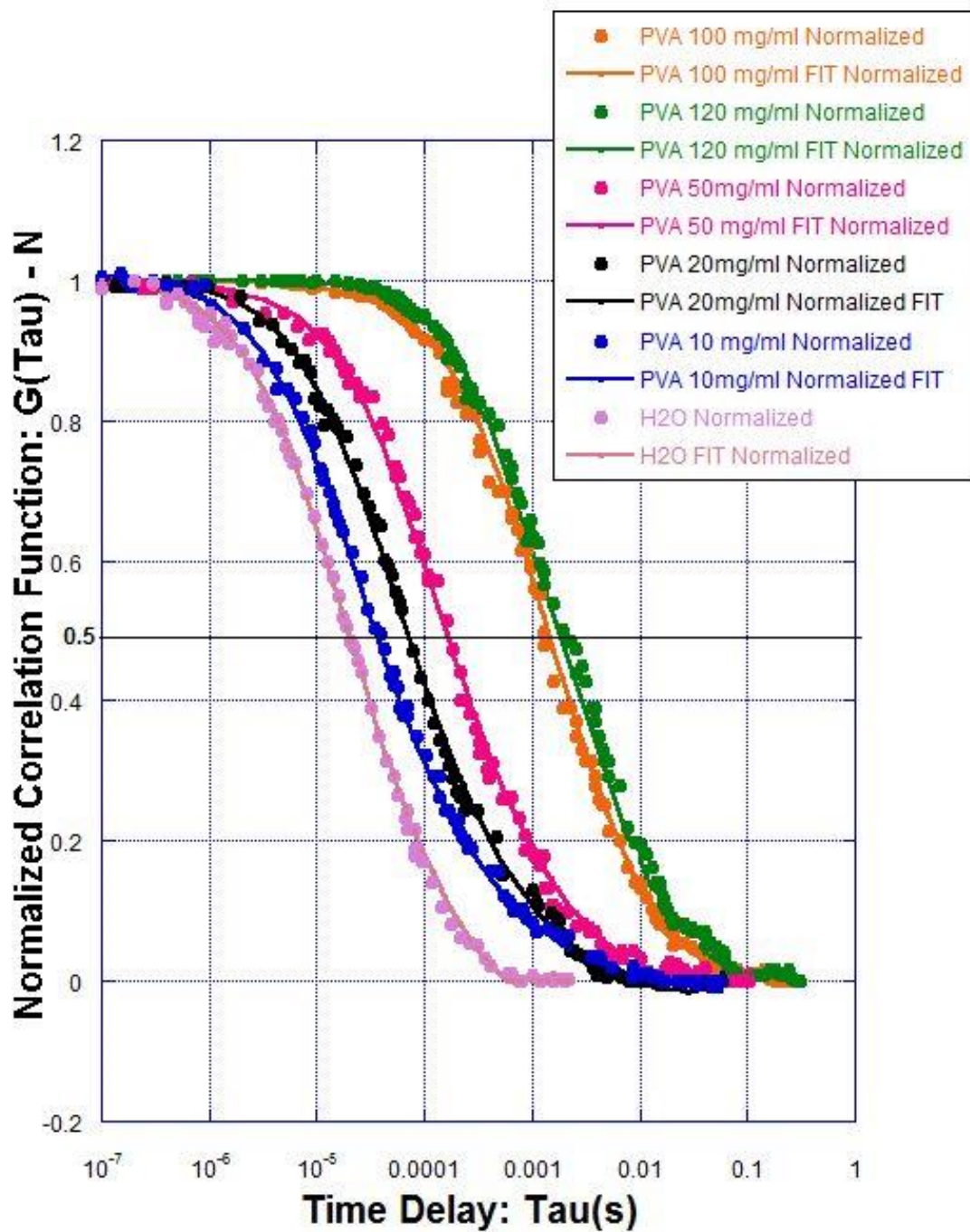


Fig 2.24: Normalized correlation functions of fluorescein in different PVA solutions. Fits of the equation 2.9 of data are represented as solid lines.

In Figure 2.23 and Figure 2.24 results of the fit (displayed as solid lines) show a good fit, indicating that diffusion as a process satisfies the changes of the correlation functions within the precision of the measurements. More importantly, the proposed expression for the 3-D diffusion fit all PVA concentrations, which means that diffusion of fluorescein slowed down as the PVA concentration increased -no measureable trapping or binding of the nanoprobe even at high PEG concentrations.

Following the same procedures with Alexa 488 fluorophore embedded in PEG, FCS correlation functions and their normalized plots are plotted as a function of delay time (Figures 2.25 to 2.28) and as observed in PVA polymers, a uniform shift of the correlation with the increase of PEG concentration is present also the 3-D model fits as well as in PVA with fluorescein.

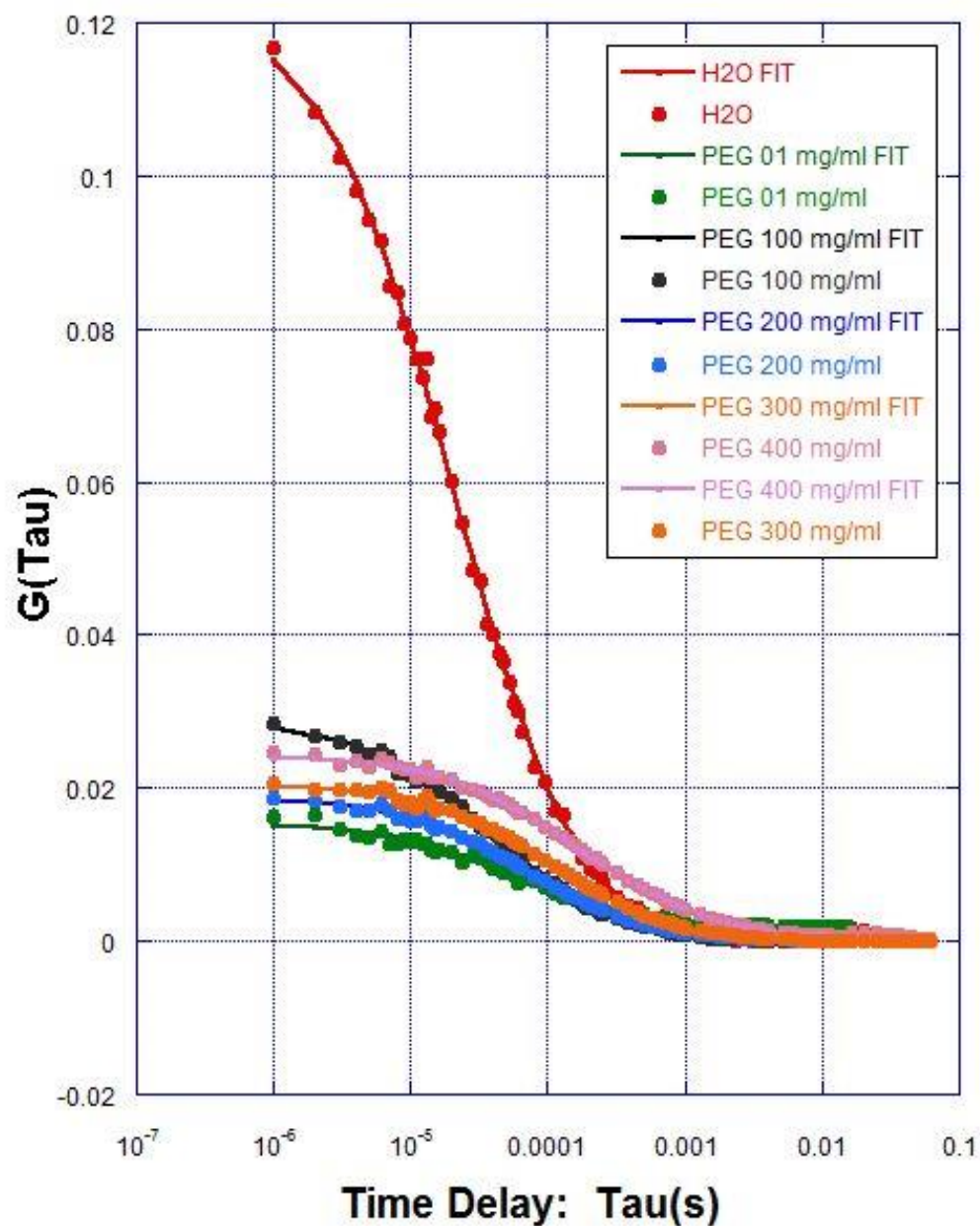


Figure 2.25: Correlation functions of Alexa 488 in different PEG solutions (from 01 to 400 mg/ml). Fits of the equation 2.9 of Data are represented as solid lines.

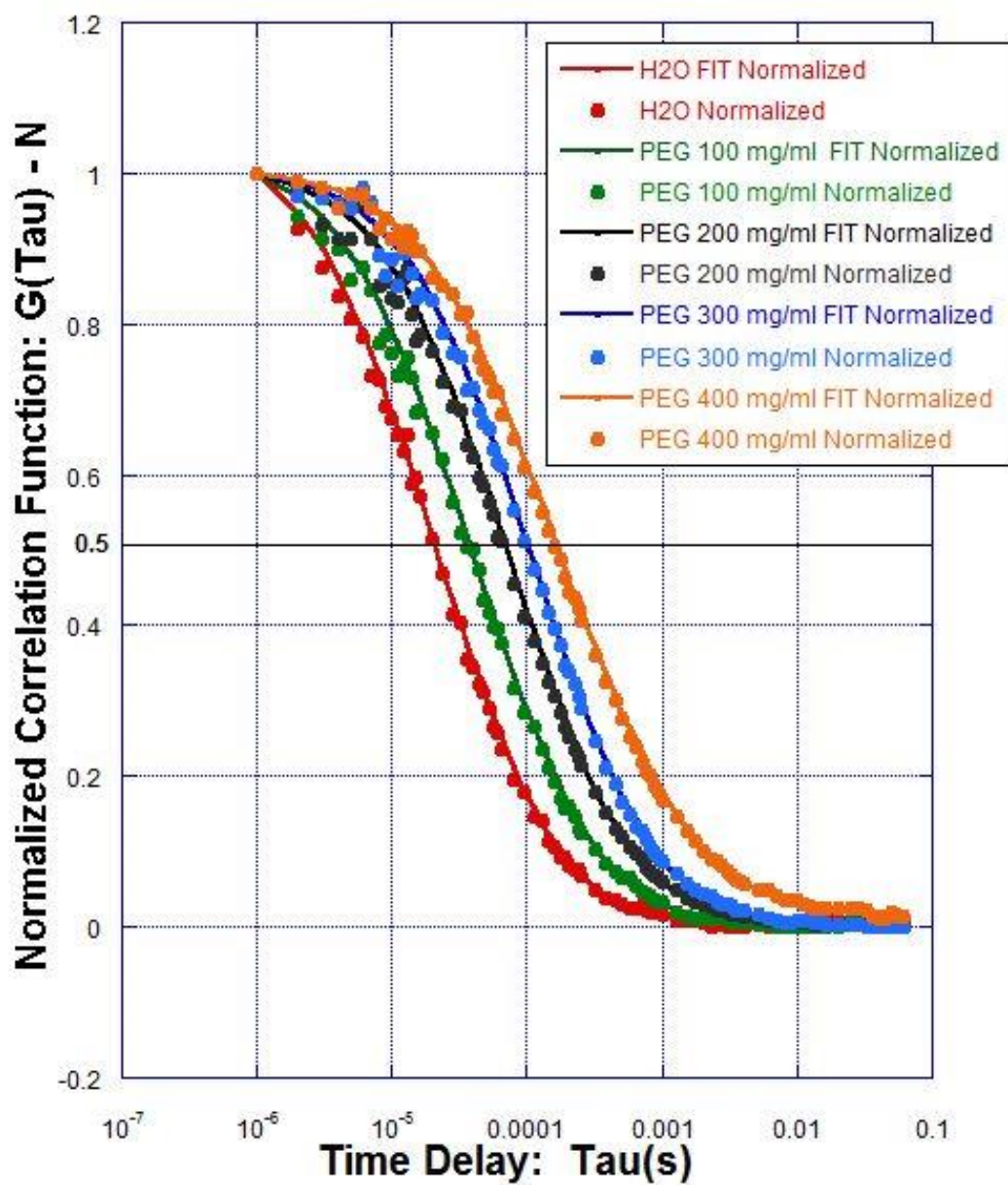


Figure 2.27: Normalized correlation functions of Alexa in different PEG solutions (from 100 to 400 mg/ml). Fits of the equation 2.9 of Data are represented as solid lines.

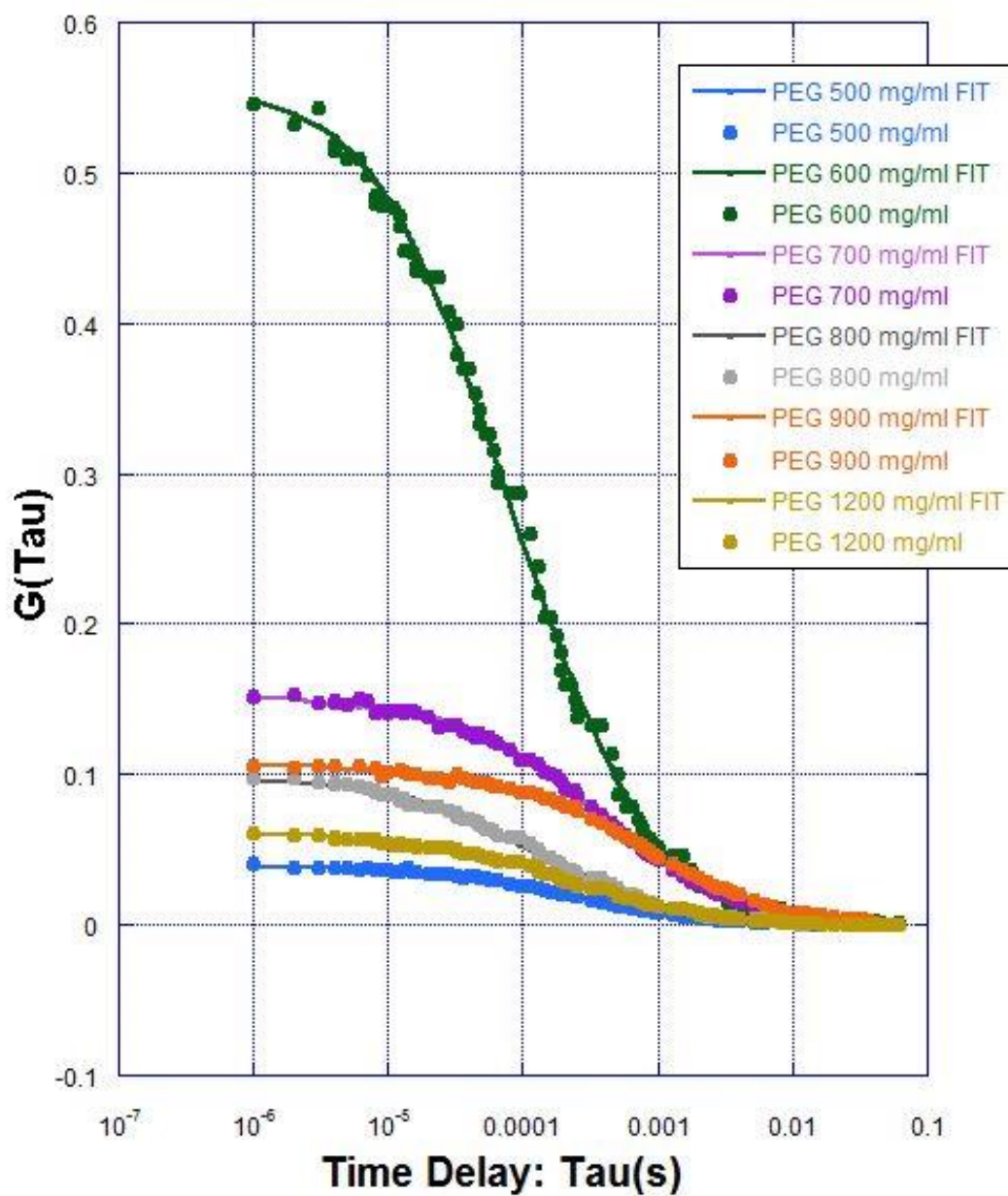


Figure 2.26: Correlation functions of Alexa 488 in different PEG solutions (from 500 to 1200 mg/ml). Fits of the equation 2.9 of Data are represented as solid lines.

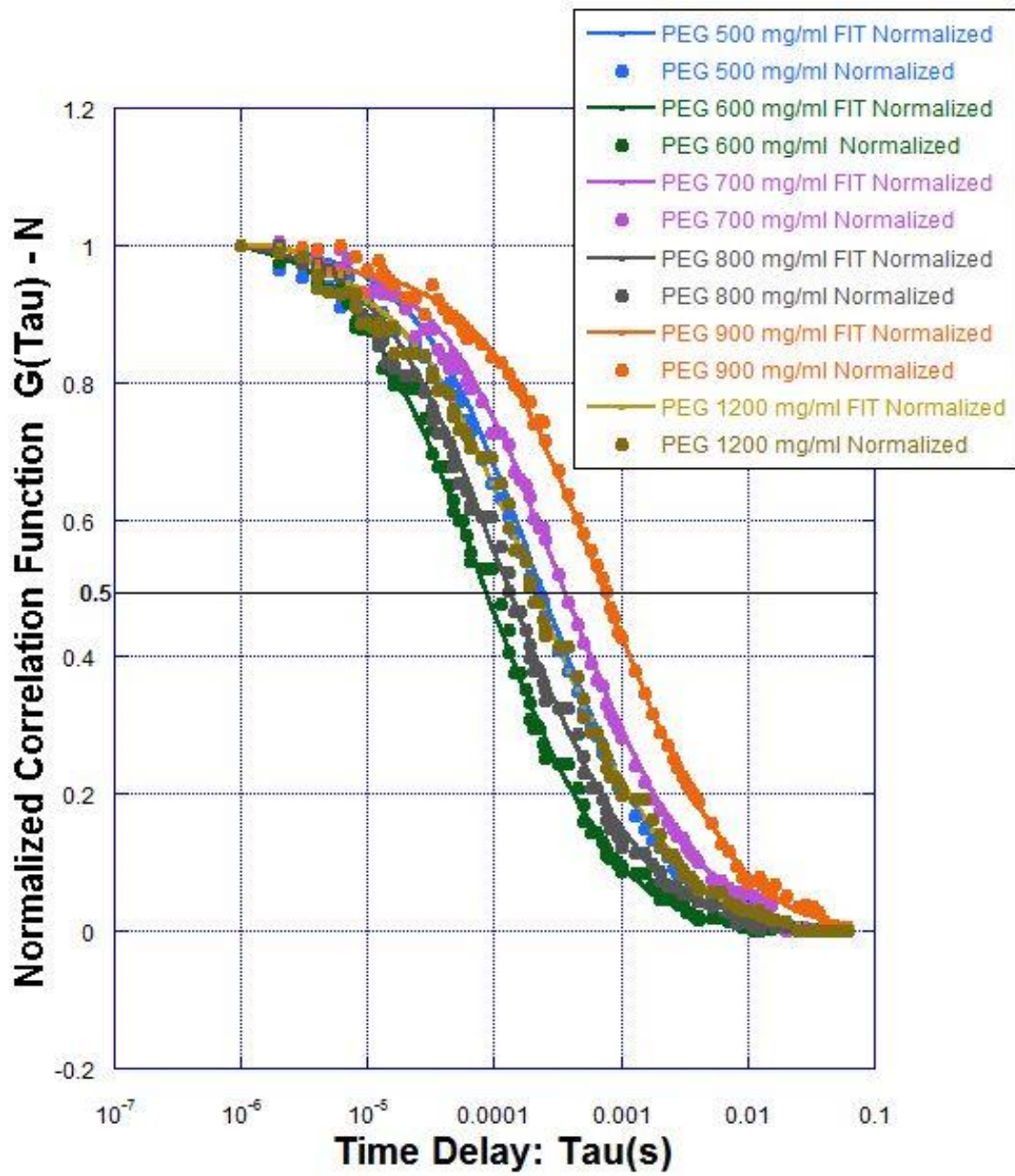


Figure 2.28: Correlation functions of fluorescein in different PEG solutions (from 500 to 1200 mg/ml). Fits of the equation 2.9 of Data are represented as solid lines.

2.5.2 Probe Diffusion in Polymeric Solutions

According to several studies, including a recent study I have published with my colleague Elton Jhamba under Dr. Boukari' Supervision (see ref [38]), changes of the translational diffusion coefficient of nanoprobe with increase of polymeric concentration appears to be best described with a stretched exponential function of the concentration of the host polymeric solution $\exp(-\alpha c^n)$ with the value of the exponent n varying between 0.5 and 1 depending on the system[67,68-74]. Langevin and Rondelez have argued that the probe diffusion is governed by topological effects, neglecting other effects such as hydrodynamics. In their model, the semi dilute polymer solution is treated as a transient statistical network of mesh size, ξ . The frictional force on the probe depends on the relative size of the diameter of the probe, d , and the mesh size, ξ , which is described by a scaling law:

$$\frac{f_0}{f_c} = \Psi\left(\frac{d}{\xi}\right) \quad (2.13)$$

where f_0 and f_c are the friction coefficients of the probe moving in pure solvent and in a solution of polymer, respectively and three regimes are identified:

$d/\xi \ll 1$, in which the effects of the polymers on the probe diffusion are neglected, suggesting that the probe diffuse in the solvent only. That is, $f_0/f_c = 1$.

$d/\xi \gg 1$, in which the size of the probe is so large that the polymeric solution appears as a continuum. Here, one can recover and apply the underlying assumptions for the derivation of the Stokes-Einstein relation with the friction, $f_c = 3\eta_c d_H$, where η_c is the viscosity of the polymer solution with concentration, c . Hence, $f_0/f_c = \eta_0/\eta_c$.

In the regime $d/\xi \sim 1$, Langevin and Rondelez suggested a specific function for $\Psi\left(\frac{d}{\xi}\right)$:

$$\Psi\left(\frac{d}{\xi}\right) = e^{-\left(\frac{d}{\xi}\right)^\delta} \quad (2.14)$$

where δ is a scaling parameter. Equation 2.14 was obtained by estimating the reduction of entropy due to distortion of the mesh unit of size ξ by the particle of size d . Experimentally, Langevin and Rondelez found the value $\delta = 1$ for sedimentation of ludox, bovine serum albumin (BSA), and viruses in poly (ethylene oxide), in agreement with predictions of several models of probe diffusion. Further, from the Nernst-Einstein equation, one has $f_0/f_c = D_T/D_0$, therefore 2.14 can be rewritten (with $\delta = 1$) as:

$$\frac{D_T}{D_0} = A e^{-\frac{d}{s} \left(\frac{c}{c^*}\right)^n} \quad , \quad (2.15)$$

where we utilize de Gennes's scaling relation for the correlation length in semidilute solution, ξ , namely

$$\xi \sim s \left(\frac{c}{c^*}\right)^{-n} \quad . \quad (2.16)$$

Here, s is the average polymer chain size, c^* the concentration where the chains begin to entangle, and n a scaling exponent related to the polymer chain excluded volume, according to Flory theory [75,76] which reflects the solvent quality. For a theta solvent, $n = 1$, and for a good solvent, $n = 3/4$. Note that Eq.3 can be rewritten as a stretched exponential:

$$\frac{D_T}{D_0} \sim e^{-\alpha c^n} \quad , \quad (2.17)$$

where

$$\alpha \sim \frac{d}{s} c^{*-n} \quad , \quad (2.18)$$

which shows the dependence of the prefactor on the size of the probe, d (or d_H , the hydrodynamic diameter).

Another competitive model of probe diffusion has been developed by Phillies, who argues that probe diffusion is largely governed by hydrodynamic interactions, as opposed to topological effects such as entanglements. Phillies asserts that this physical assumption differs from the assumptions made in the de Gennes and Doi-Edwards models, where topological constraints dominate hydrodynamic forces. His expression for probe diffusion in polymer solutions, however, has the same form as equation 2.17, where α and n are adjustable parameters. He argues that α has a dependence on the polymer molecular weight but not probe size, and n is related to solvent quality.

After obtaining $\tau_{D(PVA)}$ values from the fit (figure 2.24 for PVA) we scaled τ_D with τ_{D0} (diffusion time in H₂O) to obtain values independent of experimental parameters. From equation (2.12) the diffusion time τ_D is inversely proportional to diffusion coefficient D , using this relation to define a scaled diffusion coefficient D_{PVA}/D_{H2O} . Same steps are taken to obtain $\tau_{D(PEG)}$ values from fits(figures 2.26 and 2.28). For both PVA and PEG curves, data are times at half amplitude of respective normalized functions.

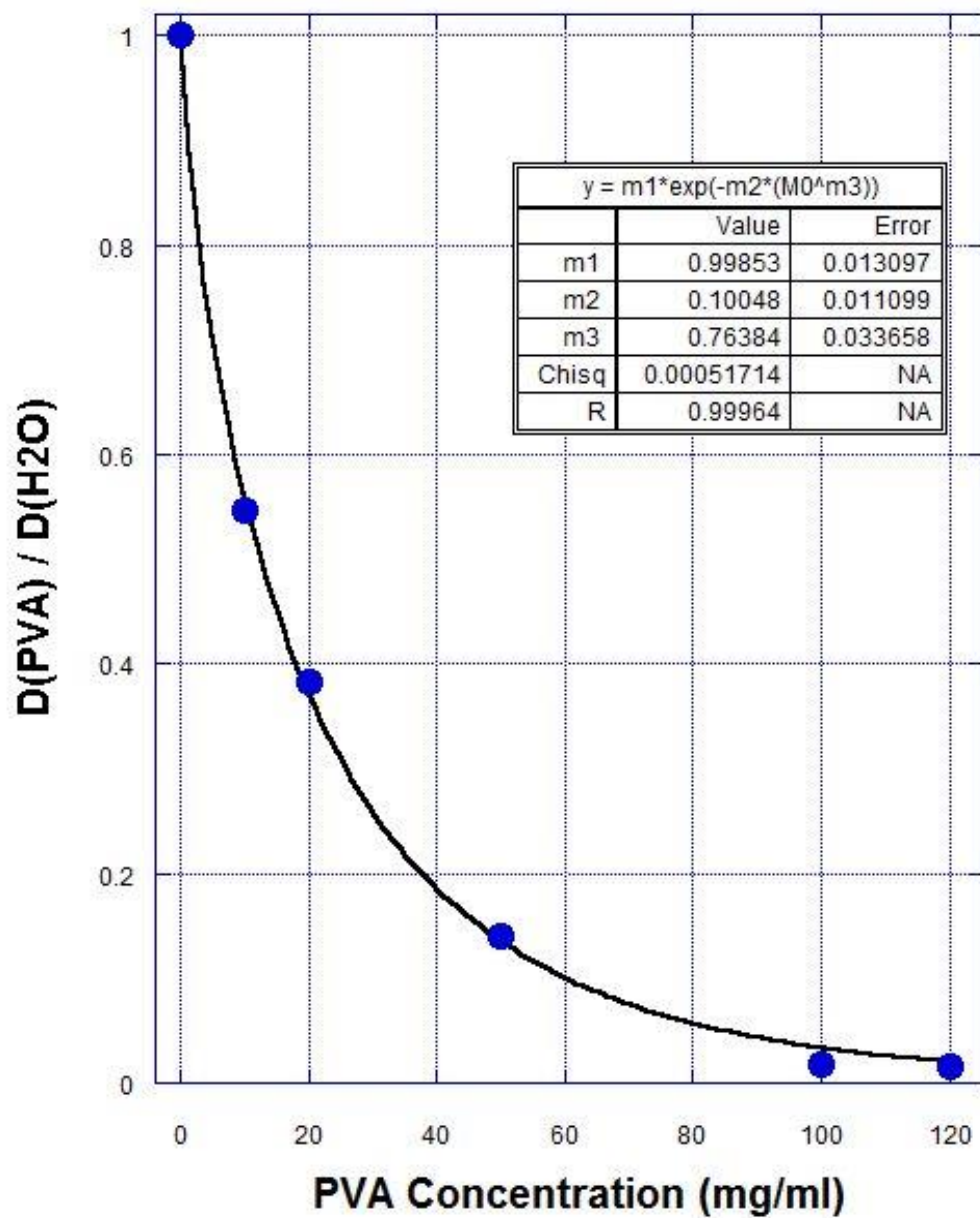


Figure 2.29: translational diffusion coefficient of Fluorescein fluorophores as function of PVA concentration

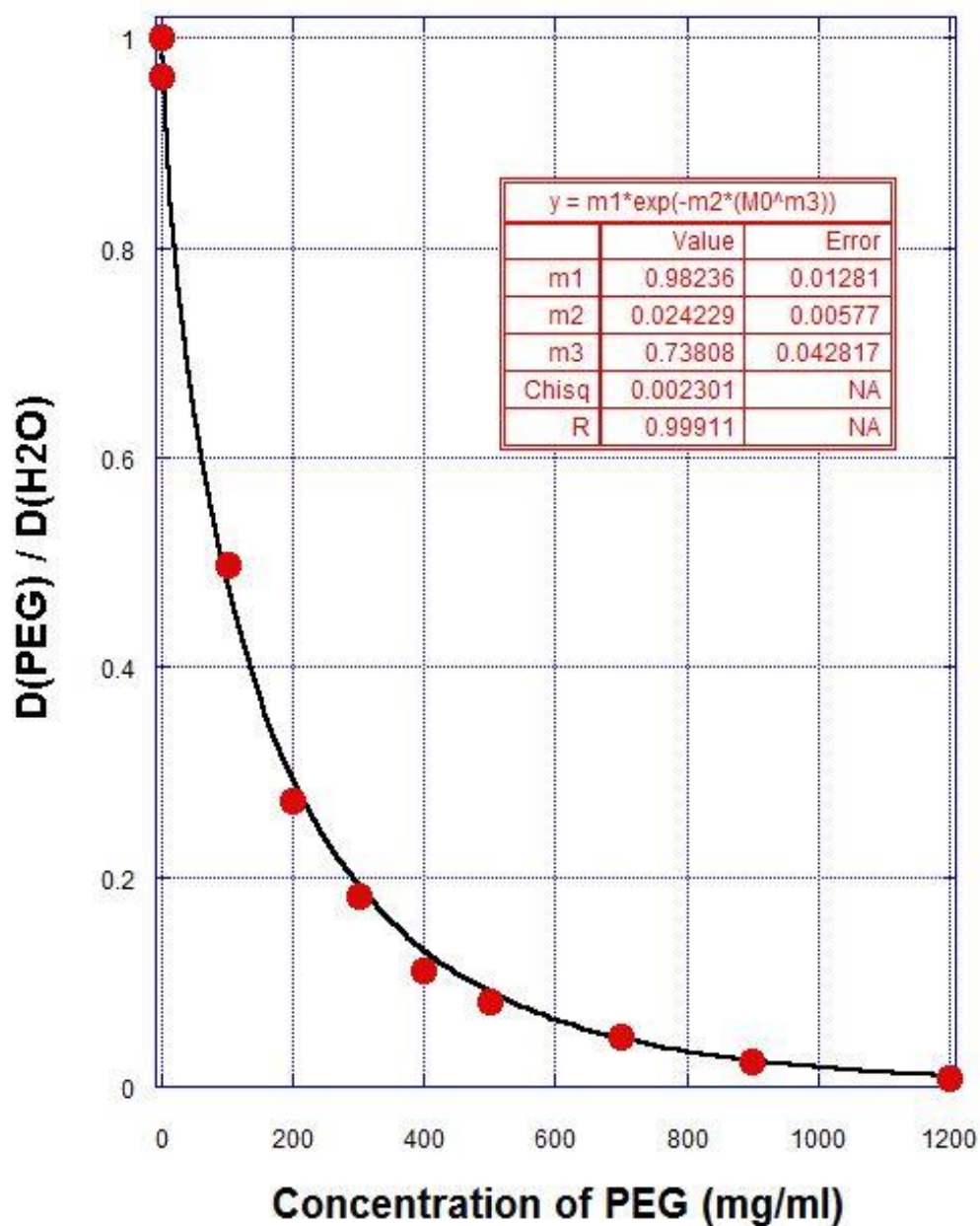


Figure 2.30: translational diffusion coefficient of Alexa488 fluorophores as function of PEG concentration

For both figures 2.29 and 2.30, we fit the concentration dependence of the apparent diffusion time derived from FCS data for both Fluorescein and Alexa488 in PVA and PEG solutions with a stretched exponential ($Ae^{-\alpha c^n}$). The resulted fits are included in the figures as solid lines. Note that for both fluorophores we determined respectively, $n = 0.763$ for fluorescein in PVA and $n = 0.738$ for Alexa488 in PEG. Both these values are close to the theoretical $n=3/4$ for associated with good quality according to Flory's theory.

Further, the scaled exponent of Alexa488 in PEG solutions, $\alpha(\text{PEG})=0.024$ shown in figure 2.30 (m_2 value in Fig 2.30), is four folds less than that of the scaled coefficient of Fluorescein in PVA $\alpha(\text{PVA}) = 0.100$ shown in figure 2.29 (m_2 value in Fig 2.29), this means that for any given concentration C (under maximum theoretical volume fraction concentration discussed in 2.5.3) of both polymers studied in this chapter, the higher the polymer concentration, the slower the translation diffusion occurs however this translation diffusion will be four exponential-times more slowly in PVA than in PEG.

2.5.3. Volume Fraction Vs. Concentration

Since the value for the solvent quality n is $n \sim 0.75$ which is the same for both polymers and since the both fluorescein and Alexa 488 have comparable sizes (~ 1.8 nm), we had to investigate the effect of molecular weight of PVA ($M_w \approx 85 \times 10^3$ g per mole) and PEG ($M_w \approx 10 \times 10^3$ g per mole) on the diffusion coefficient. The volume fraction can be estimated by $\phi = V_p / (V_w + V_p)$ where V_p is the volume occupied by the polymer in the solution and V_w the volume of water. Therefore,

$$V_p = \frac{(4\pi R^3/3)mN_A}{M_w}$$

with R is the radius of gyration; m is the polymer mass, N_A the Avogadro number, M_w is the molecular of the polymer.

The radius of gyration in water as a function of molecular mass M is given by $R = 0.02M^{0.58}$ where R is in nanometer and M in Daltons [77].we plot changes of volume fraction ϕ with mass concentration of both polymers dissolved in water leads to figure 2.31 shown below.

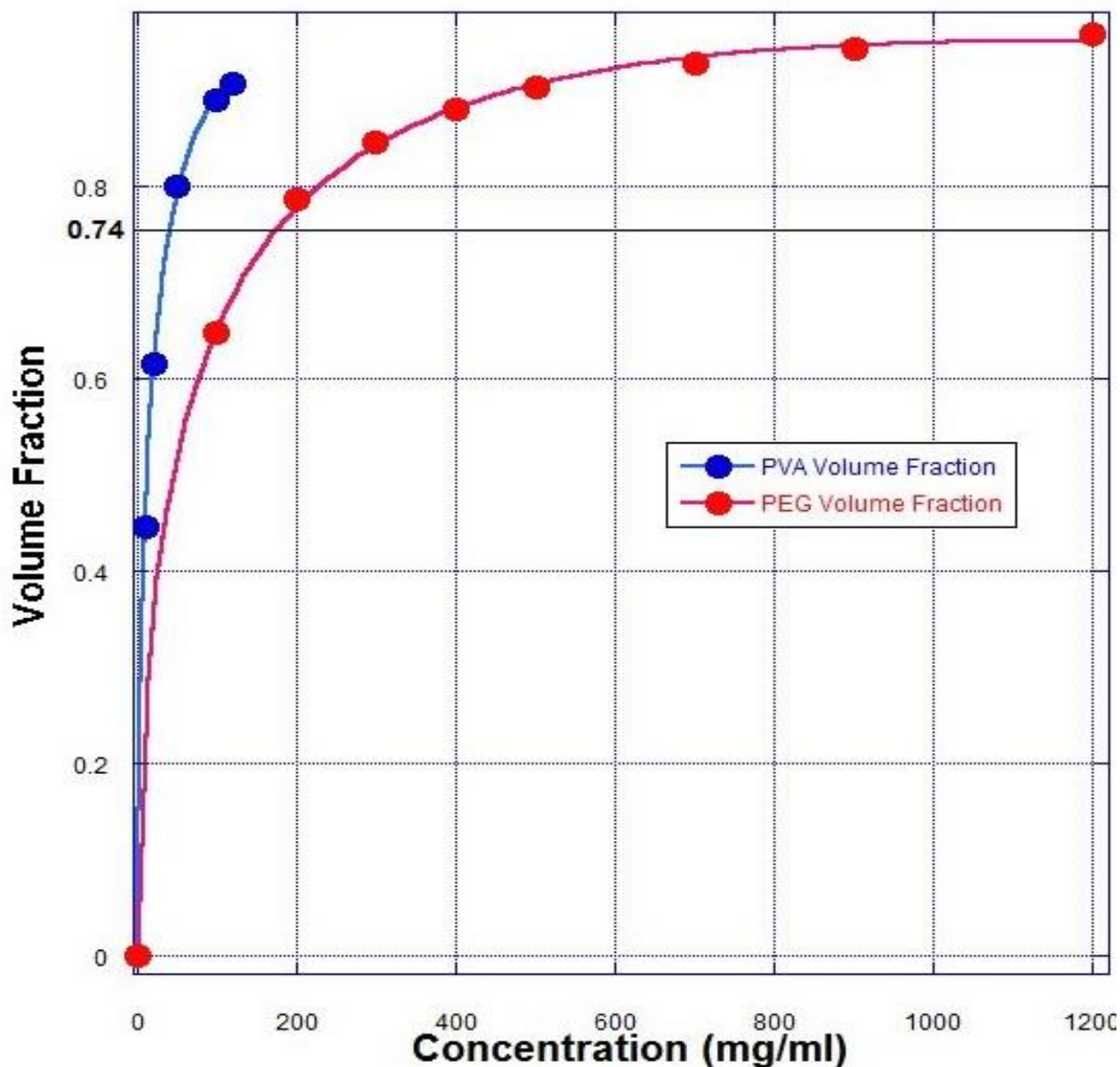


Figure 2.32: Calculated Volume fraction of PVA and PEG as a function of their respective concentrations.

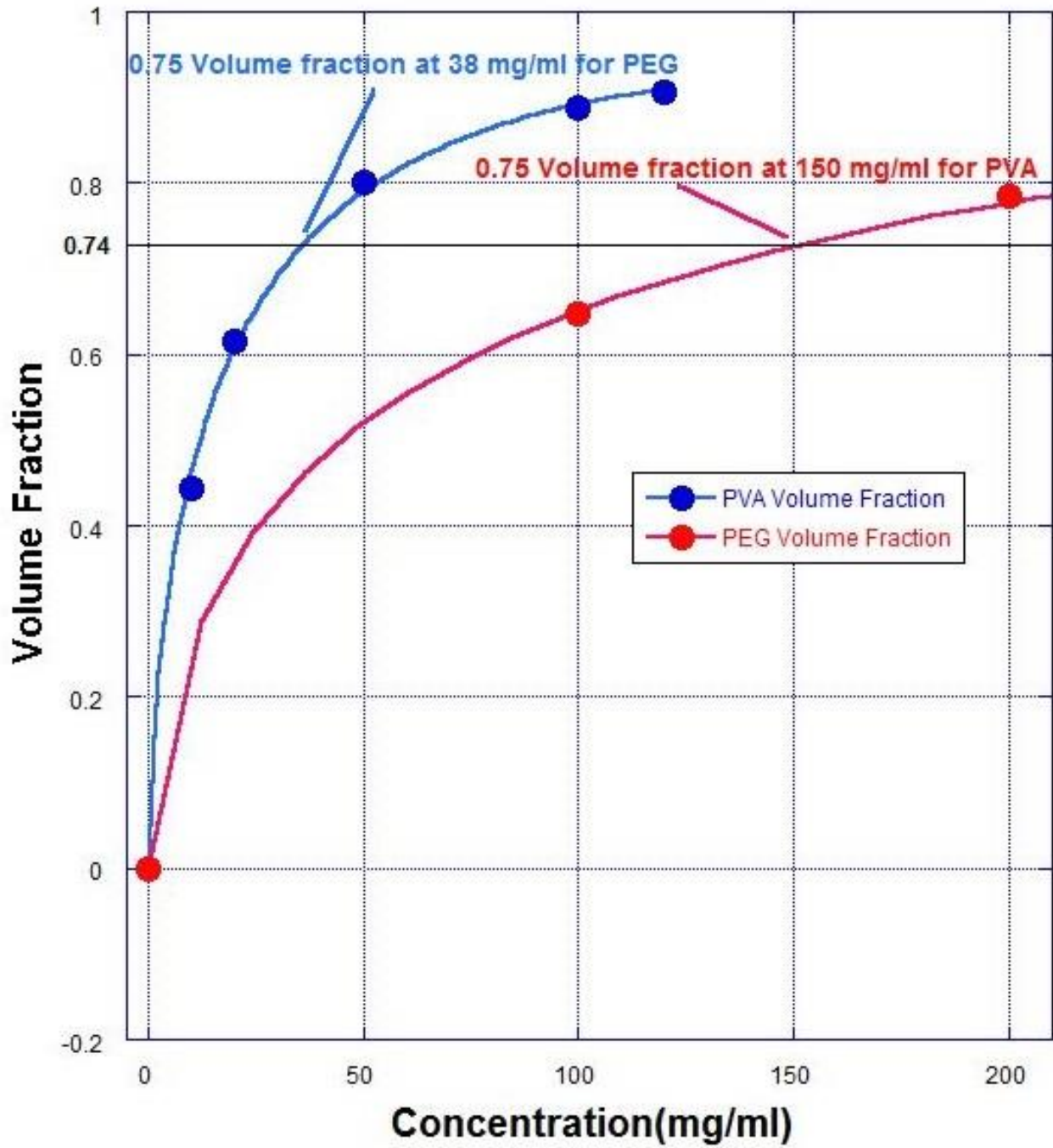


Figure 2.31: comparable Volume fraction at~ 0.74, to the respective is about 04 folds (~150 mg/ml for Fluorescein in PVA and ~38 mg/ml for Alexa488 in PEG).

We have also inserted a line associated with the maximum theoretical volume fraction (~ 0.74) that can be occupied by rigid, spherical polymer chains in the solution.

Analyzing plots of volume fractions of the polymer in water for both PEG and PVA, we have noticed that for the same volume fraction (under the maximum theoretical volume fraction), the concentration of PEG is 04 times higher than that of PVA which justifies the diffusion coefficient in (PEG) being 04 folds less than a(PVA).

Combining these two results lead to the final governing conclusion expressed in the figure 2.33 below: identical behavior for both polymers in terms of diffusion delay time with respect of the polymer volume occupancy fraction in the solution , which emphasizes that the translational diffusion coefficient of a particle diffusing in a polymeric medium suggest that the coefficient only depend inversely on the viscosity of the medium, that is the higher the polymer concentration, the slower the translation diffusion.

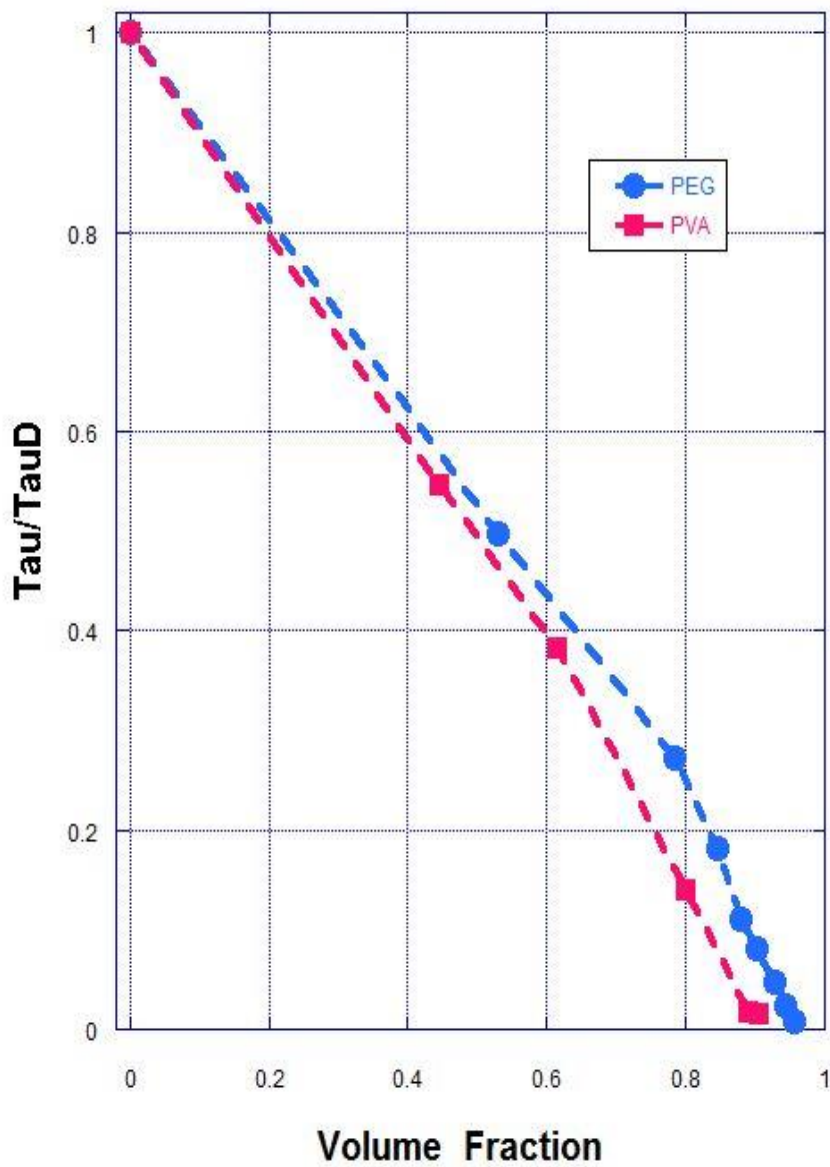


Figure 2.33: Translational diffusion time Vs. the polymer volume occupancy fraction in the solution of both PEG and PVA, The two fitting plots are in almost superposition

Also, changes of the diffusion coefficients of the studied nanoparticles cannot be accounted for by changes of the gelation status of the PVA gels for concentrations of 50, 100, 120 mg/ml, Stokes-Einstein relation was maintained in this case as well, we were unable to detect any considerable shift in the diffusion time of the probe embedded in semi diluted PVA gels(7-10 days) or completely solid PVA gel(30 days and more) proving once more that translational diffusion is solely depending on the concentration of the polymer.

6. Conclusions:

In this chapter we have demonstrated the use of FCS to measure changes of the diffusion of Alexa488 and Fluorescein in PVA and PEG linear polymer solutions. In particular, we have found that:

- PVA and PEG polymers do not affect significantly the fluorescence spectra and lifetimes of Alexa488 and Fluorescein.

The measured FCS correlation functions of the fluorescent Alexa488 and Fluorescein appeared to shift uniformly and systematically to longer times as the PVA and PEG were increased. Further, the FCS correlation functions could be adequately fit with the expression of Eq. 2.10 which describes the 3-dimensional free diffusion of the the nanoprobe in the solutions. That is, there is no measurable binding of the nanoprobe with the polymers and there is no need to apply the expression for anomalous diffusion as suggested by other reports [38].

- Since the PVA molecular weight is larger than that of PEG, the radius of gyration and the corresponding volume approximation of the suggested spherical shape of PVA polymer is about 4 times bigger than that of PEG polymer. However, we noticed that entanglement of PEG made it almost like PVA in term of volume fraction Vs. diffusion (figure 2.33). The dependence of the apparent diffusion coefficient on the PEG and PVA concentration fit well with a stretched exponential ($\exp(-\alpha c^n)$), consistent with the entropic-based model suggested by de-Gennes and his collaborators. . For both PEG and PVA solutions we found that the α -values to be close to the theoretical value for a good solvent, $n=3/4$.

CHAPTER III : ROTATIONAL DIFFUSION of Alexa488 in PEG and PVA Solutions

3.1 Introduction

In this chapter I will describe fluorescence anisotropy (FA) measurements conducted on samples of mixture solutions of fluorescent nanoprobes (Alexa488 and Fluorescein) and polymer (PVA and PEG) which were dissolved in water. The main goal is to perform a systematic study of the effects of the polymers on the rotation of the nanoprobes. Here, we applied the fluorescence anisotropy method and collected the data with an ISS K2 spectrometer. Similar to the FCS measurements described in Chapter 2, the nanoprobes were dispersed in solutions of PVA and PEG that were prepared at different concentrations (up to 120 mg/ml for PVA and 900 mg/ml for PEG). And the major question is how similarly, if it were, the effects of the polymeric crowding due to the polymers in the solutions on the translation and the rotation.

3.2 Fluorescence Anisotropy Method

In a simple experimental setup (see Figure 3.1) fluorescence anisotropy (FA) method uses a polarized incident beam on a sample containing fluorescent molecules, and measures the emitted fluorescence intensities parallel ($I_{||}$) and perpendicular (I_{\perp}) to the direction of the incident beam. A measure of the depolarization of the fluorescence is provided by the calculated anisotropy, r , defined as the following ratio:

$$r = (I_{||} - I_{\perp}) / (I_{||} + 2I_{\perp}) \quad (3.1)$$

where $I_{||} + 2I_{\perp}$ represents the total emitted intensity since the emission of the molecules is symmetric around the axis of incident polarization. The main concept in understanding the fluorescence anisotropy rests on the rotation of the fluorescent molecules which are typically driven by thermal fluctuations.

Anisotropy measurements indicate the average angular rotational displacement of fluorophores which took place between the absorption of the incident polarized beam and the emission of photons. This angular displacement depends on the rate of rotational diffusion, which itself depends on the viscosity of the host solvent, the shape, and the size of the rotating molecule during the lifetime of the excited state. For low viscosity solvent the anisotropy will be close to zero for small fluorophores since the rate of rotational diffusion is faster than the rate of emission.

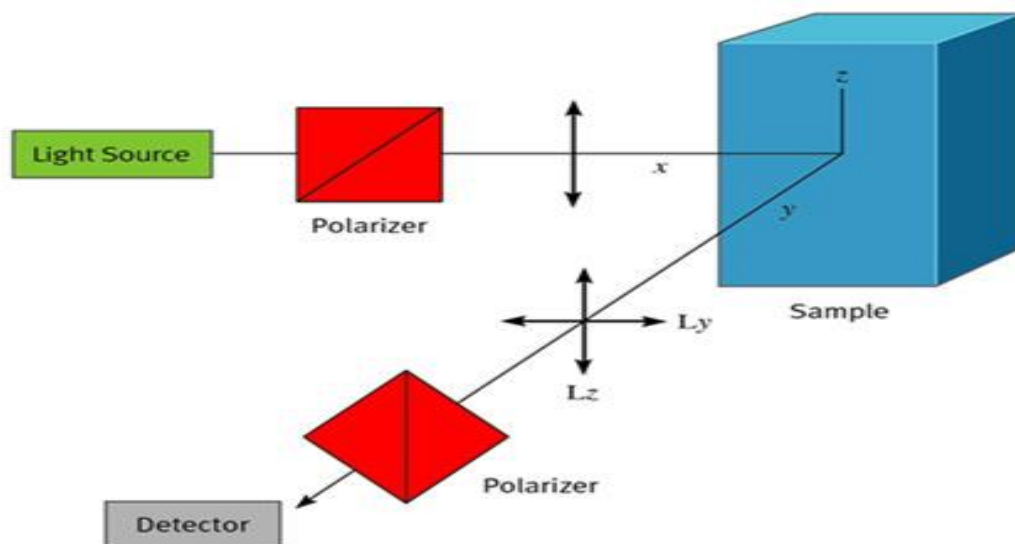


Figure 3.1[82]: Schematic drawing for the measurement of fluorescence Anisotropy

Fluorescence anisotropy has been widely used in biological applications such as studies of antigen-antibody interactions Dandliker[83]. For example, ovalbumin was labeled with fluorescein isothiocyanate and then antibodies were raised to the fluorescein-ovalbumin adduct. Then the binding of this antibody-antigen system was studied using anisotropy and intensity measurements [83]. Another example was described in Ref [84] where fluorescence polarization measurements of FITC-labeled chitosan were performed to gain better insight into

the association between chitosan and mucin under different pH and ionic conditions [84]. Recently, fluorescence anisotropy has been used for nanoparticle sizing where a particle sizing method has been developed based on analysis of rotational motion [85]. Also, it has been used for studying micellar aggregation of nonionic Brij surfactants [86].

In case of free rotation, the anisotropy decay equals to zero while for non-rotating or frozen state molecules the anisotropy approaches the residual or remaining anisotropy, r_0 . These decays of the fluorescence polarization components, $I_{||}(t)$ and $I_{\perp}(t)$, are directly attributed to the randomness and tumbling of the fluorescent part of the molecules or the overall fluorescent molecules due to rotational diffusion. Further analysis of the time dependence of the anisotropy would provide valuable information on the orientation dynamics of the fluorescent molecules, which itself is related to the host environment as well as the size and shape of the molecule.

3.3 Theoretical Background and Frequency Domain Measurements

In frequency domain setup the intensity of the excitation -in frequency-domain fluorometry- is assumed to be a sinusoidal polarized beam directed onto a sample and expressed as:

$$I(t) = I_0[1 + A_e \sin(\omega t + \phi_0)] \quad (3.2)$$

where ω is the angular frequency of the modulated excitation beam, A_e the amplitude of the modulation, and ϕ_0 an arbitrary initial phase of the incident beam. The fluorescence response is expected to decay exponentially, and since it has been excited by a sinusoidal beam we expect a sinusoidal response of the measured fluorescence given by the following expression:

$$F(t) = F_0[1 + A_f \sin(\omega t + \phi)] \quad (3.3)$$

Differential polarized phase angle (between the perpendicular and parallel components of the emission) at modulated frequency, and the ratio of the parallel and perpendicular components of the modulated emission – amplitude ratio, are the two quantities that characterize anisotropy decay in our frequency domain experiments. The modulation ratio is defined as,

$$M = \frac{A_f}{A_e} \quad (3.4)$$

Using Fourier transform (represented by a series of sinusoidal functions) to solve for these variables from time domain fluorescence response to a delta function excitation, $I_f(t)$, following the following equations and steps:

$$\tan(\phi) = \frac{C}{T} \quad (3.5)$$

$$M = \frac{A_f}{A_e} = \frac{\sqrt{C^2+T^2}}{F} \quad (3.6)$$

$$T = \int_0^\infty I_f(t) \cos(\omega t) dt \quad (3.7)$$

$$C = \int_0^\infty I_f(t) \sin(\omega t) dt \quad (3.8)$$

$$F = \int_0^\infty I_f(t) dt \quad (3.9)$$

For a single exponential decay,

$$I_f(t) = I_0 e^{-\frac{t}{\tau}} \quad (3.10)$$

the equations 3.5 and 3.6 reduce, respectively, to:

$$\tan(\phi) = \omega \tau \phi \quad (3.11)$$

$$M = \frac{1}{\sqrt{1+\omega^2\tau_m^2}} \quad (3.12)$$

where τ_θ is the lifetime phase value and τ_m is the lifetime measured by modulation.

At a single frequency, assessing phase-modulation coupling measurements can be determined through the study of the decay type fitted, so when a single exponential decay is determined then the phase and modulation lifetime will be equal. In order to get the frequency domain values we use Fourier transform on the parallel and perpendicular components of the impulse response function separately. Then, Equations (3.7) and (3.8) are expressed as:

$$T_\omega = \sum f_i \frac{\omega t_i}{(1+\omega^2\tau_i^2)} \quad (3.13)$$

and

$$C_\omega = \sum f_i \frac{1}{(1+\omega^2\tau_i^2)} \quad (3.14)$$

From T_ω and C_ω the phase and modulation values can be deduced and expressed as:

$$\phi_{c\omega} = \arctan\left(\frac{T_\omega}{C_\omega}\right) \quad (3.15)$$

and

$$M_{c\omega} = (T_\omega^2 + C_\omega^2)^{1/2} \quad (3.16)$$

In FA experiments, we need the error-weighted sum of the squared deviations between the measured and calculated values (χ^2) to be at its minimum. Therefore, the estimated values of α_i and τ_i are introduced accordingly. Using both phase and modulation values, χ^2 is expressed as:

$$\chi^2 = \sum_\omega \left[\frac{\phi_\omega - \phi_{c\omega}}{\sigma_{\phi_\omega}} \right]^2 + \sum_\omega \left[\frac{M_\omega - M_{c\omega}}{\sigma_{M_\omega}} \right]^2 \quad (3.17)$$

where for each frequency, $\sigma_{\phi\omega}$ and $\sigma_{M\omega}$ are the respective estimated uncertainties in the phase and modulation data.

For analysis of our measurements we fixed the errors margin as the following constants, $\sigma_{\phi}= 0.020$ and $\sigma_M= 0.004$, if a high value of χ^2 is persistent then this indicate a poor signal or a present problem with the setup . Once the values of the phase ratio, the modulation ratio, and the lifetime were determined, we proceeded to calculate the value of the fluorescence anisotropy. Best fit of the data were determined by the optimum χ^2 value. Note that relatively high χ^2 value even for the best fitting model it would indicate that there is a systematic error or poor signal to noise ratio.

Fluorescence anisotropy of a single fluorophore and its rotational conduct process can be expressed as an exponential decay with $r(t) = r_0 e^{-t/\theta}$ where θ is the rotational correlation time of the fluorophore at any time, t . However the average anisotropy in a steady state of rotating fluorophores is expressed as:

$$\bar{r} = \frac{\int_0^{\infty} I(t)r_0 e^{-t/\theta} dt}{\int_0^{\infty} I(t) dt} \quad (3.18)$$

$$\text{or ,} \quad \bar{r} = \frac{r_0}{1 + \frac{\tau_f}{\theta}} \quad (3.19)$$

is a better expression of the average fluorescence anisotropy in a well determined lifetime τ_f of a rotating fluorophore, the rotational correlation time θ and known initial or residual anisotropy r_0 .

In the case of slow rotation where τ_ϕ is shorter than θ , the value of \bar{r} approaches that of r_0 . In contrast, for fast rotation where τ_ϕ is much longer than θ , the value of \bar{r} approaches 0. Equation 3.19 can also be expressed as:

$$\frac{r_0}{\bar{r}} = 1 + \frac{\tau_f}{\theta} = 1 + 6D_R\tau_f \quad (3.20)$$

where we introduce the rotational diffusion coefficient, D_R , of the fluorophore that is rotating randomly in a 3-dimensional environment: $\theta = \frac{1}{6D_R}$. Equation 3.20 is commonly known as the Perrin equation.

Overall as a result of the above discussion, we should point out that in order to determine the rotational diffusion coefficient of a rotating fluorescent molecule it is required to have the values of the fluorescence lifetime of a molecule (τ_f), its average fluorescence anisotropy in its host medium (\bar{r}), as well as its fundamental or initial fluorescence anisotropy (r_0).

3.4 ISS K2 SPECTROFLUORIMETER INSTRUMENT

3.4.1 Photomultiplier tube (PMT) configuration and Light source

In the schematic diagram of Figure (3.2) we show a setup and optical paths in an anisotropy fluorescence experiment where two photomultipliers (PMT's) located at 90 angle for the incident beam on the sample. This is commonly called **T** configuration which has a major advantage for the simultaneous acquisition of both I_{\parallel} and I_{\perp} components. One needs, however, to assess the difference between the two PMT's and to include this difference in the calculation of the anisotropy.

For our measurements, it was always necessary to measure the lifetime first before running any anisotropy measurements. We have used the L configuration with only one PMT,

bypassing the need for correction and setting $g = 1$ always.

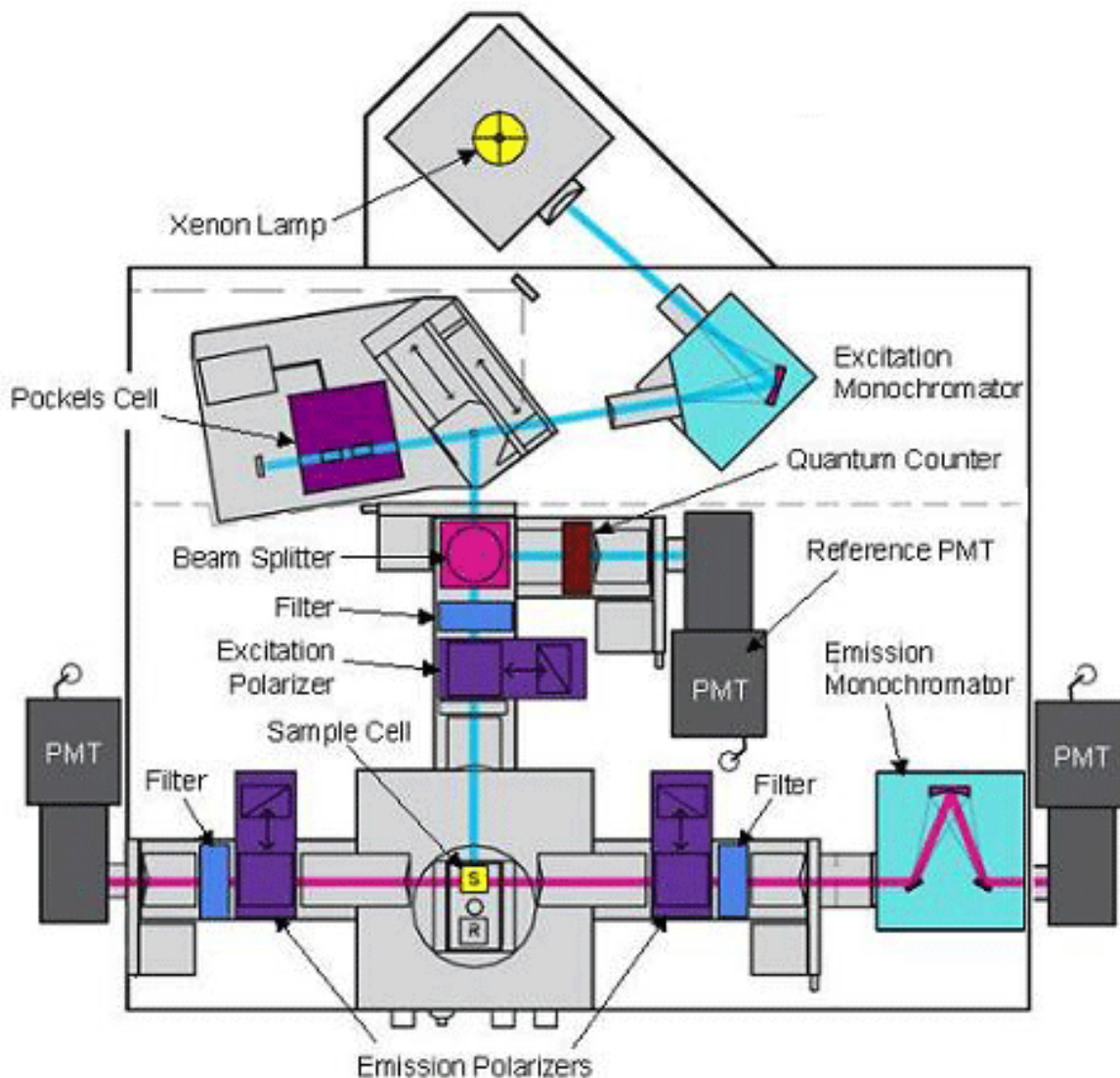


Figure 3.2[87]: ISS K2 (Champaign , IL) Spectrofluorometer

The diagram in Fig.3.2 shows also the principal components of the ISS K2 spectrofluorometer, including the Xenon arc lamp, the excitation and emission monochromators, the quartz beam splitter, quantum counting solution (Qc), three photon multiplier tubes (PMT) and one excitation (Pex) and two emission (Pem) calcite prism polarizers.

For our present discussion the most relevant light sources used in fluorescence instruments are mainly: the Xenon arc lamp, lasers, light emitting diodes (LEDs), and laser diodes which are good sources of photons. Our research was accomplished with the use of the Xenon Arc Lamp so it will be our main focus in this chapter 03. The xenon arc lamp is the most common light source in commercial instruments because it produces useable light from UV to Infrared [88]. The range is adequate for most fluorescence studies of biological samples. We note that while the range is big, the intensity depends on the wavelength. The xenon-mercury arc has the characteristics of the xenon arc source but is dominated by very prominent mercury transitions. The more prominent mercury lines are near the following wavelengths: 254, 297, 302, 313, 365, 405, 436, 543 and 578nm [89].

3.4.2 Excitation/Emission Monochromators and Polarizers

For all the experiments performed in this chapter, we used white light source (Xenon lamp 30W) and wavelength was set at 470nm using a monochromator. With the boost of an amplified master synthesizer at base frequencies, the excitation light goes through as a driven Pockel cell, which was set to modulate from 5 to 100 MHz. The modulated beam excited the sample causing the sample to emit modulated fluorescence also at base frequency. Our spectrofluorometer was also equipped with a 500-nm cut-on filter (emission filter) to allow only the desired fluorescence through to the photomultiplier tube. The PMT was modulated at the same base radio frequency as the master plus a low cross-correlation frequency (Δf) shown in below diagram (figure 3.3). The base-frequency signals were filtered to reveal the cross-correlation frequency signal, which contained all the same phase angle shift (ϕ) and

demodulation ratio (M) information as the fluorescence emission. We scanned over 10 different frequencies because of the intrinsic limitations of resolving mixtures using only one frequency.

Once the appropriate wavelength was selected, the light passed through an optical polarizer to select one plane of polarization. Our ISS K2 instrument employed the UV-grade Glan-Thompson polarizer 10 X 10 mm, L/A = 2.0.

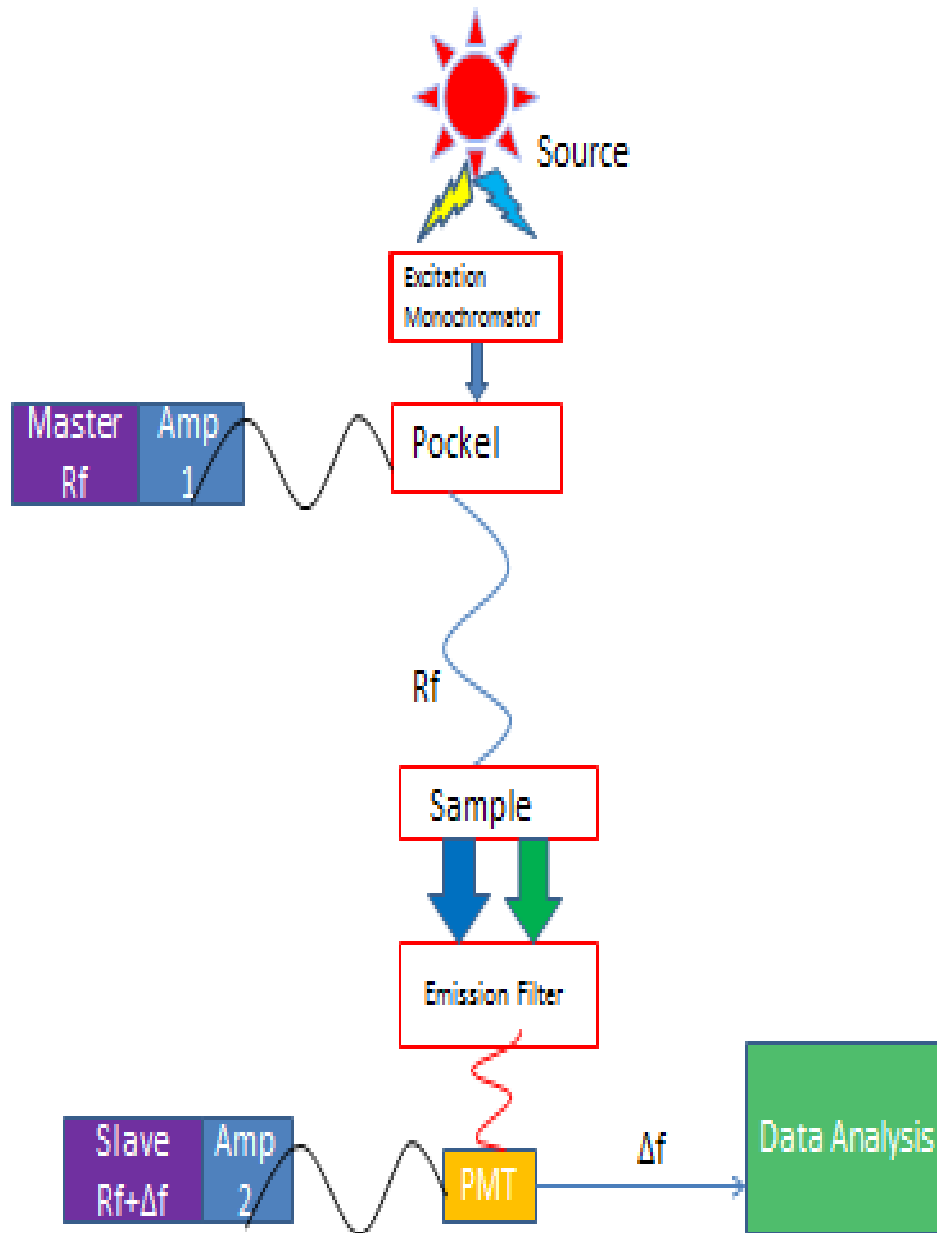


Figure 3.3[37]:MFCC Block Diagram (Multi-Frequency Cross-Correlation) setup

3.4.3 Software

We performed our main data analysis with the Vinci software package developed and provided by ISS company, Champagne, Illinois. The software offers full computer-controlled input and output of the data as well as automatic tools to fit the data (see Figure 3.4).

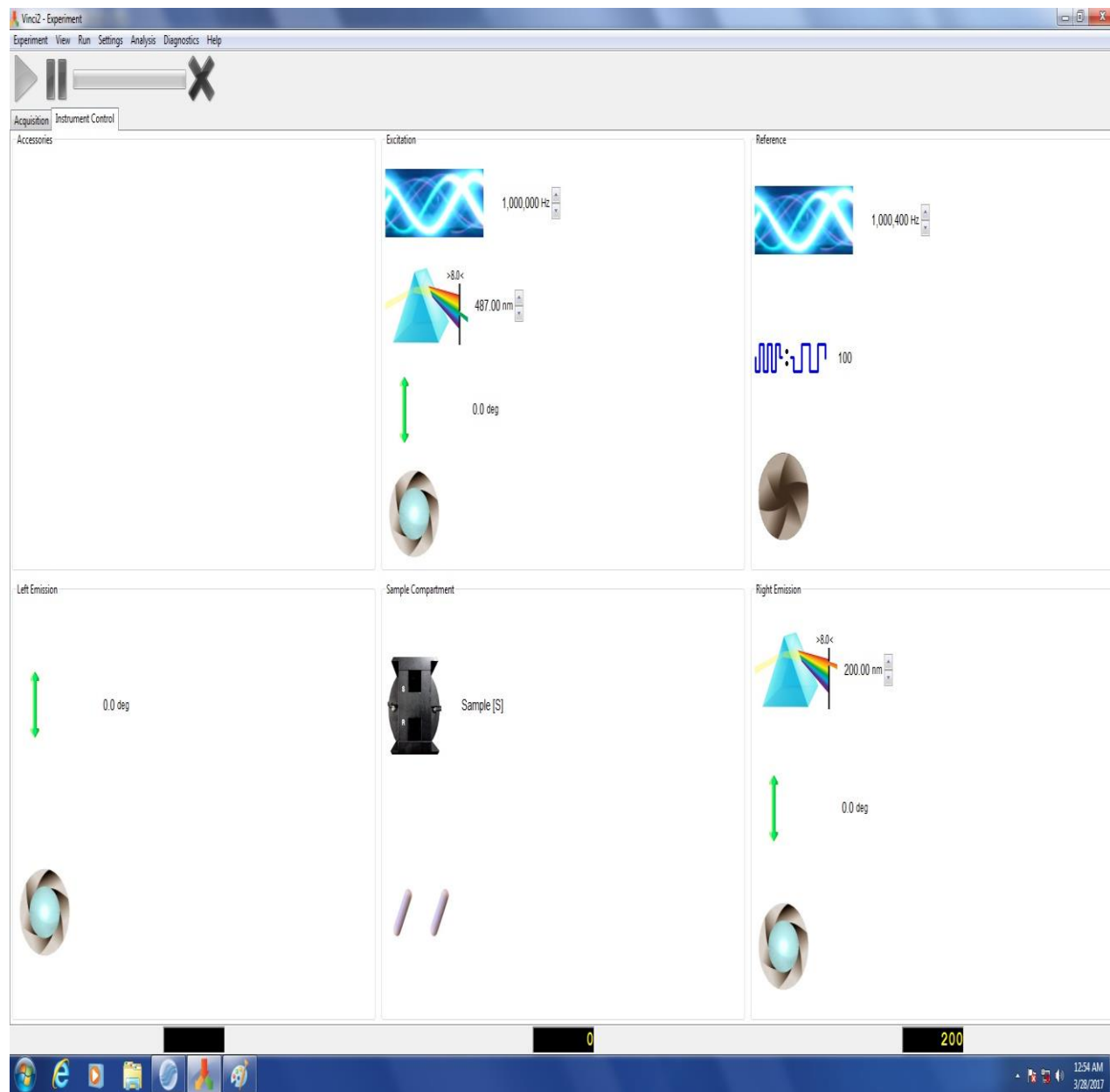


Figure 3.4: ISS K2 spectrofluorometer components with full command displayed in Vinci Software window

3.5 EXPERIMENTAL RESULTS:

3.5.1 Polymers and Nanoprobes:

We measured the fluorescence anisotropy of both Alexa 488 and Fluorescein dispersed in water as well as in PEG and PVA polymer solutions. In Figure 3.5 below, we show the measured phase delay and modulation ratio of Alexa488 and Fluorescein dispersed in water as a function of the applied modulation frequency of the incident polarized beam. Clearly, there is strong overlay of the measured phase delays and the modulation ratios of both nanoprobes in water.

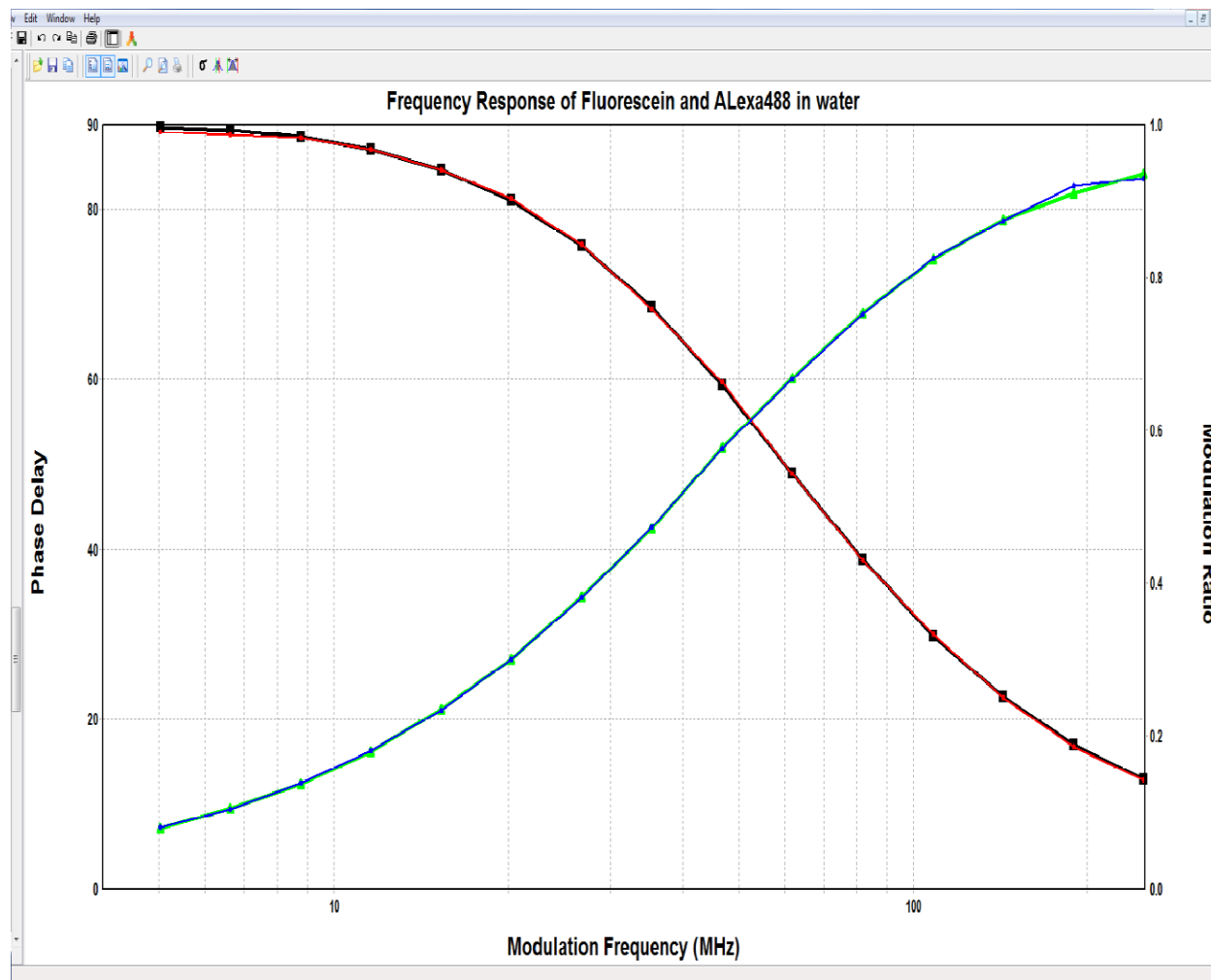


Figure 3.5 : Frequency domain intensity decays of Fluorescein in H₂O (green and black) and Alexa in H₂O (blue and red)

3.5.2 Calibration Test with Raman Spectrum:

To make sure that our instrument works well and to be certain that it functioned at the same level of accuracy throughout the experiment, Raman test was performed in the K2 spectrometer each time, before running any experiment with emission profile of scattering in water at 355 nm wavelength.

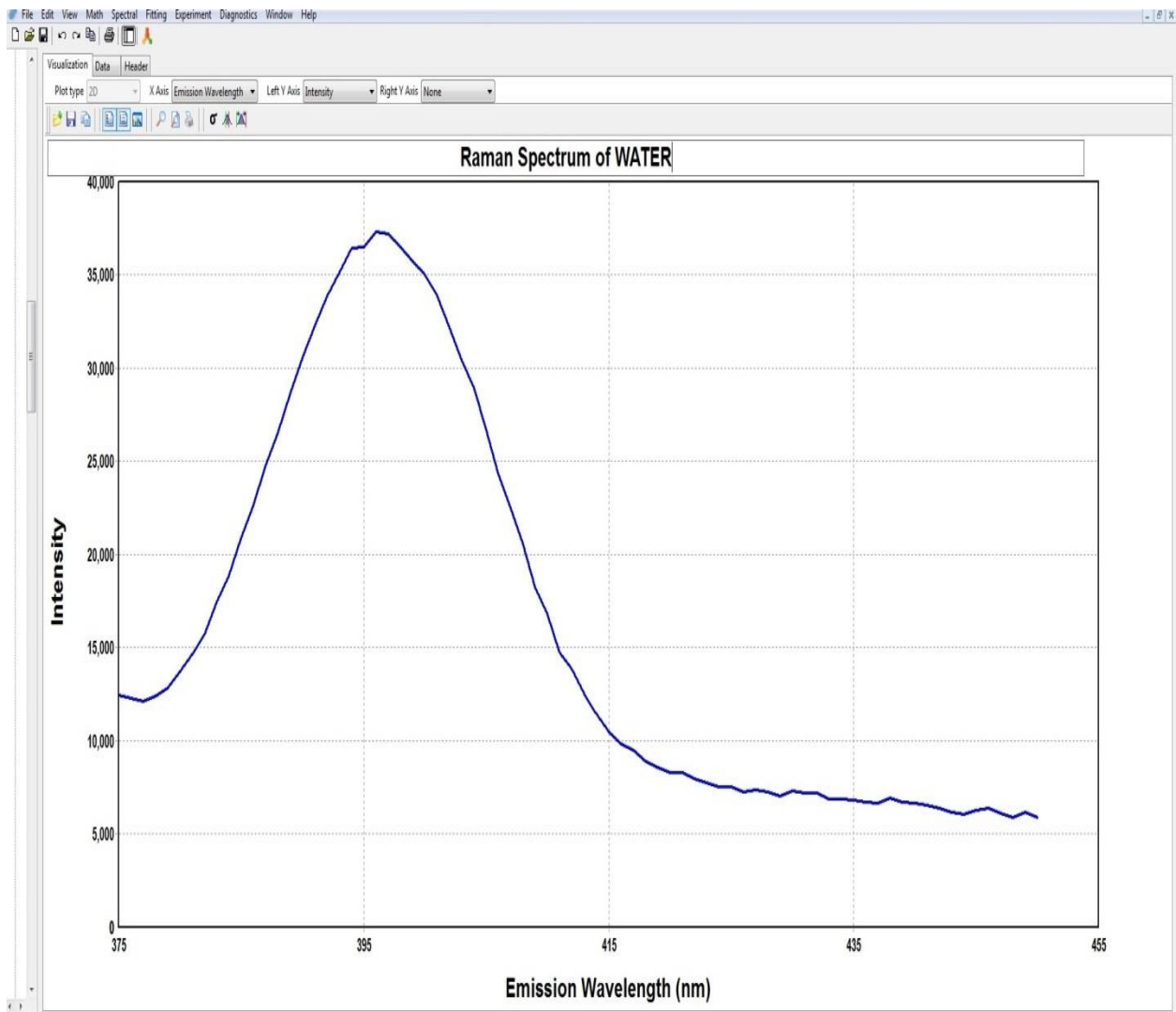


Figure 3.6: Raman spectrum of H₂O

Water is a very weak Raman scatterer, and typically is much weaker than other materials; additionally the water spectrum is very simple, with only a small number of peaks, so there is

minimum interference with peaks from the solute [90]. The intensity of the spectrum is a function of the lamp intensity and the monochromator slit bandwidths. The lamp current was set to 17 Amps on a 300 Watt Xenon lamp with a 2 mm slit on the excitation monochromator and a 1 mm slit on the emission monochromator. As shown in Figure 3.4 above the Raman spectrum obtained of water has a maximum of 398 nm and the Raman peak with 355 nm excitation (Collected with Photon counting).

3.5.3 Background Suppression, Sample, and Reference Preparation:

With the placement of a 500nm cut-off filter in the optical path after the sample, measurements were taken to measure the background spectrum from the scattered light by the polymers. The fluorescence emission spectra of PEG (500 mg/ml example) solution and Alexa488 in water are shown in Figures 3.7 and 3.8, respectively. Similar steps were performed on samples of PEG and PVA solutions to assess possible chemical interactions of the nanoprobe with the polymers. Here, filtered deionized water was used in preparation of different PEG and PVA concentrations. To ensure homogeneity, fluorophores were added and dispersed into the PEG or PVA solutions, and set aside for at least an hour. Then, the samples were poured into 10 x 10 mm optical path cuvettes.

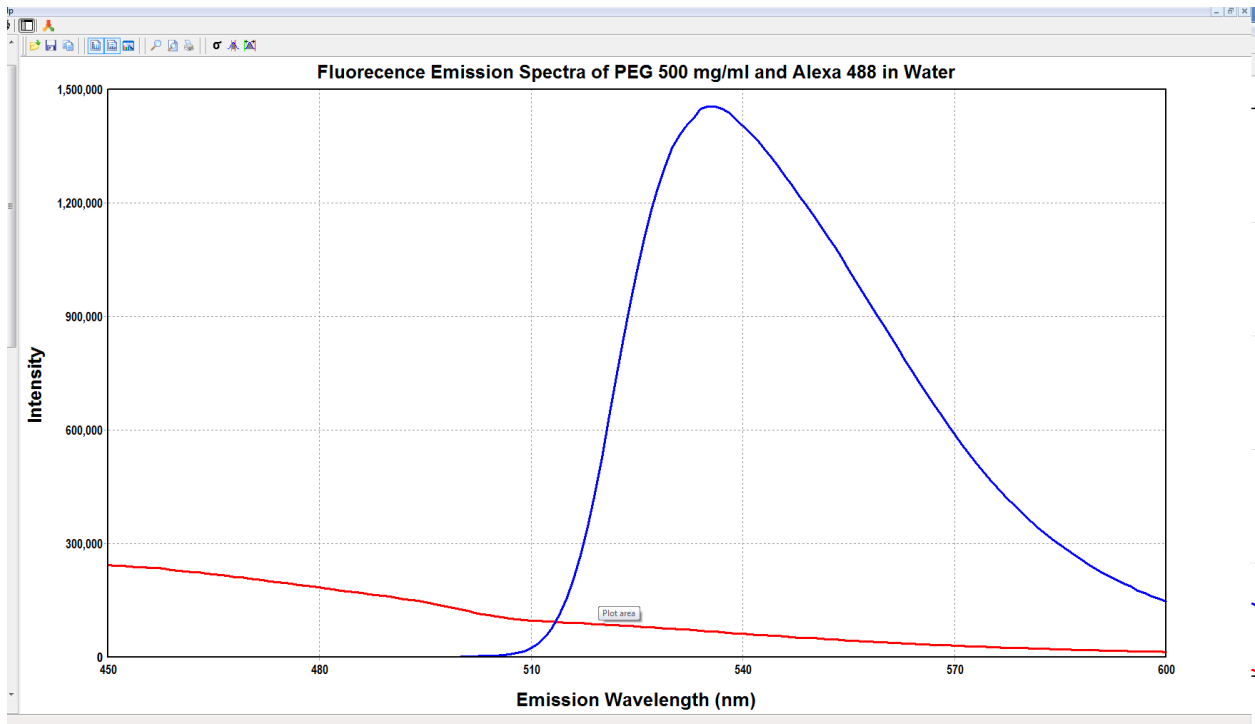


Figure 3.7: Fluorescence Emission Spectra of PEG 500 mg/ml (Red) and Alexa 488 in water (blue) without filter in the optical path.

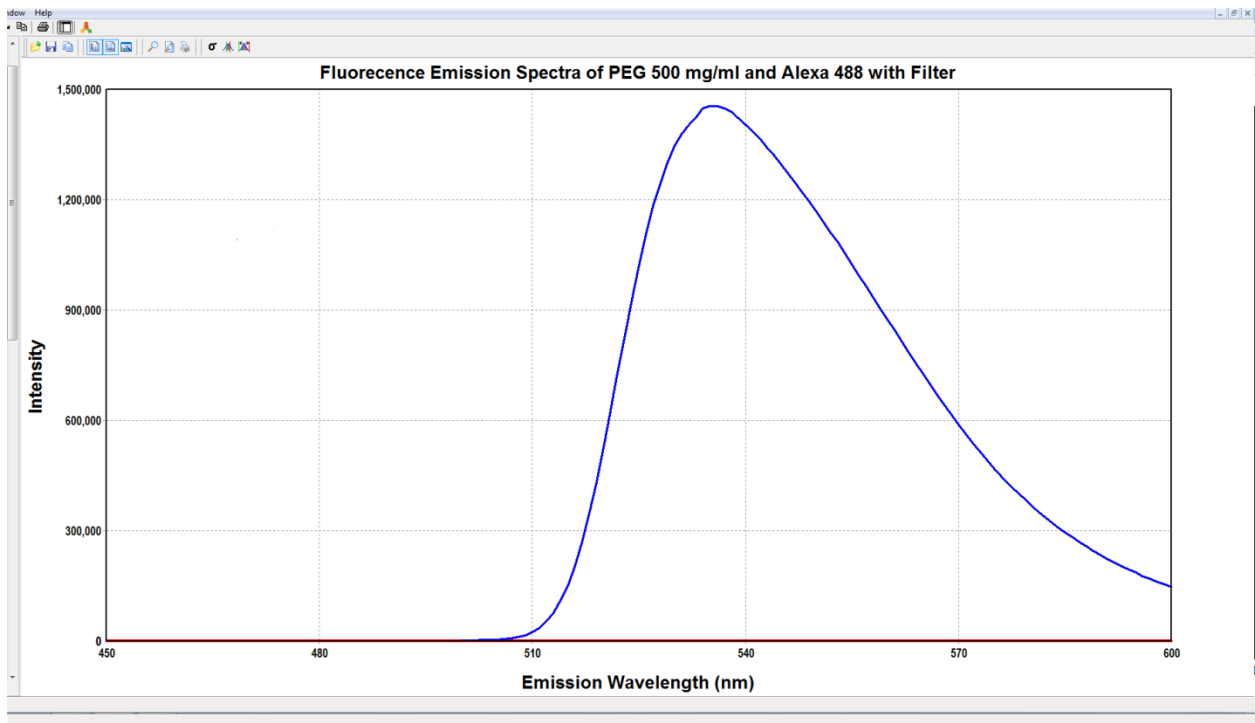


Figure 3.8: Figure: Fluorescence Emission Spectra of PEG 500 mg/ml (Red) and Alexa 488 in water (blue) with filter present in the optical path.

Using a reference solution prepared in a cuvette with a known single exponential fluorescence decay time and measuring the unknown sample mixture against this designated “Reference”, fluorescence lifetime, Rotational correlation time as well as the anisotropy can be obtained experimentally.

Our references were Alexa 488 in water with a known 4.02 ns lifetime and fluorescein in water with a known lifetime of 4.01 ns, both against all the samples at different concentrations of PEG and PVA. Figures 3.9 and 3.10 show examples of frequency domain intensity plots of different PEG and PVA concentrations with embedded Alexa488 nanoprobe.

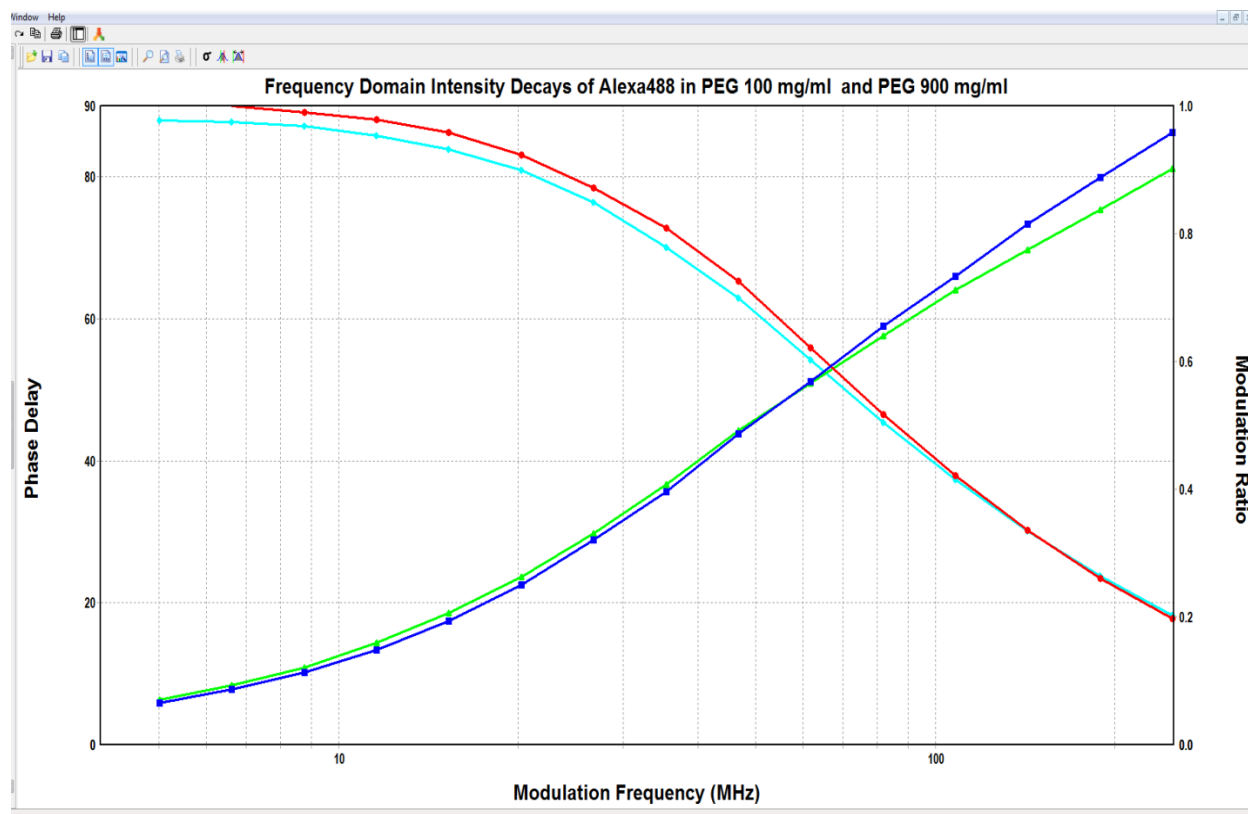


Figure 3.9: Frequency domain intensity decays of Alexa in PEG 100 mg/ml (green and light blue) and Alexa 488 in 900mg/ml PEG (dark blue and red)

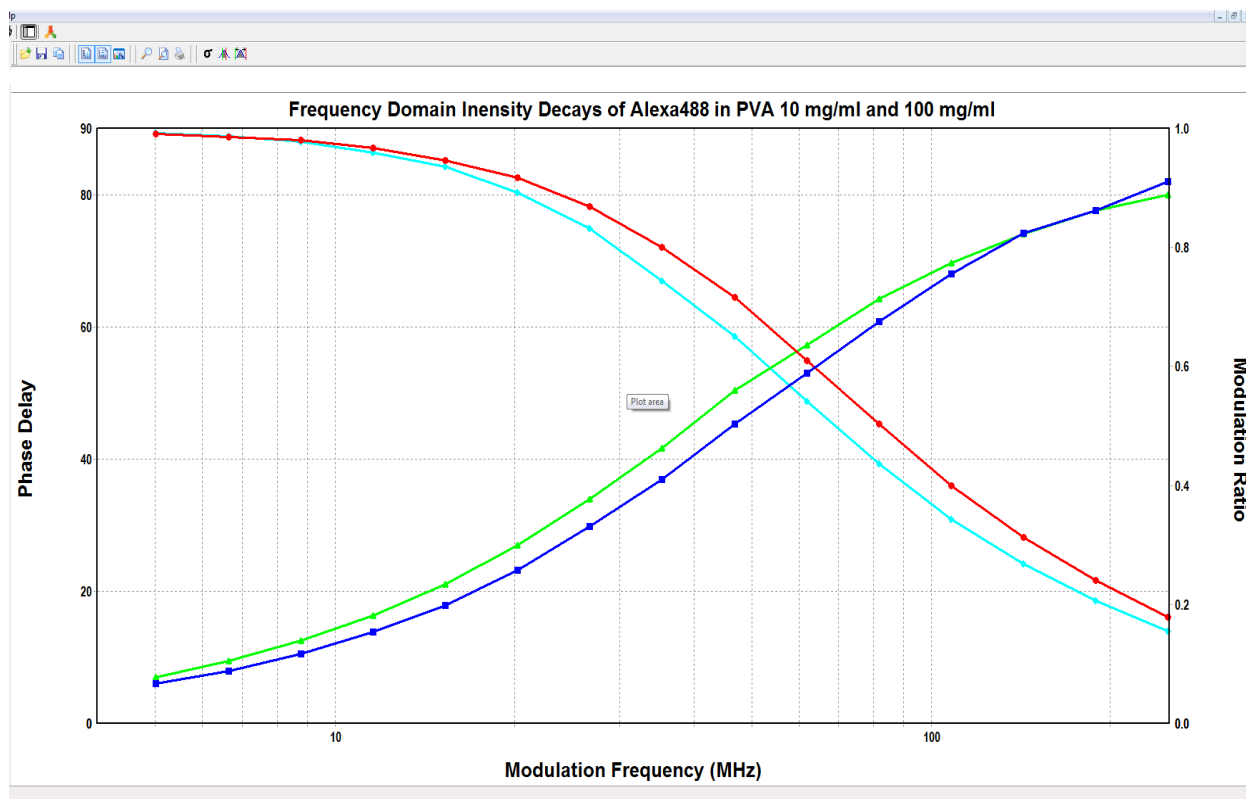


Figure 3.10: Frequency domain intensity decays of Alexa in PVA 10 mg/ml (green and light blue) and Alexa 488 in 100mg/ml PEG (dark blue and red)

3.5.4 Lifetime Measurements:

As indicated in Chapter 2 and will be listed in Tables 1 and 2 below in this chapter, there is no measureable change of the lifetimes of Alexa 488 or fluorescein as the polymer concentration was varied (see also emission spectra in Chapter 2). It is required to measure the phase angle and modulation of a sample to obtain fluorescence lifetime measurements in the frequency domain, then intensities of the sample and the reference are matched; this is achieved by diluting the sample with high counts. Intensities should be between 500-5000 photon counts and modulation should be greater than 2% at all frequencies. PMT gain settings were adjusted to help in the corrections as well. As the intensities were collected, each data point was acquired

over 0.5 seconds. We used a modulation range between 5 MHz and up to 300 MHz spanned over 15 points, and then the data were averaged. Here, 10 iteration experiments were examined.

3.5.5 Alexa488 in PEG and PVA Solutions:

Tables 1 and 2 below summarize the experimental values obtained with our fluorospectrometer on samples of Alexa488 dispersed in PEG and PVA solutions.

PEG concentration (mg/ml)	Life time (ns)	Rotational Correlation Time (ns)	Anisotropy Decay
00	4.00	0.176	0.151
50	4.10	0.281	0.248
100	4.16	0.324	0.280
200	4.10	0.570	0.290
500	4.20	1.420	0.308
700	4.10	1.700	0.313
900	4.10	3.210	0.322

PEG concentration (mg/ml)	Life time (ns)	Rotational Correlation Time (ns)	Anisotropy Decay
00	4.00	0.176	0.151
10	3.97	0.29	0.24
20	3.98	0.47	0.30
50	4.00	1.15	0.32
100	4.00	3.45	0.33
120	3.98	4.38	0.33

In the following, I will show examples of results and fitting from analysis of phase and modulation data, as well as the frequency domain differential polarization spectrum of the Alexa 488 in PEG and PVA. All FA derived values shown in Table 1 and Table 2 were obtained using the same steps as in these two examples.

Example 01: Alexa488 in PEG (500 mg/ml): Figure 3.11 shows the phase delay and modulation ratio as a function of the modulation frequency, which were measured on a sample of Alexa488 dispersed in PEG solution at [PEG]=500 mg/ml. Also, the data were fit with the expressions of Equations 3.4-3.9 and a single exponential fluorescence decay: $\tau = 4.019$ ns ($\chi^2 = 1.1$) and the results of the fits are included in Figure 3.11 as solid lines. Also, the residuals of the fits are shown in the lower window. Using Perrin equation (Equation 3.20) and the values of the lifetime of Alexa488 in PEG (4.20 ns) and fluorescence anisotropy (0.308) we determined the rotational correlation time to be 1.42 ns.

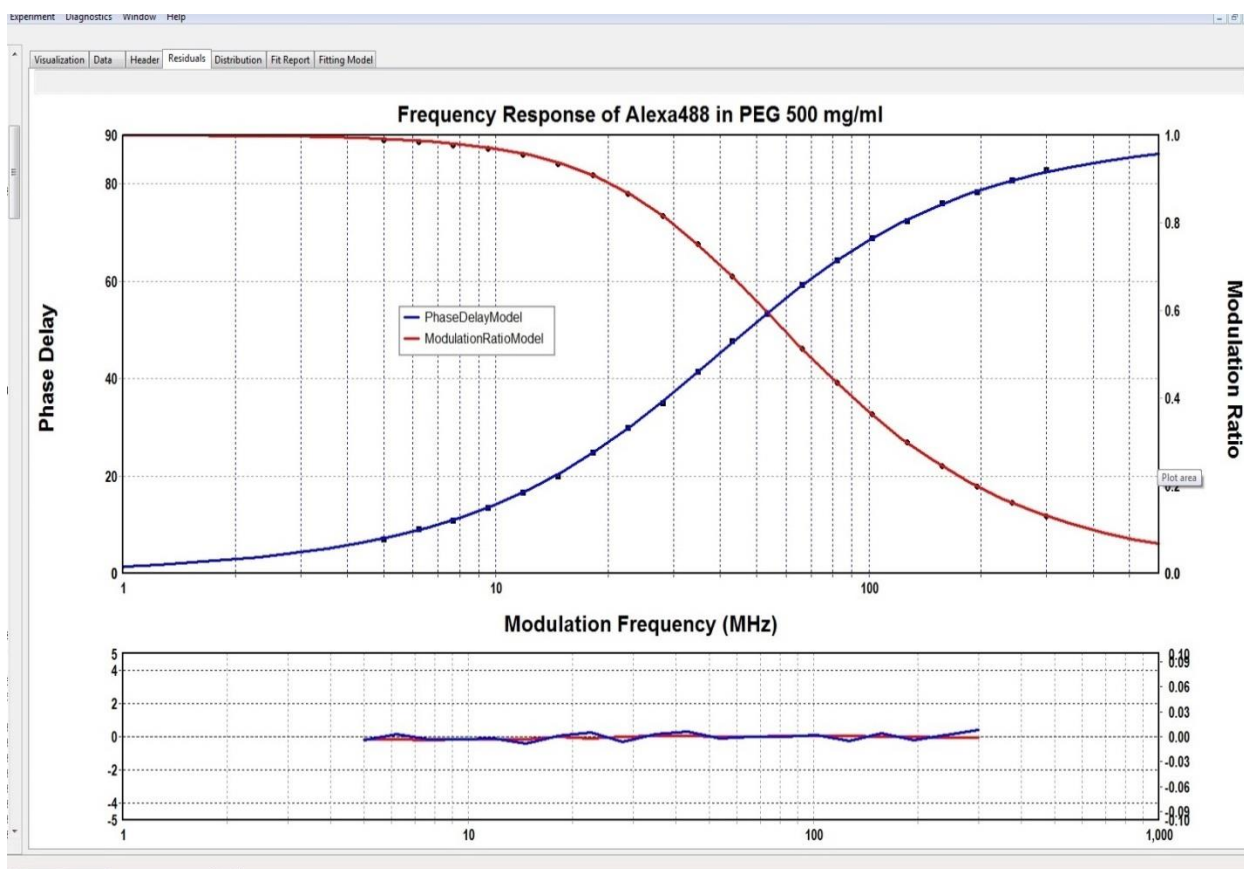


Figure 3.11: Frequency response of Alexa488 in PEG 500mg/ml. Data are the solid dots, Solid line represents the best single exponential fit

In Figure 3.12, we show the frequency domain differential polarization spectrum of Alexa 488 in [PEG]=500 mg/ml as well as its respective derivation of the fluorescence between the parallel and perpendicular orientations (modulation ratio and differential phase).

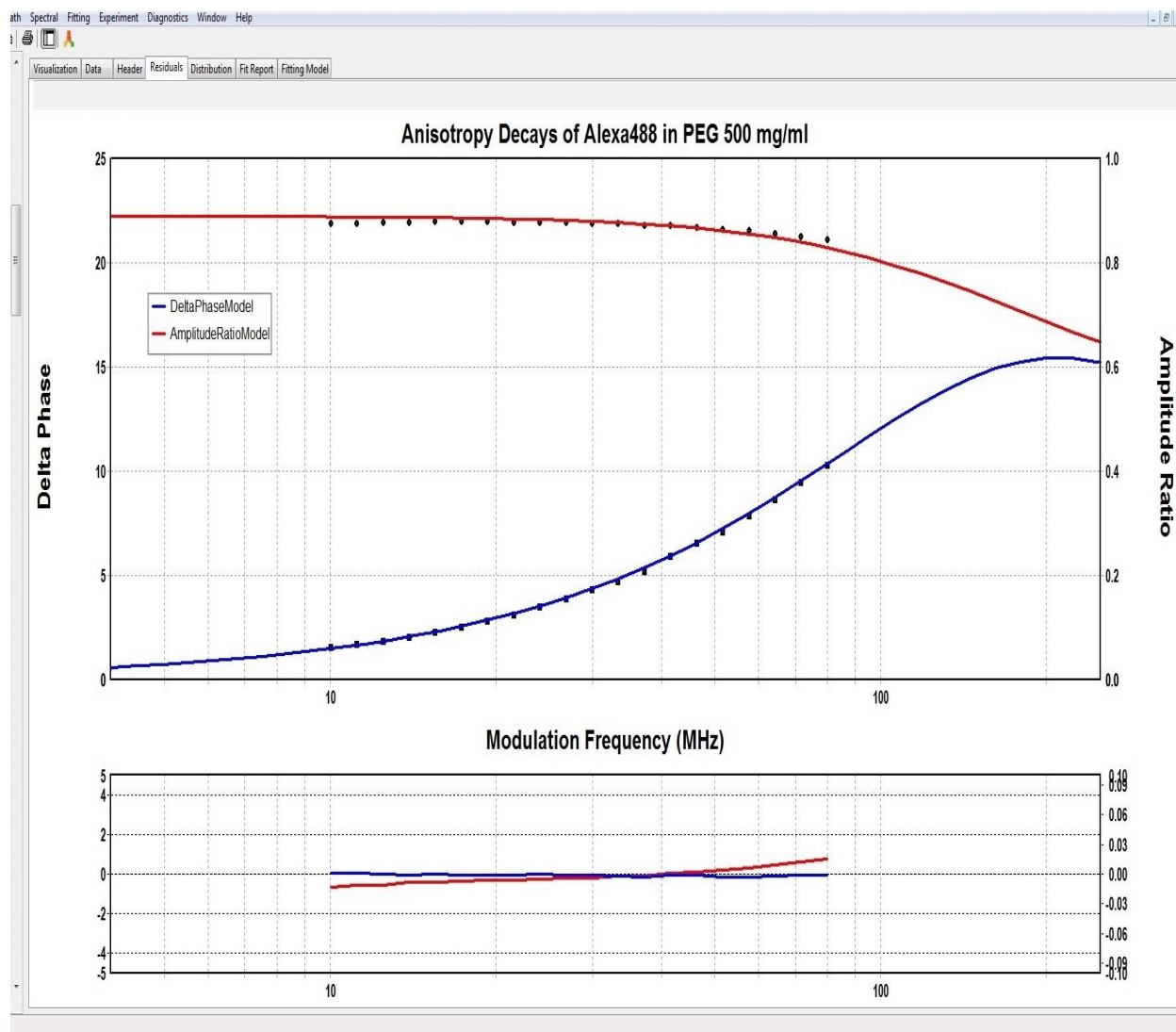


Figure 3.12: Differential Polarized Phase Angle and Amplitude Ratio (Frequency domain anisotropy decays) of Alexa 488 in PEG 500mg/ml

Example 02: Alexa488 in PVA (100 mg/ml): Using the same steps in Example 01 with PEG, we determined the rotational time of Alexa488 in PEG solution ($[PEG]=100\text{ mg/ml}$) to be 3.45 ns with the lifetime (4.00 ns) and fluorescence anisotropy of 0.33. Figures 3.13 and 3.14 show similarly the measured (markers) and fitted (solid lines) phase delay/modulation ratio and delta phase/amplitude ratio as function of the modulation frequency. The residuals of the fits are included for each set of data.

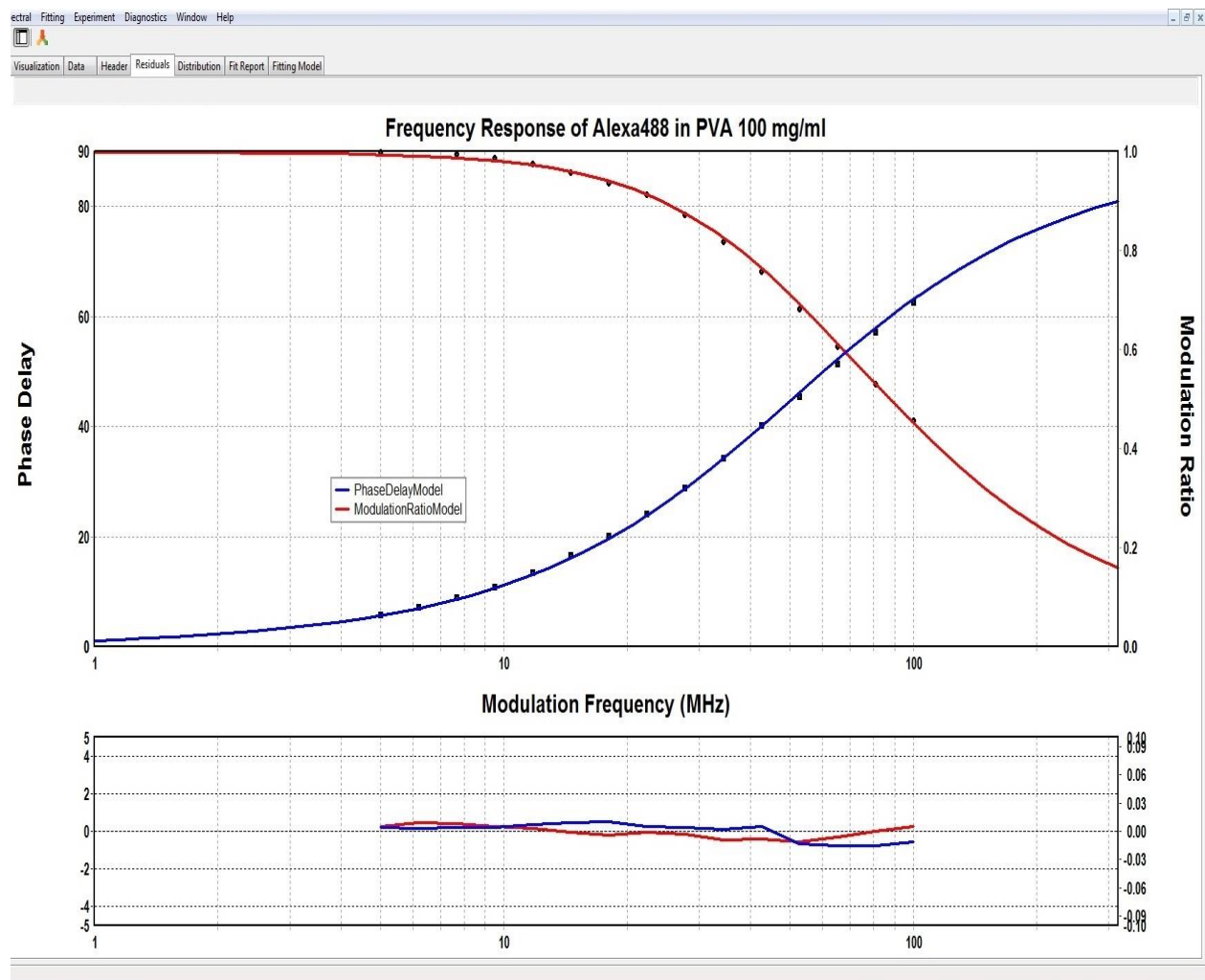


Figure 3.13: Frequency response of Alexa488 in PEG 100mg/ml. Data are the solid dots, Solid line represents the best single exponential fit

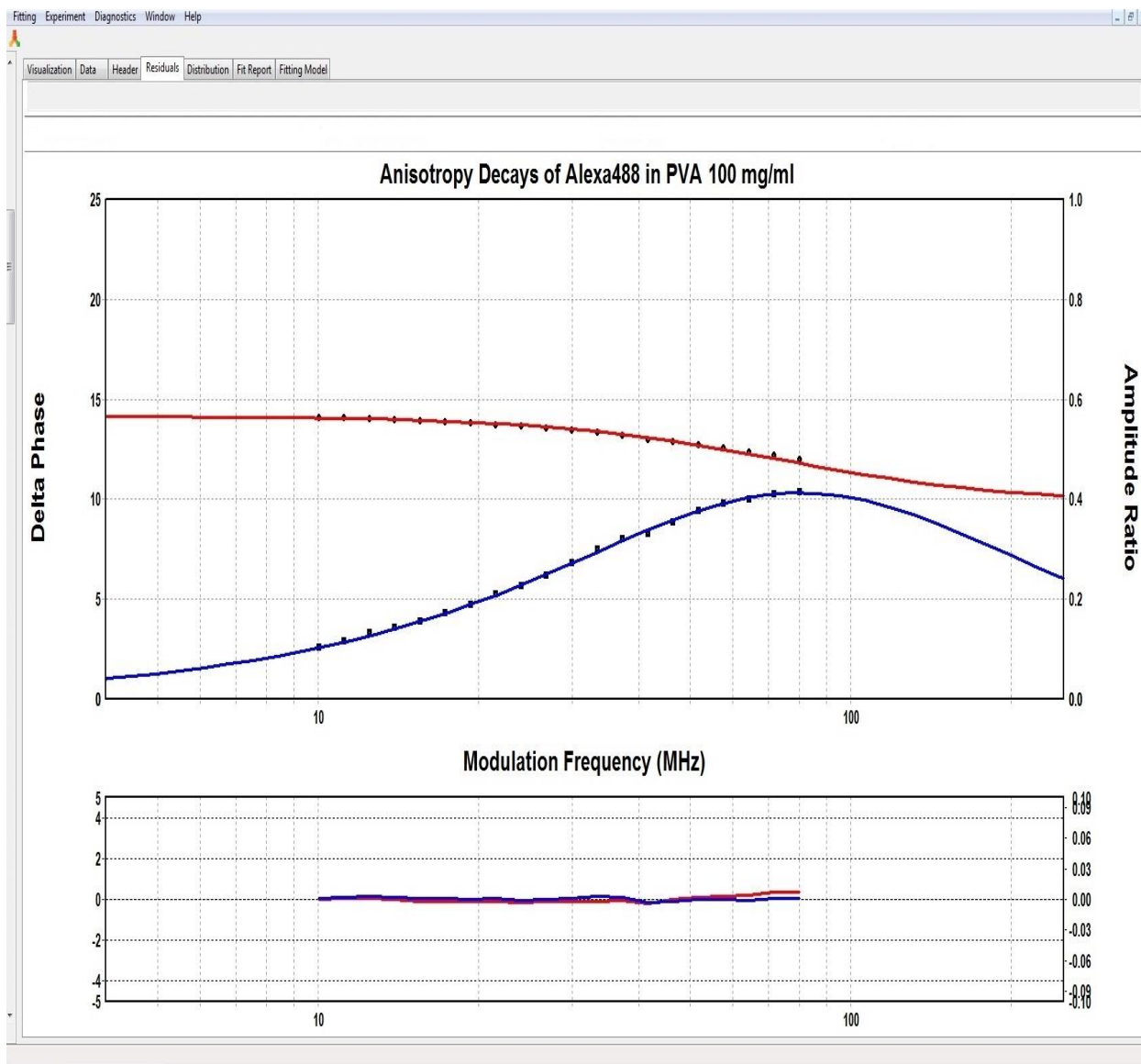


Figure 3.14: Differential Polarized Phase Angle and Amplitude Ratio (Frequency domain anisotropy decays) of Alexa 488 in PEG 100mg/ml

3.5.6 Rotational Correlation Times of Alexa488 Vs. Polymer Concentration:

In Figures 3.17 and 3.18 we show changes of the rotational correlation times of Alexa488 as a function of the concentration of PEG and PVA solutions, respectively. Both figures indicate that the higher the polymer concentration, the slower the rotation of Alexa488 as should be expected. For similarity with the data of the translational diffusion coefficient, we plot in Figures 3.19 and

3.18 the concentration dependence of the inverse of the rotational correlation time, which is proportional to the rotational diffusion coefficients, $D_{R(PEG)}$ and $D_{R(PVA)}$. Now, we fit the data were fitted with a stretched exponential ($Ae^{-\beta c^n}$) as was done with the translational diffusion data (see Figures 2.29 and 2.30). Remarkably, both fits yield similar n -values: $n=0.70\pm 0.02$ for PEG solutions and $n=0.72\pm 0.02$ for PVA solutions, which are both close to the theoretical value, $n=3/4$, for good solvents according the expression suggested by de Gennes and his collaborators (see expression in Eq. 2.17 in Chapter 2). However, the prefactor, β , appears to depend on the polymer: $\beta(PEG)=0.025 \pm 0.002$ and $\beta(PVA)=0.112\pm 0.007$.

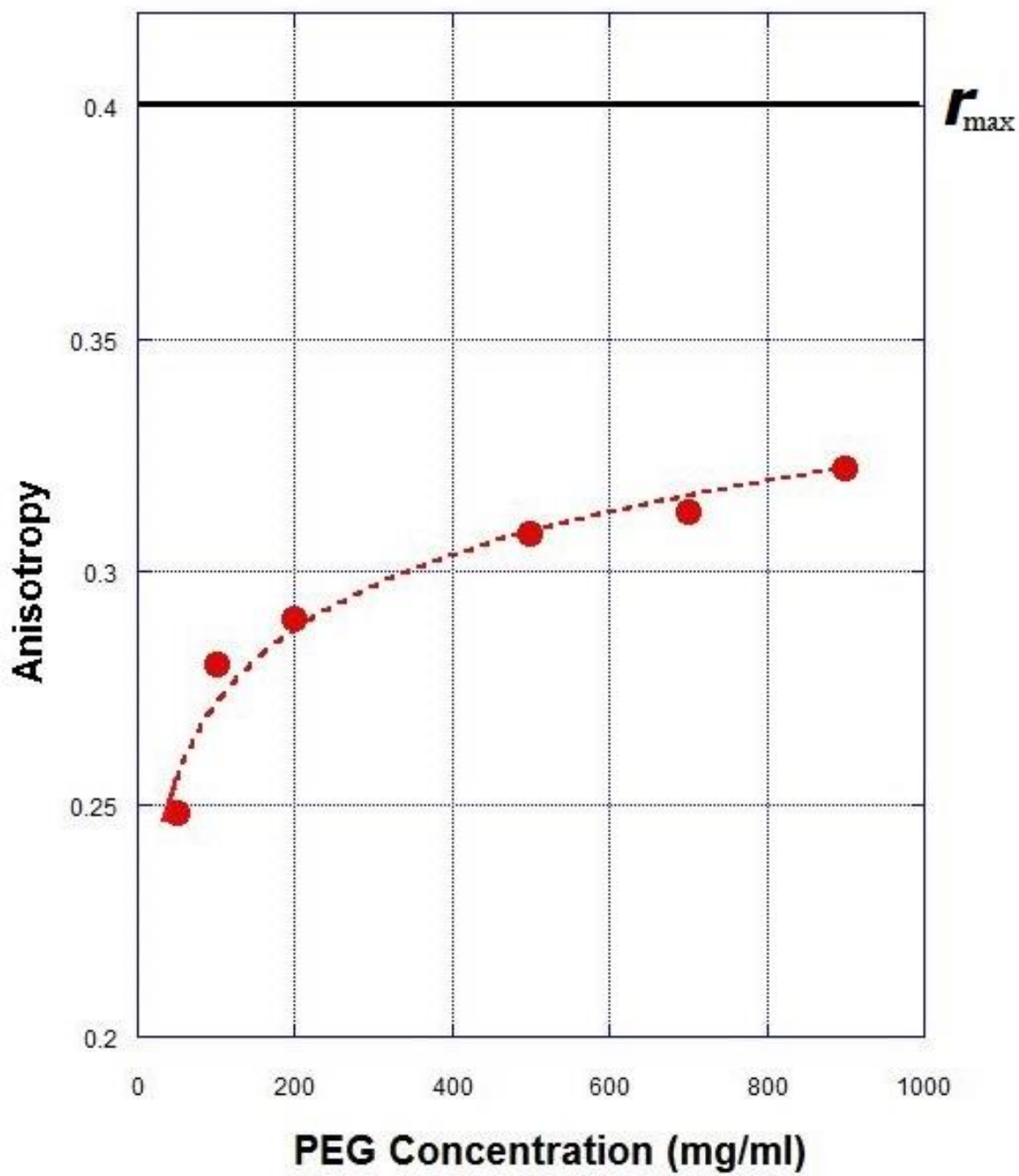


Figure 3.15: Anisotropy of Alexa488 fluorophore as function of PEG concentration

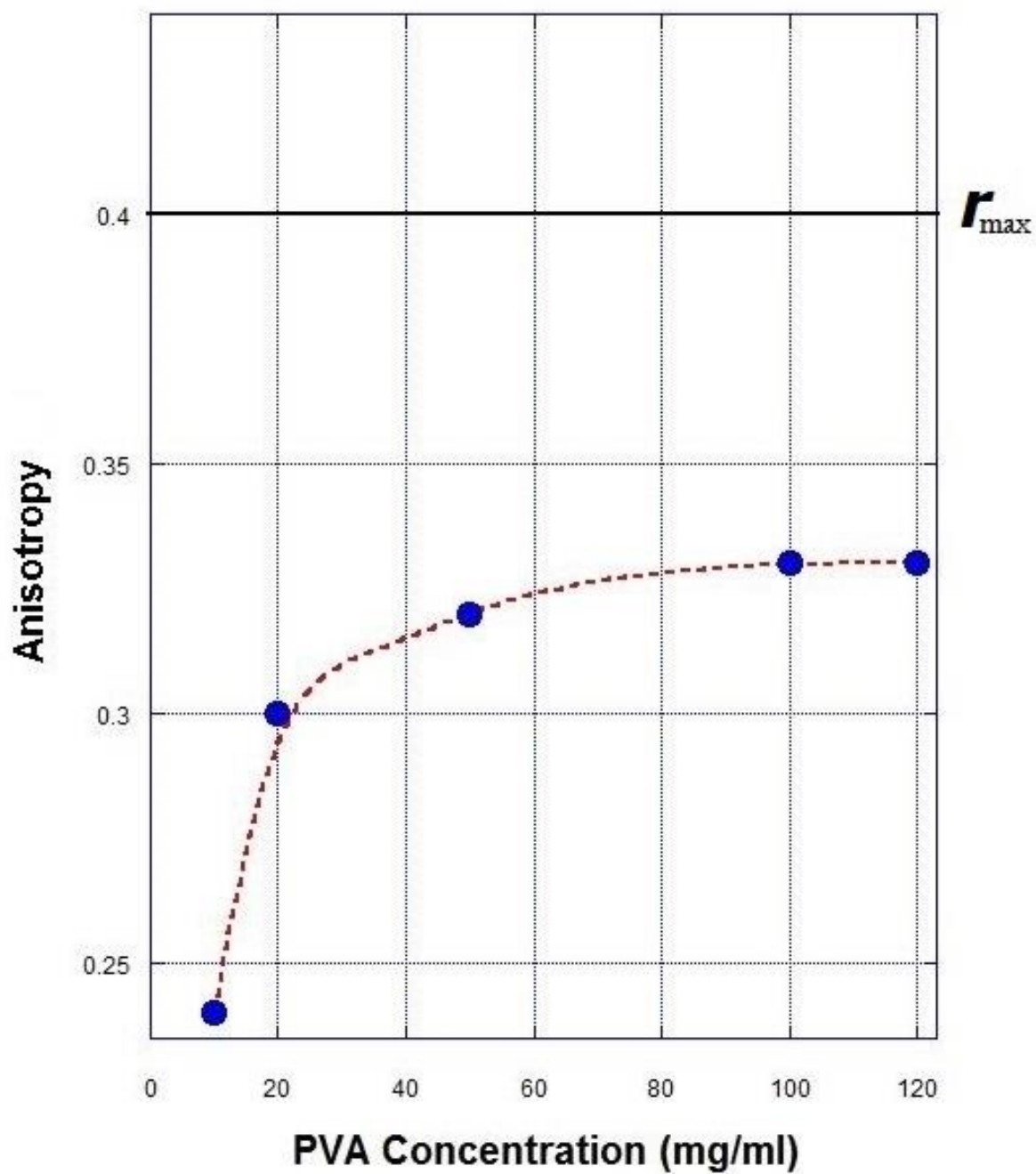


Figure 3.16: Anisotropy of Alexa488 fluorophore as function of PVA concentration

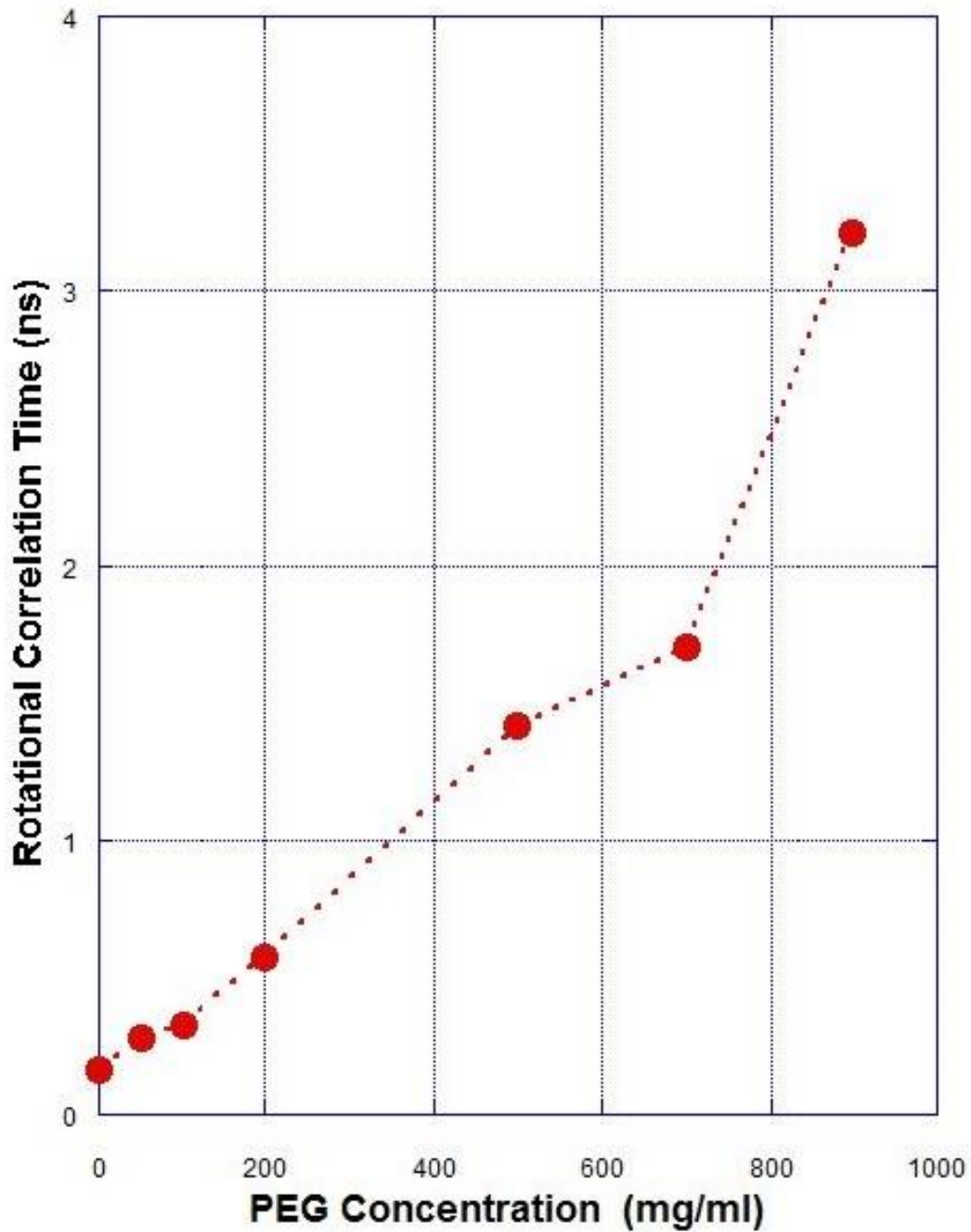


Figure 3.17: Rotational Correlation time of Alexa488 fluorophores as function of PEG concentration

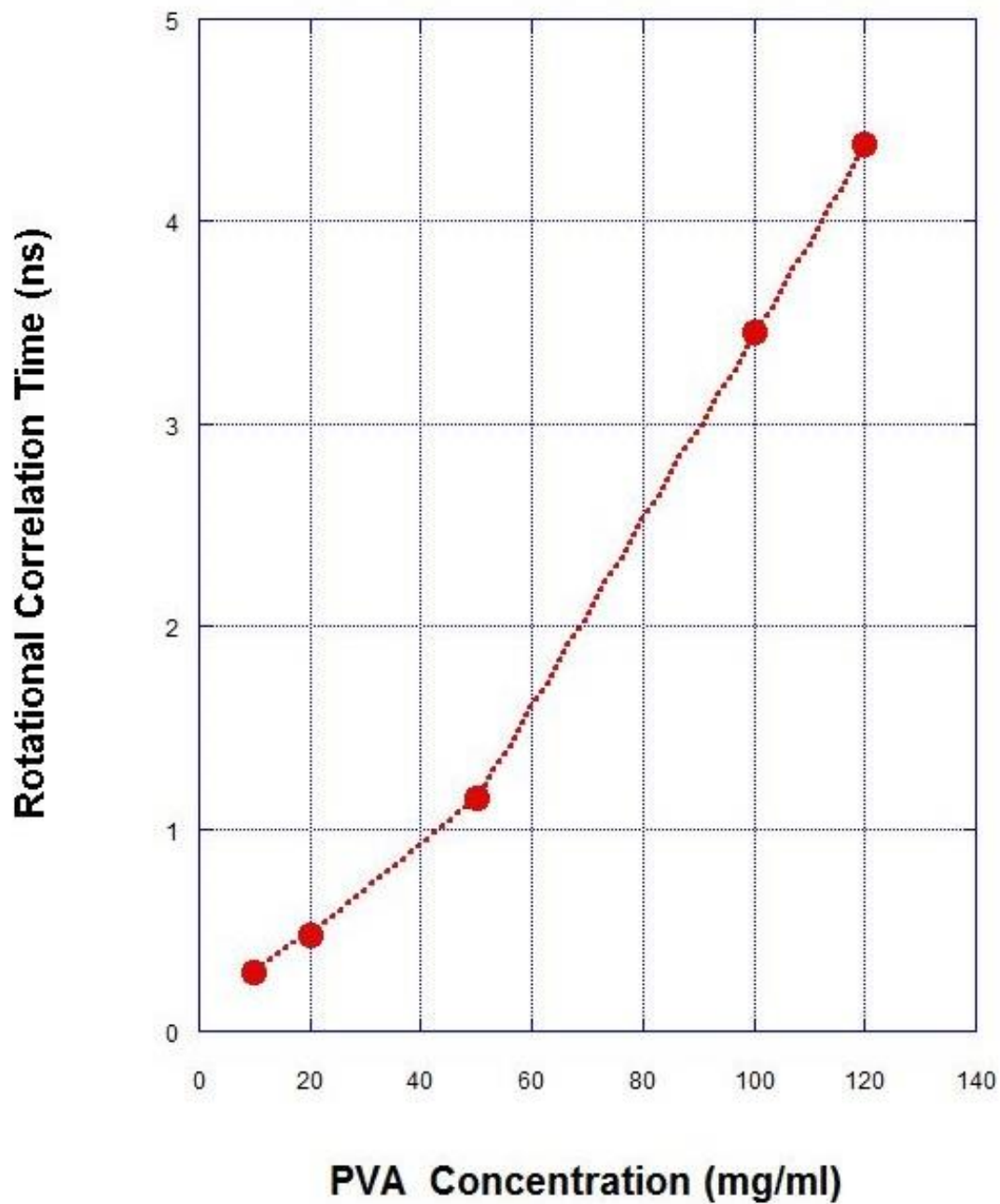


Figure 3.18: Rotational Correlation time of Alexa488 fluorophores as function of PVA concentration

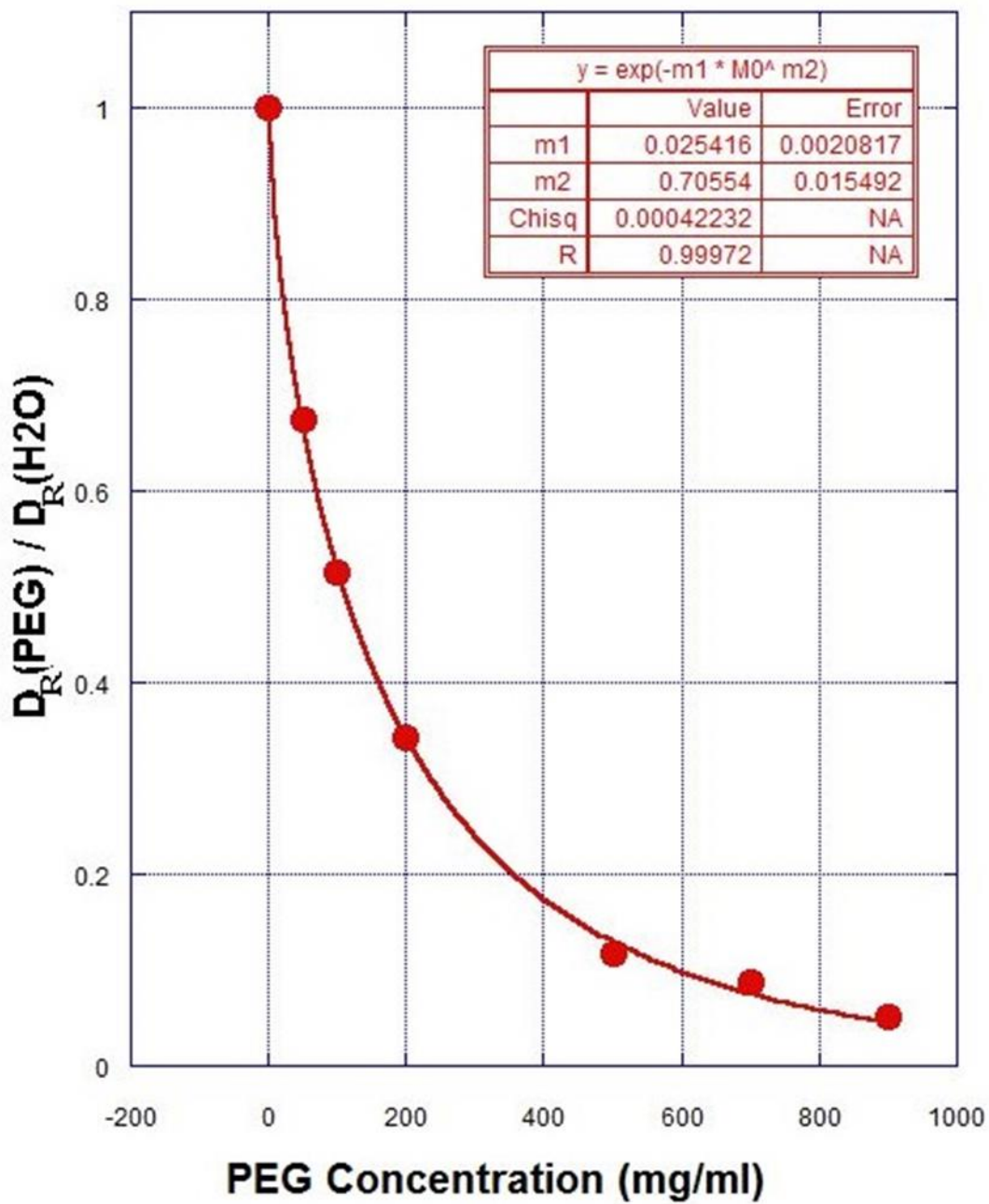


Figure 3.19: Rotational diffusion coefficient of Alexa488 fluorophore as function of PEG concentration

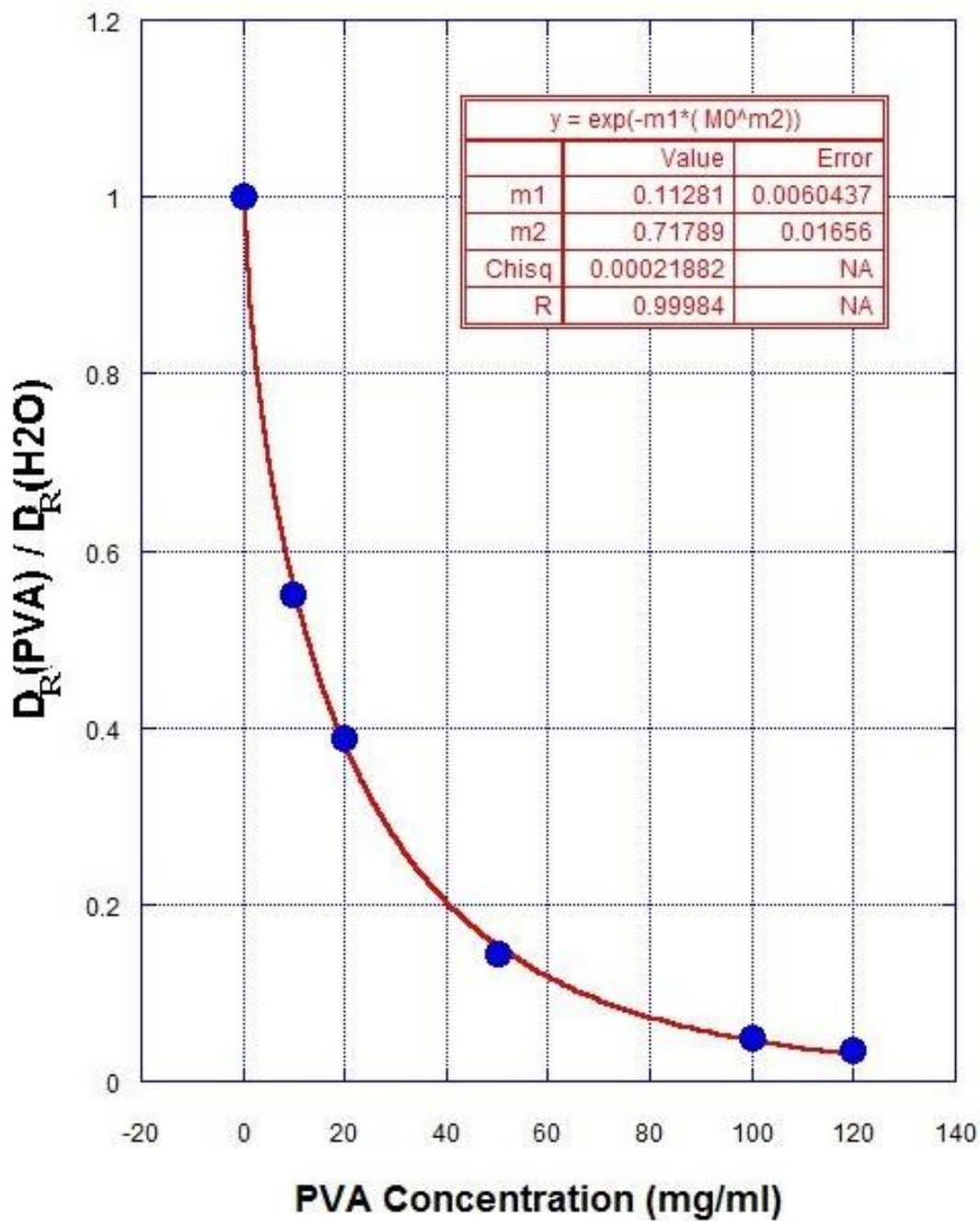


Figure 3.20: Rotational diffusion coefficient of Alexa488 fluorophore as function of PVA concentration

3.6 Summary and Conclusions of Chapter 3:

In this chapter 3 I focused on a different aspect of the effects of PEG and PVA linear polymers on the behavior of two nanoprobes, Alexa488 and Fluorescein, namely their rotational behaviors. Here, I described the fluorescence anisotropy (FA) method and FA-measurements in samples of mixtures of nanoprobe-polymer solutions, where the polymer concentration was varied. We used K2 fluorospectrometer designed and distributed by ISS company, which is based on frequency-modulation technique. Analysis of the anisotropy data indicates:

- The fluorescence anisotropy of Alexa488 increased systematically as the PEG (see Figure 3.15) or PVA (see Figure 3.16) concentration was increased, approaching steadily to the theoretical value, $2/5$, derived for immobilized fluorescent particles whose dipole moments were randomly oriented in the system.
- Using Perrin Equation and the measured lifetimes of the nanoprobes we determined the changes of the rotational correlation times of the nanoprobes with increase of PEG and PVA concentration.
- We used a stretched exponential ($Ae^{-\beta c^n}$) to fit the data, as suggested by de Gennes and his collaborators. We determined the values of the exponent, n for both polymer solutions to be close to that of a good solvent, namely $3/4$. Further, the value of the prefactor, β , appeared to depend on the polymer.

CHAPTER IV: DISCUSSION & CONCLUSIONS

Macromolecular crowding is now well-recognized to play a significant role on the behavior of macromolecules, including slowing of diffusion, enhancing polymerization or aggregation of the molecules, and inducing chemical reactions between the molecule and other molecules or macromolecules. Elucidation of this role may provide, in particular, insight into many biological processes relevant to cell division, growth, and motility. For fundamental studies it has been suggested that polymeric solutions, especially semi-dilute to concentrated polymeric solutions, may mimic the macromolecular cellular environments such as the cytoplasm. More practically, polymeric solutions represent simpler systems compared to the complex cellular structures and dynamics. In my work, here, I used two aqueous polymeric solutions of Poly(vinyl) Alcohol (PVA) and Polyethylene Glycol (PEG). Both polymers are linear and can be readily dissolved in water. And I focused on elucidating and measuring the translational and rotational diffusions of small molecules or nanoprobe dispersed in these solutions.

In an earlier investigation we undertook the initiative of elucidating the translational and rotational behavior of nanoprobe in Ficoll solutions. Ficoll is a branched polysaccharide and provides various attributes, including high solubility in water, optical transparency when dissolved in water, biocompatibility, and neutrality. We applied successfully various tools (FCS, FA, time-lapse imaging, viscometry) to measure changes of the translational and rotational diffusion of several nanoprobe (e.g. Alexa488 and FITC-Ficoll) as a function of Ficoll concentration at room temperature. In Refs [37,38], we reported that the changes of the diffusion coefficients could not be accounted for by the corresponding changes of the bulk viscosity of the Ficoll solutions as would suggest the Stokes-Einstein relations for both diffusion coefficients. As described in Chapter 2 of this dissertation, we introduced the entropic model proposed by

de-Gennes and his collaborators, and fitted each set of the measured data with a stretched exponential [$\exp(-\alpha c^n)$] with n being related to the quality of the solvent. For both sets the fits yielded n -value close to 3/4, suggesting a good solvent behavior of the host polymer-water system. The α -value for translation was very similar to that β - value of rotation in both PEG and PVA solutions, indicating similar local entropic effects on the rotation and translation, however, the α -value for translation was larger than that α - value of rotation in branched polymer like Ficoll[37] which was not discussed by de Gennes and his collaborators.

The results from the Ficoll study opened various questions when contrasted with other results derived from different types of polymers such as linear PVA [37]. For example, it was unclear whether the polymeric structure –branched vs. linear- induce different crowding effects on the translation and rotation of the nanoprobe. And this is the main focus of this work and the presented results in Chapters 2 and 3. Here, the approach developed for the study of nanoprobe in Ficoll solutions was followed with linear polymer solutions in order to get comparable data and insight. I measured both the rotational diffusion and the translational diffusion of Alexa488 and fluorescein as a function of the PVA and PEG concentration.

Most of my work capitalized on exploiting the fluorescence property of Alexa488 and fluorescein against the non-fluorescent –hence “invisible”- PEG and PVA. In Chapters 2 and 3 I extended and combined FCS and FA methods to measure changes of the apparent translational diffusion and the apparent rotational diffusion as a function of PEG or PVA concentrations. Overall, our analysis centered on comparison of the fits of the measured changes of the rotational and translational diffusion coefficients with increase of the polymer concentration. Remarkably, the dependence of the translational diffusion coefficient and the rotational diffusion coefficient of the nanoprobe on the polymeric concentration (c) appears to be adequately described by a

stretched exponential ($\exp(-\alpha c^n)$), an expression used successfully by many researchers to fit similar data [38]. More challenging has been the design of a theoretical model to interpret the results. Here, the entropic-based model proposed by de Gennes and his collaborators yields a stretched exponential for the dependence of the diffusion coefficient on the polymeric concentration. It provides a physical-based model to interpret the exponent, n , and the prefactor, α for translational diffusion and β for rotational diffusion. In the following I will discuss and analyze the experimental results described in Chapters 2 and 3, and compare the results with those obtained for Ficoll [37] and those published already on PVA system [67,82].

4.1 Results from Fluorescence Spectroscopy:

PVA and PEG do not affect significantly the fluorescence property of Alexa488 and Fluorescein.

Error! Reference source not found. 2.17-2.20 show small shift of the fluorescence spectra of Alexa488 or fluorescein with increase of PVA or PEG concentration and Figures 2.21-2.22 indicates no observable effect of PVA or PEG on the lifetime of the fluorophore with an average lifetime of 4.0 ± 0.2 ns, which is the same as that reported in the literature [38]. Both results demonstrate relative stability of the fluorophores while diffusing in the polymer solutions, and it is then reasonable to attribute observable changes in the diffusion of the fluorophores to changes in friction or entropic effects due to changes of the host polymeric system.

4.2 Results from FCS Measurements:

A particular observation should be emphasized about the systematic uniform shift of the measured FCS correlations of Alexa488 or Fluorescein as a function of the PEG or PVA concentration (see Figures 2.25- 2.28 and 2.23-2.24). More interestingly, the correlations were

readily fit with an expression (see Eq.2.10) derived for a molecule freely diffusing due to thermal fluctuations. That is, no anomalous diffusion was needed to analyze and interpret the FCS data as was already pointed out in the case of PVA solutions [67] and Ficoll solutions [37]. Both these observations should be contrasted to the anomalous diffusion observed on other types of nanoprobe (e.g. proteins) moving in different complex solutions (see Refs.[48,44,71]).

4.3 Results from FA Measurements:

In contrast to FCS, fluorescence anisotropy method is based on measurements of emitted fluorescence intensities at two perpendicular directions relative to that of the incident excitation beam. The measured fluorescence depolarization or anisotropy at the two angles depends on the relative difference between the rotational time of the fluorescent molecule (~ sub- to nano-seconds) and the modulation frequency of the K2 spectrofluorometer used in our study (up to 400 MHz). Our anisotropy measurements become more reliable and reproducible as the polymer concentration is higher, which, in principle, should hinder and slow down the rotation of the embedded Alexa488 or Fluorescein. This can be readily noticed in Figure 3.15-3.16 which shows systematic increase of the measured fluorescence anisotropy of fluorophores with increase of the polymer concentration. Further, Figures 3.15 and 3.16 indicates that the measured anisotropy was approaching the limiting theoretical value, $2/5$, related to “frozen”, non-rotating, and randomly oriented polarization axis of Alexa488 in the sample.

Figures 3.17 and 3.19 show respectively the concentration dependence of the rotational correlation times and the corresponding rotational diffusion coefficient data of Alexa488 dispersed in PEG solutions, which were derived from the measured anisotropy data in Figure 3.15. Here we assumed that the Perrin equation is valid as expressed in Equation 3.20. Figures

3.19 and 3.20 shows remarkably a stretched exponential behavior. We first note that the derivation of the expression in Eq.2.17, the stretched exponential, was argued for translational diffusion. It was unclear how to extend the expression to rotational diffusion. We argue, however, with the scaling of the frictional coefficient expressed as ϕ in section 2.5.3. In principle, one should assume that the rotation of the particle is also affected by the same friction, and we should surmise then that $f_c/f_0 = D_0/D_R$ for the rotation with D_R describing the rotational diffusion coefficient of the particle in the host polymeric system. Further, this equation would obey the same scaling function in Eq.2.17, and if we follow the same derivation in Section 2.5.2, we would end up with the same stretched exponential shown in Eq.17 for the translation. That is, the scaling argument should lead to the same stretched exponential [$\exp(-\alpha c^n)$] for both rotation and translation if the friction due to the polymeric environment affects equally the rotation and the translation. This argument provides a heuristic explanation for the n -value close to 3/4 found in both experimental data for the translation (Figures 2.29 and 2.30) and the rotation (Figures 3.19 and 3.20) in PEG and PVA solutions.

Moreover, the derived values for the prefactors (α and β) the stretched exponential appears to depend on the polymer: PVA vs. PEG. This can also be noticed in the translational data (Figure 2.29 and Figure 2.30), where we would argue that it is due to the PVA polymer (MW~85KDa) being larger than the PEG polymer (MW ~ 10KDa). Also, we should notice that unlike PEG solutions, PVA is prone to hydrogen binding, which tends to yield a gel at appropriate PVA concentration.

More noticeably is the comparative values of α and β which were derived from the rotation and the translation for the same polymeric solution: PEG (Figure 2.30 vs Figure 3.19) and PVA (Figure 2.29 vs. Figure 3.20). For PEG, $\alpha(\text{translation}) = 0.024 \pm 0.006$ and $\beta(\text{rotation})$

= 0.025 ± 0.002 , which can be considered the same given the uncertainty values from the fitting. Similarly, for PVA $\alpha(\text{translation}) = 0.100 \pm 0.011$ and $\beta(\text{rotation}) = 0.112 \pm 0.006$, can also be considered the same given the uncertainty values from the fitting. *As such, one may conclude that for both cases the polymeric frictional environment affects similarly the translation and the rotation of the nanoprobes.*

4.4 Analysis of FCS Data with Viscosity Data

Changes of both types of diffusion cannot be accounted for by changes of the bulk viscosity. Both Stokes-Einstein relations for the translational diffusion coefficient and the rotational diffusion coefficient of a particle suggest that these coefficients should depend inversely on the viscosity of the host medium. That is, the higher the polymeric concentration, the slower the translation and the rotation. Although we find systematic decrease of both coefficients with the increase of the polymer (PEG or PVA) concentration (**Error! Reference source not found.2.30** and 3.19 or Figure 2.29 and **Error! Reference source not found.3.20**), the overall increase of the bulk viscosity of the PEG or PVA solutions is much higher. The case of PVA was already discussed in the literature [67], where the viscosity data of PVA solutions were reported. It was shown that the bulk viscosity data could be appropriately used to interpret changes of the translational diffusion of relatively large beads moving freely in PVA solutions prepared at different concentration. This is consistent with the Stokes-Einstein relations. However, it is not the case with the nanoprobes, and it was argued that one has to go beyond the Stokes-Einstein relation such as the model presented by de Gennes and his collaborators (see Section 2.5.2).

For PEG solutions we used the viscosity data published by Gonzalez-Tello et al [78]. For PEG8000 Table 2 of this paper indicates an overall increase of 36.5 fold when the PEG concentration was increased from 100 mg/ml to 500 mg/ml. In contrast, the diffusion coefficient

of Alexa488 decreased by a factor of 6.2 only. That is, the changes of the diffusion coefficient cannot be accounted by those of the bulk viscosity.

The concept of microviscosity is commonly introduced to reconcile such apparent discrepancy with the Stokes-Einstein relations for rotation and translation. Microviscosity should account for the actual local structural environment of the polymeric medium surrounding the diffusing nanoprobe whereas bulk viscosity corresponds to the case of nanoparticles diffusing in a homogeneous “structureless” medium as “seen” by the nanoparticles. While water (no polymer) can be readily accepted as a homogeneous continuum medium for the studied nanoprobe, it is not the case for the present polymeric solution, especially at relatively low concentration. The entropic-based model suggested by de Gennes and his collaborators provides an alternative intuitive approach to include the relevant length scales which would validate either the assumption of the Stokes-Einstein relation or indicate possible deviation from the relation. The nanoprobe-polymer-water solution is a tertiary system with mainly two lengthscales: the size of the nanoprobe and the mesh size of the polymeric system (see Section 2.5.2). The mesh size, ξ , characterizes and reflects the statistical average distance between the polymer chains (PEG or PVA). If we use the expression in Eq. 2.17 to fit the data in Figures 2.29 and 2.30 for the translational diffusion, the resulting stretched exponential fit suggests that the value of the exponent is close $n=3/4$, which describes the solvent quality. That is, the host linear PEG and PVA systems act as a good-system in water.

4.5 Linear PEG or PVA vs Branched Ficoll Solutions:

We have recently reported FCS and FA measurements of Alexa488 dispersed in a different polymer, Ficoll (MW~70 kDa). Noticeably, Ficoll is a branched polysaccharide, and differ structurally from the linear structure of PVA or PEG. In Figures 4.1 and 4.2 we compare the dependence of the translational diffusion coefficient of Alexa488 on each polymer concentration. In each Figure we include the result of the fit of the data with a stretched exponential function.

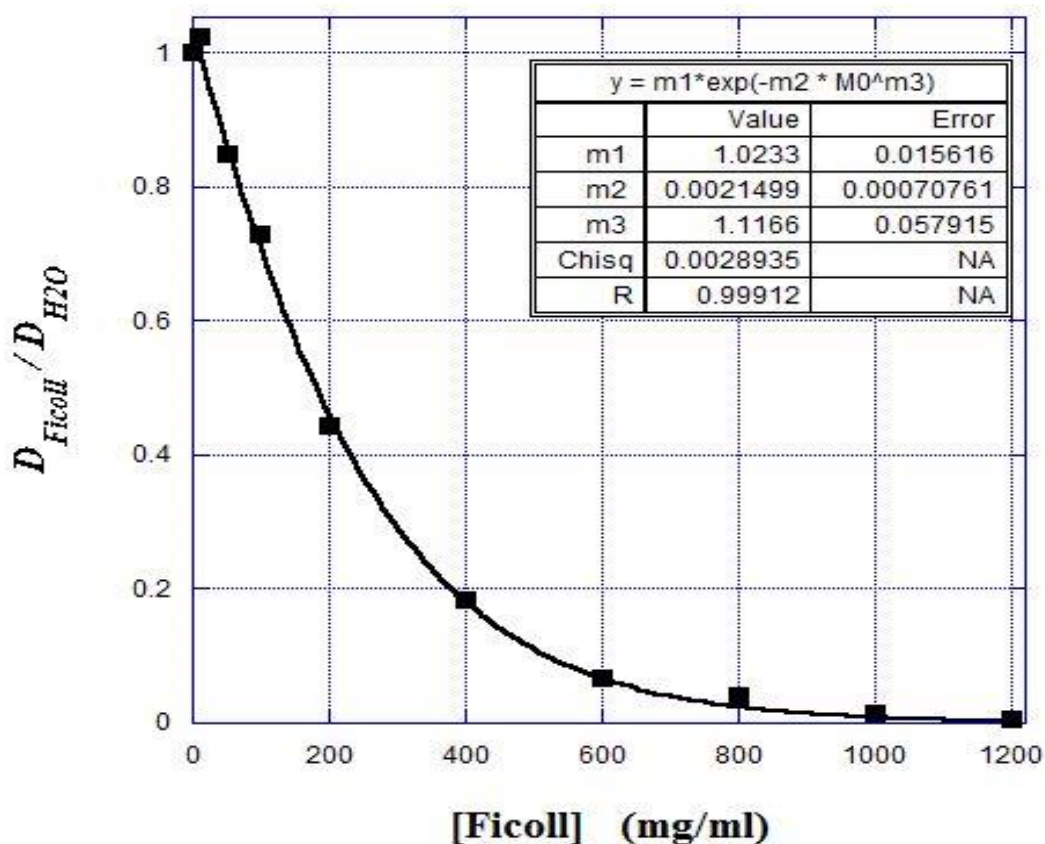


Figure 4.1: Changes of the translational diffusion coefficient of Alexa488 in Ficoll solutions

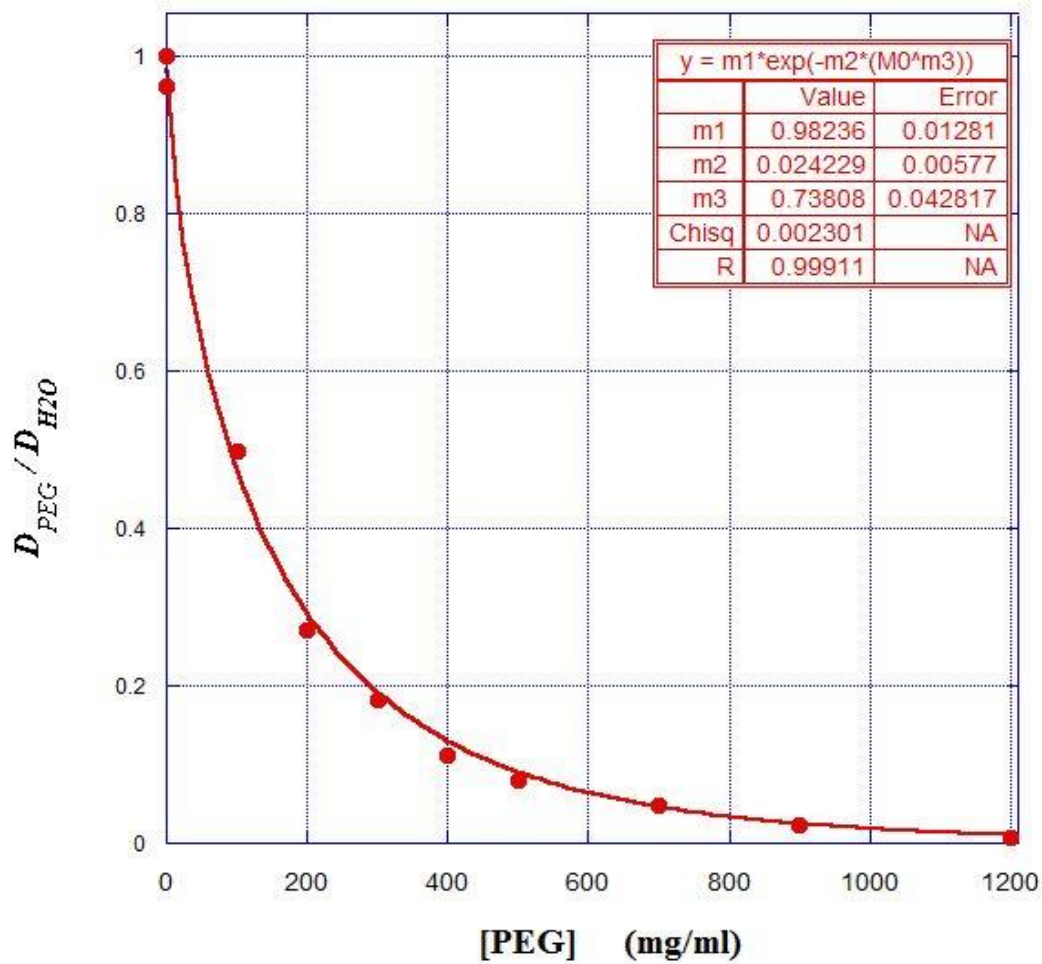


Figure 4.2: Changes of the translational diffusion coefficient of Alexa488 in PEG solutions

Here we can notice that the fitted value (1.11 ± 0.06) for the exponent of the function in the case of Ficoll is close to the theoretical value $n=1$ associated with a theta-like polymeric system. This value should be contrasted with that derived for PEG solution (0.74 ± 0.04), which is close to $n=3/4$ associated with good solvent. Whether this difference in the exponent can be related to the local structural environment created by either the branched Ficoll or the linear PEG (also by PVA) remains unclear.

Comparison of the rotational data yields the same unclear answer. In Figures 4.3 and 4.4 we show the concentration (Ficoll and PEG) dependence of the inverse of the rotational correlation time of Alexa488.

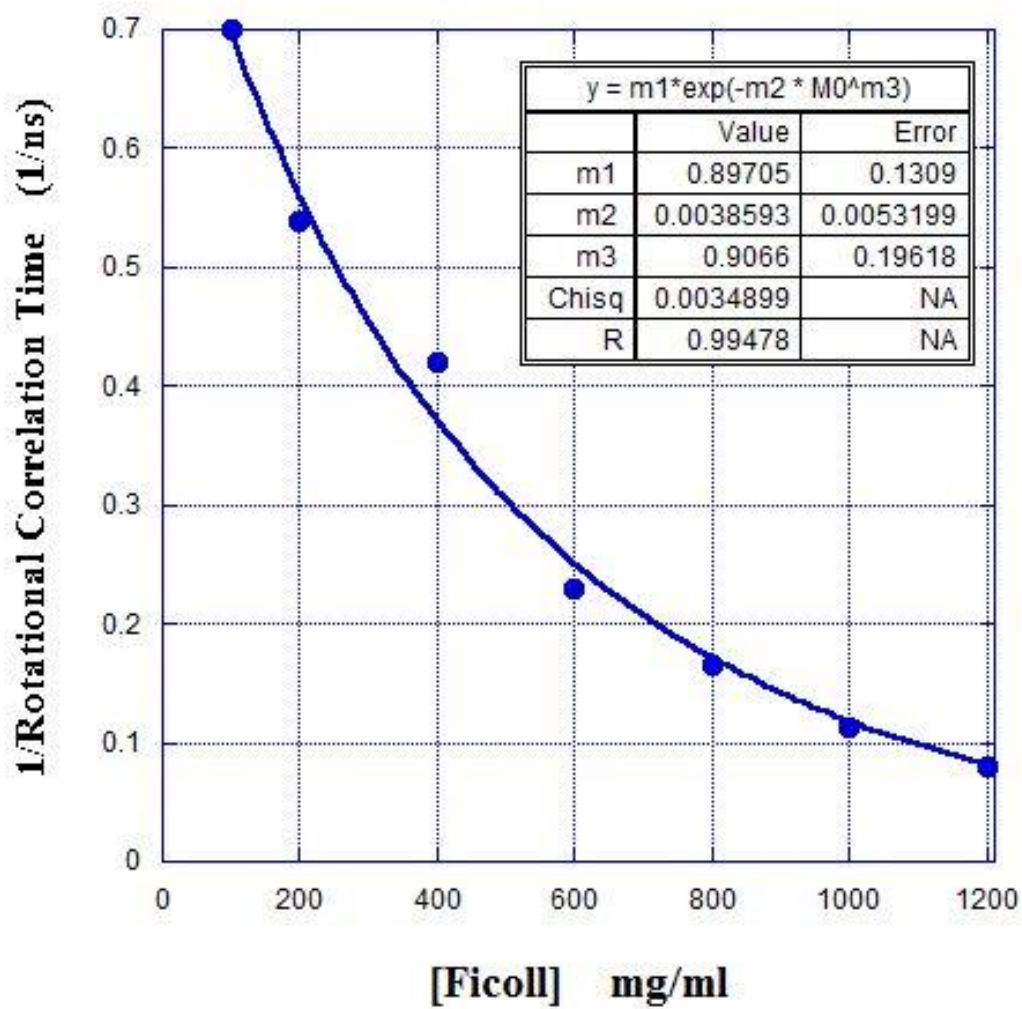


Figure 4.3: Changes of the inverse of the rotational correlation time (proportional to rotational diffusion coefficient, D_R) of Alexa488 in Ficoll solutions

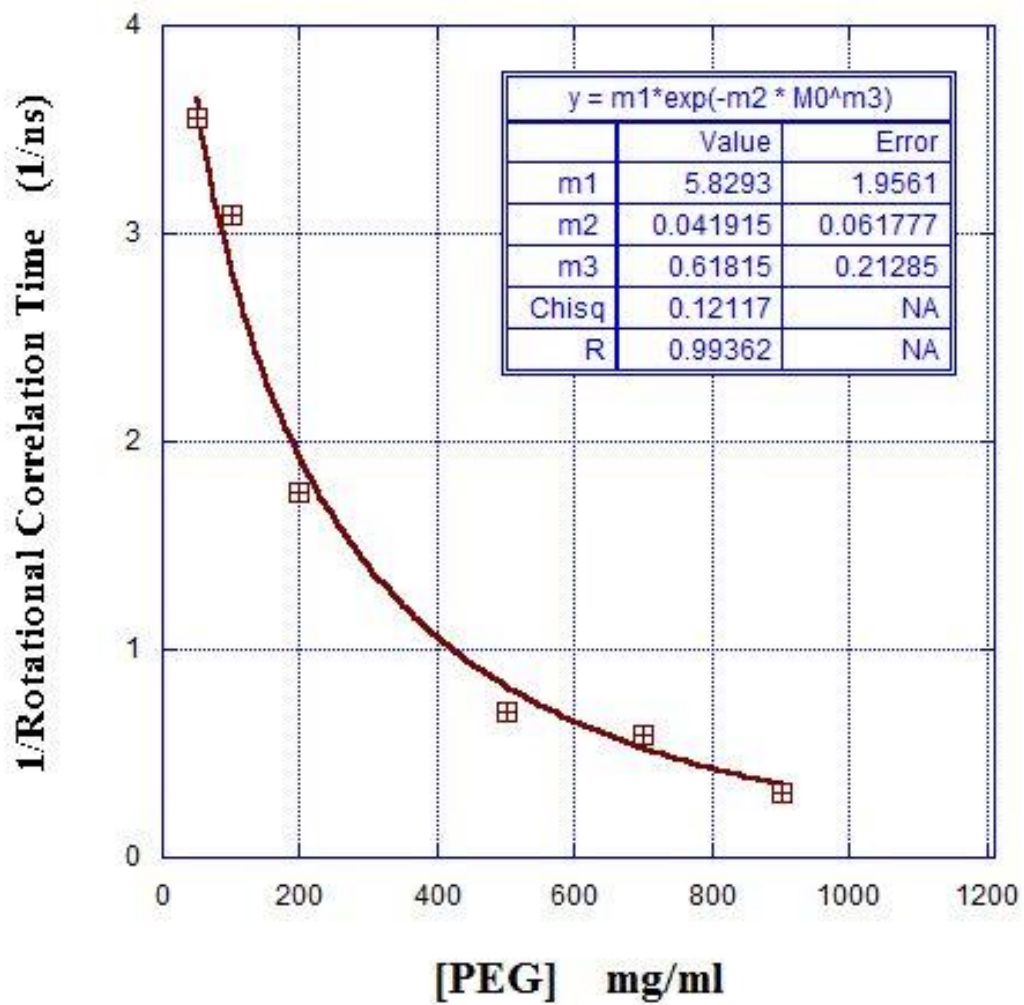


Figure 4.4: Changes of the inverse of the rotational correlation time (proportional to rotational diffusion coefficient, D_R) of Alexa488 in PEG solutions.

I have also included the results of the fits with a stretched exponential. As can be noticed it appears that the values of the exponents are different with the exponent (0.9 ± 0.2) in Ficoll closer again to the theoretical value, $n=1$, for a theta-like solvent. For PEG, the derived exponent, 0.6 ± 0.2 , tends to closer to the theoretical value, $n=3/4$, for a good solvent. Note, however, that the uncertainty values in the values of both exponents are larger in the rotational data and one needs to refrain from making a definite conclusion about the validity of this difference. Additional and more precise data are needed for either this nanoprobe (Alexa488) or others to generalize the result.

In summary, this study reinforces first the successful systematic approach that was developed previously in the case of Ficoll system for investigating the diffusion –rotation and translation- of nanoprobes. As demonstrated the optical methods (FCS and FA) provide many advantages and allowed us to probe in-situ and examine the effects of polymeric crowded environment on the behavior of the nanoprobes at nanoscopic scale. Alexa488 fluorophore (~1.5 nm) provided information about the polymeric host solutions such as solvent quality. Remarkably, the nanoprobe appears to diffuse and behave similarly if dispersed in similar linear polymers (PEG vs PVA). It is not the case when we compare PEG versus Ficoll. Additional studies with other nanoprobes and other polymeric systems are certainly needed in order to get further insight into the nanoscopic behavior of the nanoprobe.

REFERENCES:

1. Ellis, R.J.; Minton, A.P. Cell biology: Join the crowd. *Nature* 2003, 425, 27–28
2. Homouz, D.; Perham, M.; Samiotakis, A.; Cheung, M.S.; Wittung-Stafshede, P. Crowded, cell-like environment induces shape changes in aspherical protein. *Proc. Natl. Acad. Sci. USA* 2008, 105, 11754–11759.
3. Fulton, 1982; Record et al, 1998
4. Magde, D., E.L. Elson, and W.W. Webb, *Fluorescence correlation spectroscopy. II. An experimental realization*. *Biopolymers*, 1974. **13**(1): p. 29-61.
5. Elson, E.L., *Fluorescence correlation spectroscopy: past, present, future*. *Biophysical journal*, 2011. **101**(12): p. 2855-2870.
6. Schwille, P., *Fluorescence correlation spectroscopy and its potential for intracellular applications*. *Cell biochemistry and biophysics*, 2001. **34**(3): p. 383-408.
7. Mei, C.C., J.-L. Auriault, and C.-O. Ng, *Some applications of the homogenization theory*. *Advances in applied mechanics*, 1996. **32**: p. 278-348.
8. Briddon, S.J., et al., *Pharmacology under the microscope: the use of fluorescence correlation spectroscopy to determine the properties of ligand-receptor complexes*. *Trends Pharmacol Sci*, 2007. 28(12): p. 637-45.
9. Hazlett, T.L., et al., *Application of fluorescence correlation spectroscopy to hapten-antibody binding*. *Methods Mol Biol*, 2005. **305**: p. 415-38.
10. Kim, S.A., et al., *Intracellular calmodulin availability accessed with two-photon crosscorrelation*. *Proc Natl Acad Sci USA*, 2004.101(1): p. 105-10.
11. Cussler, E.L., *Diffusion: mass transfer in fluid systems*. 2009: Cambridge university press.

12. Park, H. and K. Park. *Hydrogels in bioapplications*. in *ACS Symposium Series*. 1996.
13. Hu, D.S.-G. and K.J.-N. Chou, *Kinetics of water swelling and development of porous structure in ionic poly (acrylonitrile-acrylamide-acrylic acid) hydrogels*. *Polymer*, 1996. **37**(6): p. 1019-1025.
14. Pecora, R., *Dynamic light scattering measurement of nanometer particles in liquids*. *Journal of nanoparticle research*, 2000. **2**(2): p. 123-131.
15. Reits, E.A.J. and J.J. Neefjes, *From fixed to FRAP: measuring protein mobility and activity in living cells*. *Nature cell biology*, 2001. **3**(6): p. E145-E147.
16. Peppas, N.A. and J.E. Scott, *Controlled release from poly (vinyl alcohol) gels prepared by freezing-thawing processes*. *Journal of controlled release*, 1992. **18**(2): p. 95-100.
17. Amsden, B., *Solute diffusion within hydrogels. Mechanisms and models*.
18. Cukier, R.I., *Diffusion of Brownian spheres in semidilute polymer solutions*. *Macromolecules*, 1984. **17**(2): p. 252-255.
19. Stilbs, P., *Fourier transform pulsed-gradient spin-echo studies of molecular diffusion*. *Progress in nuclear magnetic resonance spectroscopy*, 1987. **19**(1): p. 1
20. Doi, M., *Introduction to polymer physics*. 1996: Oxford university press.
21. Ying, Q. and B. Chu, *Overlap concentration of macromolecules in solution*. *Macromolecules*, 1987. **20**(2): p. 362-366.
22. Annabi, N., et al., *Controlling the porosity and microarchitecture of hydrogels for tissue engineering*. *Tissue Engineering Part B: Reviews*, 2010. **16**(4): p. 371-383.
23. Zustiak, S.P., H. Boukari, and J.B. Leach, *Solute diffusion and interactions in crosslinked poly (ethylene glycol) hydrogels studied by fluorescence correlation spectroscopy*. *Soft Matter*, 2010. **6**(15): p. 3609-3618.

24. Ahearne, M., et al., *Characterizing the viscoelastic properties of thin hydrogel-based constructs for tissue engineering applications*. Journal of The Royal Society Interface, 2005. **2**(5): p. 455-463.
25. Kang, H.-W., Y. Tabata, and Y. Ikada, *Fabrication of porous gelatin scaffolds for tissue engineering*. Biomaterials, 1999. **20**(14): p. 1339-1344.
26. Drury, J.L. and D.J. Mooney, *Hydrogels for tissue engineering: scaffold design variables and applications*. Biomaterials, 2003. **24**(24): p. 4337-4351.
27. Tibbitt, M.W. and K.S. Anseth, *Hydrogels as extracellular matrix mimics for 3D cell culture*. Biotechnology and bioengineering, 2009. **103**(4): p. 655-663.
28. Harris, J.M., *Introduction to biotechnical and biomedical applications of poly (ethylene glycol)*, in *Poly (ethylene glycol) Chemistry*. 1992, Springer. p. 1-14.
29. Lutz, P. and P. Rempp, *New developments in star polymer synthesis. Starshaped polystyrenes and star-block copolymers*. Die Makromolekulare Chemie, 1988. **189**(5): p. 1051-1060.
30. Jain, E., et al., *Fabrication of Polyethylene Glycol-Based Hydrogel Microspheres Through Electrospraying*. Macromolecular Materials and Engineering, 2015.
31. Bromberg, L., *Crosslinked poly (ethylene glycol) networks as reservoirs for protein delivery*. Journal of applied polymer science, 1996. **59**(3): p. 459-466.
32. Shao C., Kim H., Gong J., Ding B., Lee D., and Park S., Mater. Lett., 57 (2003) 1579. 7. Krumova M.
33. López D., Benavente R., Mijangos C., and Pereša J.M., Polymer, 41 (2000) 9265.
34. <http://photobiology.info/Visser-Rolinski.html> (figure.11)
35. Fluorescence Correlation Spectroscopy: Past, Present, Future ., Elliot L. Elson 101(12): 2855–2870.

36. Solute diffusion and interactions in cross-linked poly(ethylene glycol) hydrogels studied by Fluorescence Correlation Spectroscopy., Silviya P. Zustiak, Hacene Boukari, and Jennie B. Leach : [10.1039/C0SM00111B](https://doi.org/10.1039/C0SM00111B)
37. Rotational and Translational Diffusion of Nanoprobes in Ficoll solutions By ELTON JHAMBA, DSU 2016.
- 38. Rotational and Translational Diffusion of Low Molecular Weight Nanoprobes in Ficoll Solutions E. Jhamba, Z. M'Rah, and H. Boukari., DOI: 10.2174/1573413713666170110110938**
39. Tokuriki N, Kinjo M, Negi S, et al. Protein folding by the effects of macromolecular crowding. *Protein Science: A Publication of the Protein Society*. 2004;13(1):125-133. doi:10.1110/ps.03288104.
40. Aitchison JD, Rout MP. The interactome challenge. *The Journal of Cell Biology*. 2015;211(4):729-732. doi:10.1083/jcb.201510108.
41. Molecular Fluorescence: Principles and Applications. Bernard Valeur: P. 133-185
42. Elson, E. L., and D. Magde. 1974. Fluorescence correlation spectroscopy. I. Conceptual basis and theory. *Biopolymers*. 13: 1-27.
43. Krichevsky, O., and G. Bonnet. 2002. Fluorescence correlation spectroscopy: the technique and its applications. *Rep. Prog. Phys.* 65: 251-297.
44. Bacia, K., and P. Schwille. 2003. A dynamic view of cellular processes by in vivo fluorescence auto- and cross-correlation spectroscopy. *Methods*. 29: 74-85.
45. Haustein, E., and P. Schwille. 2007. Fluorescence correlation spectroscopy: novel variations of an established technique. *Annu. Rev. Biophys. Biomol. Struct.* 36: 151-169.

46. Charier, S., A. Meglio, D. Alcor, E. Cogne-Laage, J. F. Allemand, L. Jullien, and A. Lemarchand. 2005. Reactant concentrations from fluorescence correlation spectroscopy with tailored fluorescent probes. An example of local calibration-free pH measurement. *J. Am. Chem. Soc.* 127:15491-15505.
47. Krai, T., M. Langner, M. Benes, D. Baczynska, M. Ugorski, and M. Hof. 2002. The application of fluorescence correlation spectroscopy in detecting DNA condensation. *Biophys. Chem.* 95:135-144.
48. Widengren, J., U. Mets, and R. Rigler. 1999. Photodynamic properties of green fluorescent proteins investigated by fluorescence correlation spectroscopy. *Chem. Phys.* 250:171-186.
49. Haupt, U., S. Maiti, P. Schwille, and W. W. Webb. 1998. Dynamics of fluorescence fluctuations in green fluorescent protein observed by fluorescence correlation spectroscopy. *Proc. Natl. Acad. Sci. U. S. A.* 95:13573-13578.
50. Qian, H., and E. L. Elson. 2002. Single-molecule enzymology: stochastic Michaelis-Menten kinetics. *Biophys. Chem.* 101:565-576.
51. Lakowicz, J. R. 1999. *Principles of Fluorescence Spectroscopy*. Kluwer Academic/Plenum Publishers, New York.
52. Davis, L. M., and G. Q. Shen. 2006. Accounting for triplet and saturation effects in FCS measurements. *Curr. Pharm. Biotechnol.* 7:287-301.
53. Widengren, J., and P. Schwille. 2000. Characterization of photoinduced isomerization and back-isomerization of the cyanine dye Cy5 by fluorescence correlation spectroscopy. *J. Phys. Chem. A* 104:6416-6428.
54. Koppel, D. E. 1974. Statistical accuracy in fluorescence correlation spectroscopy. *Phys. Rev. A* 10:1938-1945.

55. Qian, H. 1990. On the statistics of fluorescence correlation spectroscopy. *Biophys. Chem.* 38:49-57.
56. Kask, P. Gunther, R. Axhausen, P. 1996. Statistical accuracy in fluorescence fluctuation experiments. *Eur. Biophys J.* 25:163-169.
57. S. R. Aragón, *J. Chem. Phys.* 64, 1791 (1976).
58. Odian, G., *Principles of Polymerization*, p. 574, 748.
59. Hermanson, G.T., *Bioconjugate Techniques* 2nd ed. 2008: Elsevier.
60. Peppas, N.A. and E.W.Merrill, Poly(vinyl alcohol) hydrogels: Reinforcement of radiation-cross linked networks by crystallization. *Journal of polymer science - Polymer chemistry edition*, 1976. 14: p. 441-457.
61. Peppas, N.A. and N.K. Mongia, Ultrapure poly(vinyl alcohol) hydrogels with mucoadhesive drug delivery characteristics. *Eur J Pharm Biopharm*, 1997. 43: p. 51-58.
62. Zhang, X.e.a., Double network hydrogel with high mechanical strength prepared from two biocompatible polymers. *Journal of Applied Polymer Science*, 2009. 112: p. 3063-3070.
63. T. Wohland, R. Rigler, and H. Vogel, *Biophys. J.* **80**, 2987 (2001).
64. D. E. Koppel, *Phys. Rev. A* **10**, 1938 (1974).
65. K. Hassler, T. Anhut, R. Rigler, M. Gösch, and T. Lasser, *Biophys. J.* **88**, 1 (2005).
66. <http://www.biochemsoctrans.org/content/44/2/624>
67. Michelman-Ribeiro, A., Horkay, F., Nossal, R., and Boukari, H. "Probe diffusion in aqueous Poly(vinyl alcohol) solutions studied by fluorescence correlation spectroscopy," *Biomacromolecules* 8 (5), 1595–1600 (2007).
68. Langevin, D., and Rondelez, F., "Sedimentation of large colloidal particles through semidilute polymer solutions," *Polymer* 19 (8), 875–882 (1978).

69. Phillies, G. D. J., Brown, W., and Zhou, P., "Chain and sphere diffusion in Polyisobutylene-CHC13: A reanalysis," *Macromolecules* 25, 4948-4954 (1992).
70. Phillies, G. D. J., and Clomenil, D., "Probe diffusion in polymer solutions under θ and good conditions," *Macromolecules* 26, 167-170 (1993).
71. Cukier, R. I., "Diffusion of brownian spheres in semidilute polymer solutions," *Macromolecules* 17, 252-255 (1984).
72. Altenberger, A. R., and Tirrell, M., "On the theory of self-diffusion in a polymer gel," *J. Chem. Phys.* 80, 2208-2213 (1984).
73. Ogston, A. G., Preston, B. N., and Wells, J. D., "On the transport of compact particles through solutions of chain-polymers," *Proc. R. Soc. London A.* 333, 297-316 (1973).
74. Phillies, G. D. J., "Dynamics of polymers in concentrated solutions: The universal scaling equation derived," *Macromolecules* 20, 558-564 (1987).
75. S. M. Bhattacharjee, A. Giacometti, and A. Maritan, *J. Phys. Condens. Matter* **25**, 503101 (2013).
76. A. Michelman-Ribeiro, H. Boukari, R. Nossal, and F. Horkay, *Macromol. Symp.* **227**, 221 (2005).
77. Crossover regime for diffusion of nanoparticles in polyethylene glycol solutions: influence of depletion layer Natalia Ziębacz, Stefan A. Wiczorek, Tomasz Kalwarczyk, Marcin Fiałkowski, Robert Hołyst.
78. Density and Viscosity of Concentrated Aqueous Solutions of Polyethylene Glycol **by** :Pedro Gonzalez-Tello, Fernando Camacho, and Gabriel Blazquez . *Journal of Chemical & Engineering Data* 1994 39 (3), 611-614 DOI: 10.1021/je00015a050

79. Zahra Sekhavat Pour and Mousa Ghaemy., Removal of dyes and heavy metal ions from water by magnetic hydrogel beads based on poly(vinyl alcohol)/carboxymethyl starch-g-poly(vinyl imidazole)
80. Alberts B, Johnson A, Lewis J, et al. *Molecular Biology of the Cell*. 4th edition. New York: Garland Science; 2002. Protein Function.
81. Rotational behavior of the fluorescent probe molecules near the critical point of phase separation., Shigeaki Morita , Hideharu Ushiki
82. http://www.iss.com/resources/research/technical_notes/PC1_FP.html
83. W. B. Dandliker and G. A. Feigen, "Quantification of the antigen-antibody reaction by the polarization of fluorescence," *Biophysical and biochemical research communications*, vol. 5, pp. 299-304, 1961.
84. R. B. Qaqish and M. M. Amiji, "Synthesis of a fluorescent chitosan derivative and its application for the study of chitosan-mucin interactions," *Carbohydrate Polymers*, vol. 38, pp. 99-107, 1999.
85. T. Hayashi, Y. Ishizaki, M. Michihata, Y. Takaya, and S. I. Tanaka, "Nanoparticle sizing method based on fluorescence anisotropy analysis," *Measurement*, vol. 59, pp. 382-388, 2015.
86. M. Sowmiya, A. K. Tiwari, and S. K. Saha, "Fluorescent probe studies of micropolarity, pre-micellar and micellar aggregation of non-ionic Brij surfactants," *Journal of colloid and interface science*, vol. 344, pp. 97-104, 2010.
87. Craig J. Sansonetti, Marc L. Salit, and Joseph Reader: Wavelengths of spectral lines in mercury pencil lamps

88-Jameson DM, Croney JC, Moens PD:Fluorescence: basic concepts, practical aspects, and some anecdotes

89. <http://www.iss.com/fluorescence/instruments/k2.html>

90. <http://www.horiba.com/scientific/products/raman-spectroscopy/raman-academy/raman-faqs/can-raman-spectra-be-obtained-from-aqueous-materials/>